IN THIS ISSUE

IMAGE: OBSERVATORY WITH STAR TRAILS ON MOUNTAINS FOR CLEAR SKY

Great Britain Journals Press

www.journalspress.com

LONDON JOURNAL OF ENGINEERING RESEARCH

Volume 24 | Issue 3 | Compilation 1.0

Print ISSN: 2631-8474
Online ISSN: 2631-8482
DOI: 10.17472/LJER

© 2024 Great Britain Journals Press

COMPILED IN UNITED KINGDOMS

ENGLISH

London Journal of Engineering Research

Volume 24 | Issue 3 | Compilation 1.0

PUBLISHER

Great Britain Journals Press
1210th, Waterside Dr, Opposite Arlington Building, Theale, Reading
Phone:+444 0118 965 4033 Pin: RG7-4TY United Kingdom

SUBSCRIPTION

Frequency: Quarterly

Print subscription
$280USD for 1 year
$500USD for 2 year
(*color copies including taxes and international shipping with TSA approved)*
Find more details at https://journalspress.com/journals/subscription

ENVIRONMENT

Great Britain Journals Press is intended about Protecting the environment. This journal is printed using led free environmental friendly ink and acid–free papers that are 100% recyclable.

Copyright ©2024 by Great Britain Journals Press

All rights reserved. No part of this publication may be reproduced, distributed, or transmitted in any form or by any means, including photocopying, recording, or other electronic or mechanical methods, without the prior written permission of the publisher, except in the case of brief quotations embodied in critical reviews and certain other noncommercial uses permitted by copyright law. For permission requests, write to the publisher, addressed "Attention: Permissions Coordinator," at the address below. Great Britain Journals Press holds all the content copyright of this issue. Great Britain Journals Press does not hold any responsibility for any thought or content published in this journal; they belong to author's research solely. Visit https://journalspress.com/journals/privacy-policy to know more about our policies.

Great Britain Journals Press Headquaters

1210th, Waterside Dr,
Opposite Arlington
Building, Theale, Reading
Phone:+444 0118 965 4033
Pin: RG7-4TY
United Kingdom

Reselling this copy is prohibited.
Available for purchase at www.journalspress.com for $50USD / £40GBP (tax and shipping included)

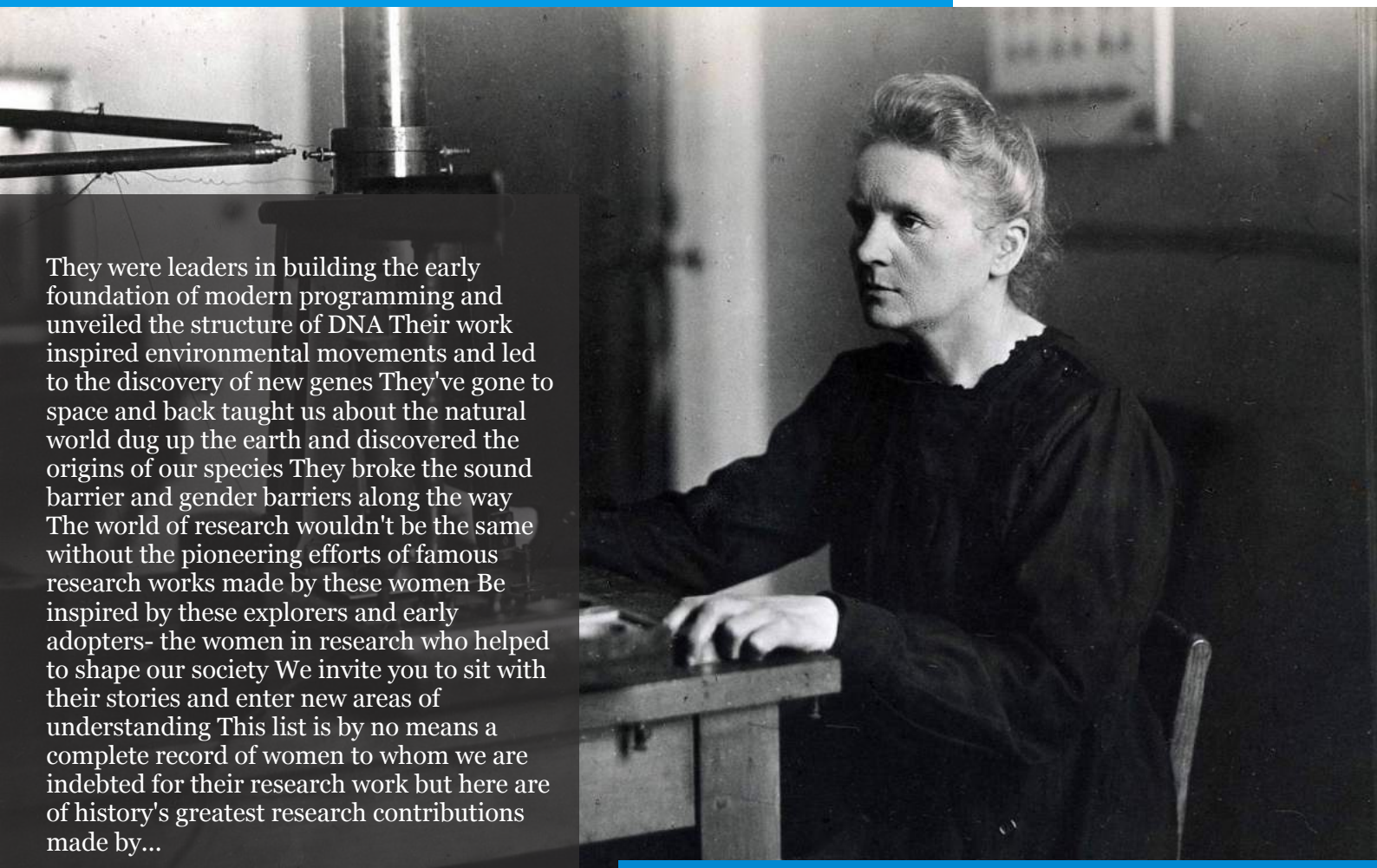

They were leaders in building the early foundation of modern programming and unveiled the structure of DNA Their work inspired environmental movements and led to the discovery of new genes They've gone to space and back taught us about the natural world dug up the earth and discovered the origins of our species They broke the sound barrier and gender barriers along the way The world of research wouldn't be the same without the pioneering efforts of famous research works made by these women Be inspired by these explorers and early adopters- the women in research who helped to shape our society We invite you to sit with their stories and enter new areas of understanding This list is by no means a complete record of women to whom we are indebted for their research work but here are of history's greatest research contributions made by...

Read complete here:
https://goo.gl/1vQ3lS

Women In Research

Computing in the cloud!

Cloud Computing is computing as a Service and not just as a Product Under Cloud Computing...

Read complete here:
https://goo.gl/VvHC72

Writing great research...

Prepare yourself before you start Before you start writing your paper or you start reading other...

Read complete here:
https://goo.gl/np73jP

©2024 Great Britain Journals Press

Journal Content
In this Issue

Great Britain Journals Press

©2024 Great Britain Journals Press

Editorial Board

Curated board members

Dr. Sharif H. Zein

School of Engineering,
Faculty of Science and Engineering,
University of Hull, UK Ph.D.,
Chemical Engineering Universiti Sains Malaysia,
Malaysia

Prof. Hamdaoui Oualid

University of Annaba, Algeria Ph.D.,
Environmental Engineering,
University of Annaba,
University of Savoie, France

Prof. Wen Qin

Department of Mechanical Engineering,
Research Associate, University of Saskatchewan,
Canada Ph.D., Materials Science,
Central South University, China

Dr. Luisa Molari

Professor of Structural Mechanics Architecture,
University of Bologna,
Department of Civil Engineering, Chemical,
Environmental and Materials, PhD in Structural
Mechanics, University of Bologna.

Prof. Chi-Min Shu

National Yunlin University of Science
and Technology, Chinese Taipei Ph.D.,
Department of Chemical Engineering University of
Missouri-Rolla (UMR) USA

Dr. Fawad Inam

Faculty of Engineering and Environment,
Director of Mechanical Engineering,
Northumbria University, Newcastle upon Tyne,
UK, Ph.D., Queen Mary, University of London,
London, UK

Dr. Zoran Gajic

Department of Electrical Engineering,
Rutgers University, New Jersey, USA
Ph.D. Degrees Control Systems,
Rutgers University, United States

Prof. Te-Hua Fang

Department of Mechanical Engineering,
National Kaohsiung University of Applied Sciences,
Chinese Taipei Ph.D., Department of Mechanical
Engineering, National Cheng Kung University,
Chinese Taipei

Dr. Rocío Maceiras

Associate Professor for Integrated Science,
Defense University Center, Spain Ph.D., Chemical
Engineering, University of Vigo, SPAIN

Dr. Rolando Salgado Estrada

Assistant Professor,
Faculty of Engineering, Campus of Veracruz,
Civil Engineering Department, Ph D.,
Degree, University of Minho, Portugal

Dr. Abbas Moustafa

Department of Civil Engineering,
Associate Professor, Minia University, Egypt, Ph.D
Earthquake Engineering and Structural Safety,
Indian Institute of Science

Dr. Wael Salah

Faculty of Engineering,
Multimedia University Jalan Multimedia,
Cyberjaya, Selangor, Malaysia, Ph.D, Electrical and
Electronic Engineering, Power Electronics and Devices,
University Sians Malaysia

Prof. Baoping Cai

Associate Professor,
China University of Petroleum,
Ph.D Mechanical and Electronic Engineering,
China

Dr. Kao-Shing Hwang

Electrical Engineering Dept.,
Nationalsun-Yat-sen University Ph.D.,
Electrical Engineering and Computer Science,
Taiwan

Dr. Mu-Chun Su

Electronics Engineering,
National Chiao Tung University, Taiwan,
Ph.D. Degrees in Electrical Engineering,
University of Maryland, College Park

Nagy I. Elkalashy

Electrical Engineering Department,
Faculty of Engineering,
Minoufiya University, Egypt

Dr. Vitoantonio Bevilacqua

Department of Electrical and Information
Engineering Ph.D., Electrical Engineering
Polytechnic of Bari, Italy

Prof. Qingjun Liu

Professor, Zhejiang University, Ph.D.,
Biomedical Engineering,
Zhejiang University, China

Research papers and articles

Volume 24 | Issue 3 | Compilation 1.0

Scan to know paper details and
author's profile

Reaching Pandemic Milestones with Country Primary and Secondary Vaccination Inflection Points: An Assessment of Foundational and Hybrid Forecasting Methodologies

Marco M. Vlajnic & Steven J. Simske

Colorado State University

ABSTRACT

The devastating worldwide impact of the COVID-19 pandemic created a need to better understand the effects of vaccination on case fatality rates (CFR) in a pandemic setting. Foundational time series forecasting models (ARIMA, Prophet, LSTM) and novel hybrid models (SARIMA-Bidirectional LSTM and SARIMA-Prophet-Bidirectional LSTM) were compared for performance and accuracy to forecast vaccination inflection points for 26 countries. Correlation analyses demonstrated that stringency index, age 65 and older, life expectancy, and positive test rate, are factors correlating the most with the vaccination and case fatality rates. The primary vaccination inflection point was reached at 83.27 days (15-367 days), at the vaccination rate of 13.1% (0.1% - 50%), with 42% of countries seeing the initial impact in <50 days.

The secondary vaccination inflection point (SVIP) was reached at 339.31 days (161-560 days) at the cumulative vaccination rate of 67.8% (28% - 89%), with 23.1% of countries reaching it in < 300 days, 73% in the second half of 2021, and 27% in early 2022.

Index Terms: COVID-19, primary vaccination inflection point, secondary vaccination inflection point, ARIMA, prophet, LSTM, double hybrid, triple hybrid, SARIMA-bidirectional LSTM, SARIMA-prophet-bidirectional LSTM.

Classification: LCC Code: HB1-3840

Language: English

Great Britain Journals Press

LJP Copyright ID: 392941
Print ISSN: 2631-8474
Online ISSN: 2631-8482

London Journal of Engineering Research

Volume 24 | Issue 3 | Compilation 1.0

© 2024. Marco M. Vlajnic & Steven J. Simske. This is a research/review paper, distributed under the terms of the Creative Commons Attribution- Noncom-mercial 4.0 Unported License http://creativecommons.org/licenses/by-nc/4.0/), permitting all noncommercial use, distribution, and reproduction in any medium, provided the original work is properly cited.

Reaching Pandemic Milestones with Country Primary and Secondary Vaccination Inflection Points: An Assessment of Foundational and Hybrid Forecasting Methodologies

Marco M. Vlajnic[α] & Steven J. Simske[σ]

ABSTRACT

The devastating worldwide impact of the COVID-19 pandemic created a need to better understand the effects of vaccination on case fatality rates (CFR) in a pandemic setting. Foundational time series forecasting models (ARIMA, Prophet, LSTM) and novel hybrid models (SARIMA-Bidirectional LSTM and SARIMA-Prophet-Bidirectional LSTM) were compared for performance and accuracy to forecast vaccination inflection points for 26 countries. Correlation analyses demonstrated that stringency index, age 65 and older, life expectancy, and positive test rate, are factors correlating the most with the vaccination and case fatality rates. The primary vaccination inflection point was reached at 83.27 days (15-367 days), at the vaccination rate of 13.1% (0.1% - 50%), with 42% of countries seeing the initial impact in <50 days.

The secondary vaccination inflection point (SVIP) was reached at 339.31 days (161-560 days) at the cumulative vaccination rate of 67.8% (28% - 89%), with 23.1% of countries reaching it in < 300 days, 73% in the second half of 2021, and 27% in early 2022. The highest vaccination rate was achieved in Portugal (89%) and the lowest in Bulgaria (28%). All assessed machine and deep learning methodologies performed with high accuracy relative to COVID-19 historical data, demonstrated strong forecasting value, and were validated by anomaly and volatility detection analyses. The novel triple hybrid model performed the best and had the highest accuracy across all performance metrics. Countries prioritizing the health of elderly and frail populations and utilizing AI technology will be better prepared for any future pandemic.

Index Terms: COVID-19, primary vaccination inflection point, secondary vaccination inflection point, ARIMA, prophet, LSTM, double hybrid, triple hybrid, SARIMA-bidirectional LSTM, SARIMA-prophet-bidirectional LSTM.

Author α σ: Systems Engineering Department, Colorado State University, Engineering Building Suite 202, 400 Isotope Dr, Fort Collins, Colorado, 80523-6029 United States of America.

I. INTRODUCTION

COVID-19 is an infectious disease, caused by the Severe Acute Respiratory Syndrome Coronavirus 2 (SARS-CoV-2) characterized by high morbidity and mortality, and a significant burden on hospital systems and country economies. Over the last three years, the COVID-19 virus infected over 300 million people, caused death for approximately seven million people [1], and had a negative impact of $3.8 trillion on economies around the world. At the end of 2023, COVID-19 is still present with different virus mutations continuing to cause infections and deaths across the world [2, 3, 4].

The experience with the COVID-19 pandemic demonstrated the inadequate levels of preparedness across countries. Two thirds of world countries have a good capacity for public health threat surveillance and analytics in order to drive policy and planning. However, half of the countries have a limited capacity to systematically monitor care, including the impact of vaccination [5]. Both surveillance and

London Journal of Engineering Research

©2024 Great Britain Journals Press

monitoring are needed to adequately plan and prepare for possible infectious disease outbreaks with novel viruses [6, 7, 8, 9, 10, 11, 12, 13].

Vaccination is an effective way to obtain individual and herd immunity [14]. When the herd immunity threshold is reached, naturally or through vaccination, it creates an environment that is sufficient to control large outbreaks, reduce the number of infected individuals and possible deaths, protect vulnerable individuals in the society, and relax other public health measures [15]. There are many factors that influence a success of a vaccination campaign, such as availability of vaccine supply (e.g. speed of development, level of demand, difficulties with production and distribution of vaccines worldwide), vaccination strategy outlining priority groups for vaccination, and population acceptance of vaccination (e.g. anti-vaccination movement).

The vaccination efforts for COVID-19 started in December of 2020 for most of the countries in the world. There were several types of vaccines that were available: genetically engineered messenger RNA, viral vector, and protein subunit vaccines. The initial vaccinations from 2020 were followed with booster doses in 2021, 2022 and 2023, for a total of four booster doses, specifically in developed countries [16]. Understanding the impact of vaccination campaigns, the correlation of vaccination rates, incidence of COVID-19, and mortality rates was researched over the last two years. The results confirmed that successful vaccination efforts (e.g. availability of vaccines, public acceptance, strong government programs, etc.) can significantly reduce the negative effects of the COVID-19 pandemic, with a sharp decrease in the fatality rate [17, 18, 19]. Some researchers were able to define the vaccination threshold, identifying that a mean level of administering about 80 doses of vaccines per 100 inhabitants can sustain a reduction of confirmed cases and number of deaths [11], or when the mean cumulative vaccination rate reaches 29.06 doses per 100 people and 7.88 doses per 100 people, respectively, for spread and mortality [19]. Many researchers also looked at the sentiment around vaccination. Attitudes toward COVID-19 and vaccination, conspiracy beliefs, misconceptions, and complaints about COVID-19 control, were documented as dominant sentiments [21, 22, 23]. Researchers used data from different sources (local, national, and global registries) and different time frames (e.g., periods of 3 or 6 months post initial vaccination).

Diverse research methodologies were applied to increase sensitivity of analyses and achieve more accurate results, such as neural networks with cut effect [17], Augmented Artificial Neural Network Model for the COVID-19 Mortality Prediction relative to the vaccination rates [24]; Deep Learning Sequence Models for Forecasting COVID-19 Spread and Vaccinations with two recurrent neural network-based approaches, LSTM and GRU [25]; amalgamation of neural network with two powerful optimization algorithms, firefly algorithm and artificial bee colony based feed-forward neural networks to look at the effect of vaccinated population on the COVID-19 prediction [26]; and a multi-path long short term memory (LSTM) neural network for COVID-19 forecasting of new viral variants and vaccination [27]. Other researchers explored other models, structured and unstructured machine learning (ML) models [22], structural topic modeling [23], Latent Dirichlet Allocation (LDA) [28], deep learning and NLP [29, 30]. Cheng applied newly developed ARIMA models to improve the accuracy of weekly COVID-19 case growth rates and forecast COVID-19 spread according to protective behavior and vaccination [31]. Dhamodharavadhani and colleagues used hybrid models to forecast the vaccination rate, such as HARIMA, a hybrid of ARIMA and HGRNN, a hybrid of Generalized Regression Neural Network and the Gaussian Process Regression model [32]. Yi-Tui Chen and colleagues explored the effect of vaccination patterns and vaccination rates on the spread and mortality of the COVID-19 pandemic [19], and Kumar utilized the recurrent neural network (RNN) Convolutional Residual Network (RNNCON-Res) [33].

Nicholson and colleagues used both supervised and unsupervised methodologies to identify the critical county-level factors for studying COVID-

©2024 Great Britain Journals Press

19 propagation prior to the widespread availability of a vaccine [40].

Published research has increased collective knowledge and has answered many questions. With limitations of every research, availability of more data and novel methodologies, there is a need and a responsibility to continue to expand the knowledge around pandemic vulnerability that can allow for better understanding of the dynamics of vaccination, infection rates and mortality.

This research was conducted to identify the vaccination inflection points and the time needed to reach the critical cumulative vaccination rate thresholds to observe continuous decrease of the case fatality rates. It was conducted both at an aggregate and at the country level. COVID-19 historical data was utilized to develop models that can be used for future pandemics. Applying advanced AI methodologies to forecast time to country specific vaccination inflection points, and assessing the vaccination rates relative to the case fatality rates, can provide another useful tool to guide countries in their pandemic risk preparedness.

II. MATERIALS AND METHODS

2.1 Data

This research utilized data from the Oxford University Our World in Data Covid 19 Dataset. This dataset contains data points collected on an ongoing basis from Johns Hopkins University, Center for Systems Science and Engineering COVID-19 data, European Centre for Disease Control, and OXFORD COVID-19 Government Response Tracker, from January 2020 to the present. The original dataset contains data from 207 countries and territories from which 26 countries were selected for this research: United States, Canada, Italy, Ireland, Finland, Iceland, Denmark, Belgium, Sweden, United Kingdom, Switzerland, Slovenia, Austria, Portugal, France, Netherlands, Luxembourg, Spain, Romania, Latvia, Cyprus, Estonia, Czechia, Slovakia, Serbia, and Bulgaria. Data for this research paper was accessed and downloaded on Dec 30, 2022 [35], and this longitudinal dataset was used from the period of December 2020, when most of the countries in the research dataset started vaccinating their population, to December 30, 2022.

The analyses in this research used 16 variables. Table 1 presents the 14 variables that represent the actual values from the research dataset. Two additional variables, case fatality rate and vaccination rate, were derived. The case fatality rate (CFR), an epidemiologic metric defined as the proportion of deaths within an observed population of interest [34], was calculated by dividing the respective values in the total deaths column by the total cases column of the dataset, for each of the 26 countries. The vaccination rate was calculated by dividing the number of people vaccinated (with at least one dose) by the total population of each country, for each of the 26 countries.

For a more meaningful interpretation of the data variables used to assess the correlation with the vaccination and CFR rates, data variables were organized into novel public health

©2024 Great Britain Journals Press

Table 1: Public Health Indices definitions from the *Our World in Data* metadata file [20]

Population Health Index (PHI)	Pandemic Sensitivity Index (PSI)
cardiovasc death rate: death rate from the cardiovascular disease in 2017 (annual number of deaths per 100,000 people)	*stringency_index:* Government response stringency index: composite measure based on 9 response indicators including school and workplace closures, and travel bans.
diabetes prevalence: Diabetes prevalence (% of population aged 20 to 79) in 2017	*positive_rate:* The share of COVID-19 tests that are positive given as a rolling 7-day average
female smokers: Share of women who smoke, most recent years available	*hosp_ patients:* Number of COVID-19 patients in hospital on a given day
male smokers: Share of men who smoke, most recent years available	*icu_patients:* Number of COVID-19 patients in intensive care unit (ICUs) on a given day
life_expectancy: Life expectancy at birth in 2019	*reproduction_ rate:* Real time estimate of the effective reproduction rate of COVID-19
aged 65 or older: Share of the population that is 65 years or older, most recent years available	*total_cases:* Total confirmed cases of COVID-19
median age: Median age of the population, UN projection for 2020	*total_deaths:* Total deaths attributed to COVID-19

indices, the Population Health Index, PHI [35], and Pandemic Sensitivity Index, PSI (Table 1). The PHI contains the parameters that describe the health of the population such as: cardiovascular death rate, diabetes prevalence, female smokers, male smokers, life expectancy, age 65 and older, and median age. The PSI Index represents variables that are directly impacted by the pandemic, such as total COVID-19 cases and deaths, number of COVID-19 hospital and ICU admissions, Government response stringency index (a composite measure based on nine response indicators including school and workplace closures, and travel bans), reproduction rate of transmission of COVID-19, and positivity rate of COVID-19.

This research was conducted to identify the vaccination inflection points and the time needed to reach the critical cumulative vaccination rate thresholds to observe continuous decrease of the case fatality rates. It was conducted both at an aggregate and at the country level. To accommodate for the peaks and troughs of the case fatality rate curves, the vaccination inflection points were assessed at two different timepoints. The first vaccination inflection time point, primary vaccination inflection point (PVIP) was assessed from the vaccination start date to the date of the first CFR drop post vaccination. The secondary vaccination inflection point (SVIP) was assessed from the vaccination start date to the steepest, most significant CFR decline post vaccination. It represents the time point when the cumulative vaccination rate reached a critical threshold showing a continuous decrease of the case fatality rate, signaling the turnaround in the pandemic. Table 2 provides an overview of descriptions of critical variables used in this research relative to the vaccination inflection point. COVID-19 historical data was utilized to develop models that can be used for future pandemics.

In this research, it was assumed that all vaccines produced by different technologies and manufacturers have the same effectiveness. It was also assumed that distribution of different vaccines in different countries includes a combination of initial two-dose and single-dose vaccines and single dose booster vaccines over the two-year period (Dec 2020-Dec 2022). Since all vaccines require approximately two weeks to produce immunity, the effect of performance of vaccines on CFR was examined two weeks after the start of vaccination.

Several types of vaccines were available at the time of the initial vaccination: genetically engineered messenger RNA Pfizer/BioNTech and Moderna, viral vector vaccines (Janssen/Johnson

©2024 Great Britain Journals Press

& Johnson and University of Oxford/AstraZeneca, Sputnik V), protein subunit vaccine (Novavax, Sinovac). The initial vaccinations in 2020 were delivered, in most cases, in sets of 2-doses, with a 3-week period in between (Pfizer/BioNTech, Moderna, Sinovac, Sputnik V). Some initial vaccines were delivered as a single dose vaccine (J&J, AZ/Oxford). Consequently, booster doses were delivered as single dose vaccines, starting in the third quarter of 2021 (Sep 2021 in the US, Oct/Nov 2021 in the EU) and continuing in 2022 (approved boosters in Mar and Sep 2022 in the US) and 2023 (approved in Sep 2023 in US and EU), for a total of four booster doses [16]. Today there are approximately 40 COVID-19 vaccines that were approved by regulatory agencies for full emergency use authorization. Of those 40, 16 have full authorization in only one country, 12 in ten or fewer countries, and 12 in more than 10 countries [36]. Emergence of new variants may be a challenge for the vaccines, reducing their protective power with the transmissibility of new variants substantially higher than the pre-existing SARS-CoV-2 variants. Booster dose vaccines were introduced to boost the protection power of vaccines and help the individuals with weakened immune systems. Efficacy of most vaccines range from 70-95%, mainly against symptomatic disease [37, 38]. All countries from this dataset (26 countries) are classified in three categories relative to their GDP per capita (>$50,000, $35,000-$50,000, and <$35,000) [20]. Table 3 summarizes the distribution of countries. This research was solely conducted by using publicly available data.

Table 2: Description of derived variables used for vaccination inflection point analyses

Variables	Description
vaccination start date	first documented date when vaccination started at the country level
CFR at vaccination start	Case fatality rate at the time on the 1st day of vaccination
CFR + 14 days	case fatality rate at the time when initial immunity from vaccination should be developed
vaccination rate at CFR +14 days	vaccination rate at the time of initial immunity
Primary vaccination inflection point (PVIP)	date when the first case fatality rate reduction is observed post vaccination, measured on the day of the 1st CFR peak post vaccination + one day
CFR at PVIP	case fatality rate at PVIP, measured on the day of the 1st CFR peak post-vaccination + one day
vaccination rate at PVIP	vaccination rate at the PVIP, measured as the vaccination rate on the day of the 1st CFR peak post vaccination + one day
Secondary vaccination inflection point (SVIP)	date when the most significant CFR reduction is observed post vaccination, measured on the day of the CFR peak that is followed by the most significant and continuous CFR reduction post vaccination + one day
CFR at SVIP	case fatality rate at the SVIP, measured as the CFR rate on the day of CFR peak that is followed by the most significant CFR reduction post vaccination + one day
vaccination rate at SVIP	vaccination rate at the SVIP, measured as the vaccination rate on the day of the CFR peak that is followed by the most significant CFR reduction post vaccination + one day

Table 3: Distribution of countries based on GDP per capita

GDP per Capita	Country Distribution
> 50,000	Ireland, Luxembourg, Switzerland, United States
35,000-50,000	Austria, Belgium, Canada, Denmark, Finland, France, Iceland, Italy, Netherlands, Sweden, United Kingdom.
< 35,000	Bulgaria, Cyprus, Czechia, Estonia, Latvia, Portugal, Romania, Serbia, Slovakia, Slovenia, Spain.

©2024 Great Britain Journals Press

2.2 Methodologies

Data utilized in this research was pre-processed by assigning the original time series dataset to training and testing datasets temporally. For each country, the training set included data from the beginning of the pandemic (March 1, 2020) until a few weeks post vaccination start. The testing set included the remaining data post vaccination until the end of the dataset (December 30, 2022).

Data cleaning was conducted by resolving the problem of missing and duplicate values, resolving data inconsistencies, removing outliers, and smoothing variables used for forecasting (*vaccination_rate* and *case_fatality_rate*), including all exogeneous variables (*stringency_index, aged_65_older, life_expectancy, and positive_rate)*. Smoothing was conducted by using a window of seven days to remove all noisy data. The current day value was calculated using the mean of the previous seven days for each variable. In this type of dataset, it is common that some data is missing, both at random and not at random. For this research, it was important that the data on the total number of cases and deaths was complete since it was used to derive the case fatality rates. This missing data was resolved by taking the mean values of the total number of cases and deaths from the previous day and the next day. Other missing data was managed in a similar manner. Data quality assessments (completeness, reliability, consistency, validity, and no redundancy) were also completed. Exploratory Data Analysis was conducted by exploring graphs and visuals in order to observe trends over time of the vaccination and case fatality rates for each country.

Three foundational forecasting methodologies were applied: Autoregressive Integrated Moving Average (ARIMA), Prophet, and Long-Short Term Memory (LSTM) models. These models were then enhanced and combined to develop novel double and triple hybrids, SARIMA-Bidirectional LSTM and SARIMA-Prophet-Bidirectional LSTM models. They were used to forecast the primary and secondary vaccination inflection points (PVIP and SVIP) relative to the case fatality rates, for each of the 26 countries. All machine learning and deep learning analyses were done using Python version 3.10.1 and the scikit-learn library version 1.2.0 [39]. In addition, the novel Vaccination Inflection Point Score was developed, and countries were classified according to the score.

2.2.1 Correlation Analysis

The correlation analysis was performed using Ordinary Least Squares Multifactor Regression Methodology to identify the top four variables that correlate the most with vaccination and case fatality rates for implementation into forecasting methodologies. These analyses were performed as an aggregate analysis of 14 variables that were assessed for correlation with vaccination and case fatality rates. All variables were used for the correlation assessment with the vaccination rate. Two variables, *total_cases* and *total_deaths* were not used in the assessment of the case fatality correlation since the CFR is a ratio of these two variables. In order to derive the list of the top four variables most correlated with both vaccination and case fatality rates together, the ranking order was assessed across both target variables (vaccination and case fatality rates).

2.2.2 Foundational Forecasting Methodologies

Baseline forecasting methodologies were selected based on literature search, model strengths and limitations.

A. Autoregressive Integrated Moving Average (Arima)

ARIMA (Autoregressive Integrated Moving Average) model is selected for its characteristics of being well-suited for forecasting time series data that exhibits trends and seasonality. It is deemed to be effective in forecasting a variety of real-world phenomena, which has good applicability for COVID-19, showing greater flexibility, accuracy, interpretability, and robustness. The parameters of the ARIMA model are defined as follows: p is the lag order, which represents the number of lag observations incorporated in the model, d is the degree of differencing, which denotes the number of times raw observations undergo differencing, and q is

©2024 Great Britain Journals Press

the order of the moving average, which indicates the size of the moving average window [41].

B. Prophet

The Facebook Prophet algorithm is an open-source software developed by Facebook's core Data Science Team. If the time series data has strong seasonal effects, this model works the best. It is a regression model for forecasting, specifically designed to forecast time series data that exhibits trends, seasonality, and coverage for holidays. It is also fast and scalable, and similar to ARIMA, this model is interpretable, robust, flexible, and accurate [42].

C. Long Short-Term Memory (LSTM)

LSTM Model is a neural network model that can learn long-term dependencies in time series data, handle nonstationary and noisy data, as well as leverage additional features. It is also accurate, flexible, and scalable [43, 83].

1) Double Hybrid Forecasting Model: Sarima-Bidirectional LSTM

Review of published literature showcases the use of different forecast models and enhancements in COVID-19 research, demonstrating better accuracy and performance in forecasting by hybrid models. For example, ARIMA-LSTM hybrid model was used to predict future COVID-19 transmissions in China where ARIMA-LSTM model was paralleled by weight of regression coefficient performing better than ARIMA alone [45]; the same group also looked at COVID-19 prediction using data from Germany and Japan and utilized three enhanced hybrid models: PSO-LSTM-ARIMA, MLR-LSTM-ARIMA, and BPNN-LSTM-ARIMA. The research showed that BPNN-LSTM-ARIMA had the best prediction accuracy [46]. Priya and colleagues compared time series forecasting models utilizing ARIMA, Facebook Prophet, Holt-Winters Model, and Hybrid ARIMA-ANN (to take advantage of the unique characteristics of ARIMA and ANN models in linear and nonlinear modeling). The Hybrid model showed better accuracy and root mean square error [47]; Morais looked at forecasting daily Covid-19 cases with a hybrid ARIMA and neural network model to capture the linear and non-linear structures of daily Covid-19 cases (MLP-ARIMA) [48]; and Nawi researched a hybrid ARIMA-SVM model [49]. Borges looked at COVID-19 ICU demand forecasting utilizing Prophet-LSTM approach vs a stand-alone approach in Brazil, confirming better performance of the hybrid model [50], and Long researched an efficient forecasting tool for Monkeypox outbreak in the US using ARIMA, Prophet, Neural Prophet, stacking model, and LSTM models. NeuralProphet achieved the optimal performance [51]. In addition, Guha, in his paper, presented two recurrent neural network-based approaches to predict the daily confirmed COVID-19 cases, daily total positive tests and total individuals vaccinated using LSTM and gated recurrent unit (GRU) [25]; Shastri looked at time series forecasting of Covid-19 using deep learning models: the recurrent neural network based variants of long-short term memory (LSTM) such as Stacked LSTM, Bi-directional LSTM and Convolutional [52]; Devaray utilized ARIMA, LSTM, Stacked LSTM (SLSTM) and Prophet approaches [53]; Zhenyu Li researched convolutional neural network combined with the stacked long-short-term-memory network model (CNN-Stack BiLSTM) [54]. The Stacked LSTM (SLSTM) model was also researched by Maaliw [55] and Ali, who also use the bidirectional enhancement to create a stacked Bi-directional long short-term memory (Stacked Bi-LSTM) network that forecasts COVID-19 more accurately [56]. Sah compared different COVID-19 forecasting models, Prophet, ARIMA, LSTM, and stacked LSTM-GRU models demonstrating better prediction results with the hybrid stacked LSTM-GRU model [57]. Other researchers looked at the Ensemble Empirical Mode Decomposition and Deep Learning creating an EEMD-LSTM hybrid model [58] and EEMD method with the Autoregressive Integrated Moving Average Exogenous inputs (ARIMAX) method, which they called EEMD-ARIMAX [59].

Hybrid models for this research were selected based on the literature search, strengths, and limitations of the individual components for forecasting performance, available enhancements

©2024 Great Britain Journals Press

to address limitations, and for their specific complementary characteristics that land them well for hybrid application. SARIMA-Bidirectional LSTM hybrid model combines the strengths of two powerful forecasting techniques, ARIMA enhanced with a seasonality component (the S) in SARIMA and enhancing the LSTM model to analyze data in both directions (Bidirectional component). This hybrid combines a linear and non-linear model, benefits from forecasting time series data that exhibits trends and seasonality and at the same time, an ability to learn long-term dependencies in time series data, as well as capture both forward and backward dependencies. SARIMA-Bidirectional LSTM complements the strength of each model and is expected to achieve better forecasting accuracy than either model individually [44].

2) Triple Hybrid Forecasting Model: Sarima-Prophet-Bidirectional LSTM

The triple hybrid SARIMA-Prophet-Bidirectional LSTM forecasting model enhances the previously mentioned hybrid model with a Facebook Prophet forecasting model that is specifically designed to forecast time series data that exhibits trends, seasonality, and holidays. The new triple hybrid combines the strengths of all three forecasting techniques with an ability to capture short-, medium-, and long-term dependencies, handle non-stationary and noisy data, and leverage additional features. Due to the complementary nature of the hybrid model components and a better fit for the data being researched, it would be expected that the new models would achieve better forecasting accuracy than either model individually.

3) Accuracy and Performance Assessment

Accuracy and performance assessment was conducted across all the models (foundational and hybrid models) evaluating vaccination and case fatality rates: Mean Absolute Error (MAE), Mean Squared Error (MSE), Root Mean Squared Error (RMSE) and Entropy, relative to the actual data. In addition, the accuracy of the forecasting results of each model was compared with actual historical data from the Our World in Data dataset, specifically, to the actual time needed to reach the vaccination inflection points for each country.

4) Anomaly and Volatility Analyses

Anomaly and Volatility analysis and assessments were conducted across all-time series analysis and forecasting models utilizing Isolation Forest and Generalized Autoregressive Conditional Heteroskedasticity (GARCH) models, both well-studied in this field. These methodologies were selected based on the review of published literature that showcase their good performance as well as being valuable algorithms for anomaly and volatility detection in the context of COVID-19 vaccination forecasting [60]. The results obtained upon performing anomaly and volatility detection were used to select the best performing model for forecasting the time to COVID-19 vaccination inflection point for each country.

A. Isolation Forest

The last part of the research was focused on the assessment of anomaly and volatility detection analysis across the time series analysis models. These analyses were conducted to identify unusual or unexpected patterns in data, to prevent overfitting, improve the accuracy, performance, and reliability of machine learning models and complex systems. It is often used in Systems Engineering to detect unusual activity in system logs, performance bottlenecks in systems, and anomalous patterns in system data and to improve overall reliability, efficiency, and security of complex systems. The first algorithm used in this research is Isolation Forest.

Isolation Forest can detect anomalies in an unsupervised manner. This model is used to compare the accuracy of different forecasting models and considered to be efficient, scalable, and robust to outliers. It works by randomly selecting features and splitting values to create partitions of the data. This process is repeated until isolation of the anomalies. It is particularly well-suited for high-dimensional data, which is the case with COVID-19 vaccination data, which includes features such as vaccination rate, case

©2024 Great Britain Journals Press

fatality rate, population density, and socio-economic factors. It is also relatively insensitive to outliers, which can be a problem for other anomaly detection algorithms. Isolation Forest can be used to detect anomalies in the vaccination and case fatality rates. This can be useful for identifying periods where the vaccination and CFR rate are significantly higher or lower than expected, adjusting, or improving the forecasts for the vaccination inflection point [61].

Isolation Forest measured three parameters: Precision, Recall, and F1-score. Precision measures the proportion of detected anomalies that are actually true anomalies, where high precision (closer to 1) is very accurate in its anomaly detections, with few false positives. A good threshold for Isolation Forest is 0.7 or higher. Recall measures the proportion of true anomalies that are correctly identified by the model, high recall (closer to 1) means the model is sensitive and can capture most anomalies. A good threshold for Isolation Forest is 0.7 or higher. F1-score combines precision and recall into a single metric, balancing their trade-off. A high F1-score (closer to 1) indicates a good balance between precision and recall, suggesting a reliable anomaly detector. Isolation Forest results at 0.7 or higher for all parameters are considered to be good results [61].

B. Generalized Autoregressive Conditional Heteroskedasticity (Garch)

The second algorithm used to compare the accuracy of different forecasting models is the Generalized Autoregressive Conditional Heteroskedasticity (GARCH) model. The GARCH model is a powerful tool employed to capture and model volatility patterns in the residuals. This model considers the conditional variance and accounts for the time-varying volatility and is especially well suited for time-series analysis, which is the case with COVID-19 vaccination and case fatality rate data.

The GARCH model was used to forecast the volatility of the COVID-19 vaccination and CFR rate. This helped to identify periods where the vaccination and CFR rates are likely to increase or decrease more rapidly than expected. If the model detects anomalies, this could indicate that the vaccination and CFR rates are not following the expected patterns [62].

Isolation Forest and GARCH models are both well-suited for anomaly and volatility detection, respectively, in the context of COVID-19 vaccination inflection point forecasting. They are both efficient, important for anomaly and volatility detection in large datasets, and robust to outliers. This can be a problem in COVID-19 vaccination data due to factors such as data entry errors and reporting delays. These models are also flexible, due to ease of adaptation to a variety of different anomaly detection tasks. The GARCH model also has several limitations, such as sensitivity to the choice of parameters, less robust performance for very short time series datasets, and the inability to capture all types of anomalies.

The GARCH model measures three parameters: Volatility Persistence, Relative Importance of ARCH Term, and Relative Importance of GARCH Term. Volatility Persistence represents the degree to which shocks to volatility persist over time, with an acceptable range between 0.7 and 1. Values below 1 are considered acceptable, ensuring stationarity of the volatility process. However, values closer to or exceeding 1, indicate stronger persistence, meaning shocks have longer-lasting impacts on volatility and might suggest issues like integrated volatility or model misspecification. The range that is typical and acceptable for Relative Importance of ARCH Term is 0 to 0.4. Relative Importance of GARCH Term captures the persistence of volatility shocks over time with an acceptable range of 0.3 to 0.9 [62].

1. Vaccination Inflection Point Score

Vaccination Inflection Point score was developed to categorize countries based on their actual time to achieving secondary vaccination inflection point, representing the time of the most significant CFR reduction post vaccination, and therefore, identifying the critical threshold signaling the turnaround in the pandemic. Countries were categorized into three groups

©2024 Great Britain Journals Press

corresponding to scores 1, 2, and 3, with a score of 1 indicating that the country needed the shortest amount of time to reach their secondary vaccination inflection point. This tool can help with the interpretation of changes in the pandemic dynamic, serve as a learning tool for the importance of the contribution of vaccination to achieving faster herd immunity, and improving the overall pandemic risk of countries.

III. RESULTS

3.1 Correlation Analysis Results

The correlation analysis was performed using Ordinary Least Squares Multifactor Regression Methodology. These analyses were performed as aggregate analysis with 14 variables. The correlation was assessed first with the vaccination rate as the target variable, followed by the case fatality rate. The top four variables most correlated with vaccination rate were: *stringency_index, life_expectancy, positive_ rate, and total_deaths*. The top four variables for the case fatality rate were: *stringency_index, aged_65_older, life_expectancy, and positive_ rate*. The top four variables that are the most correlated with both vaccination and case fatality rates together were derived by using the ranking order of variables across both vaccination and case fatality rates. The final ranking order of the four variables was: *stringency_index, aged_ 65_older, life_expectancy, and positive_ rate,* representing the exogeneous variables that were used in the primary and secondary vaccination inflection point forecasting analyses. The stringency index and positive rate were variables representing the PSI index and aged 65 and older and life expectancy represented the PHI index.

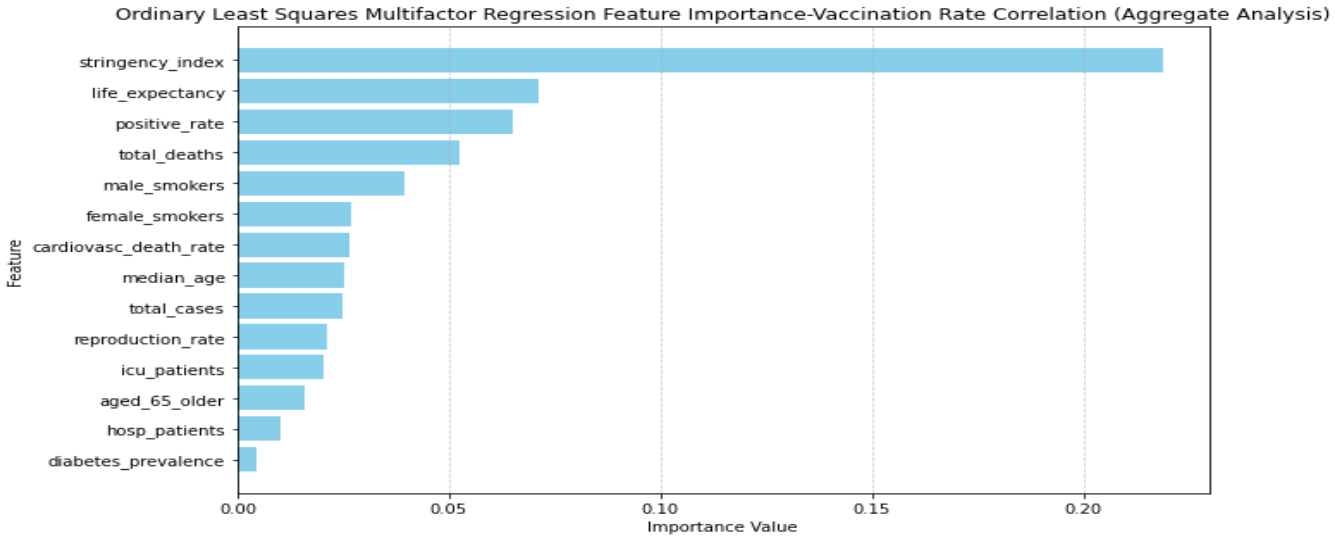

Figure 1: Correlation Analysis for Vaccination Rate (Aggregate Analysis)

©2024 Great Britain Journals Press

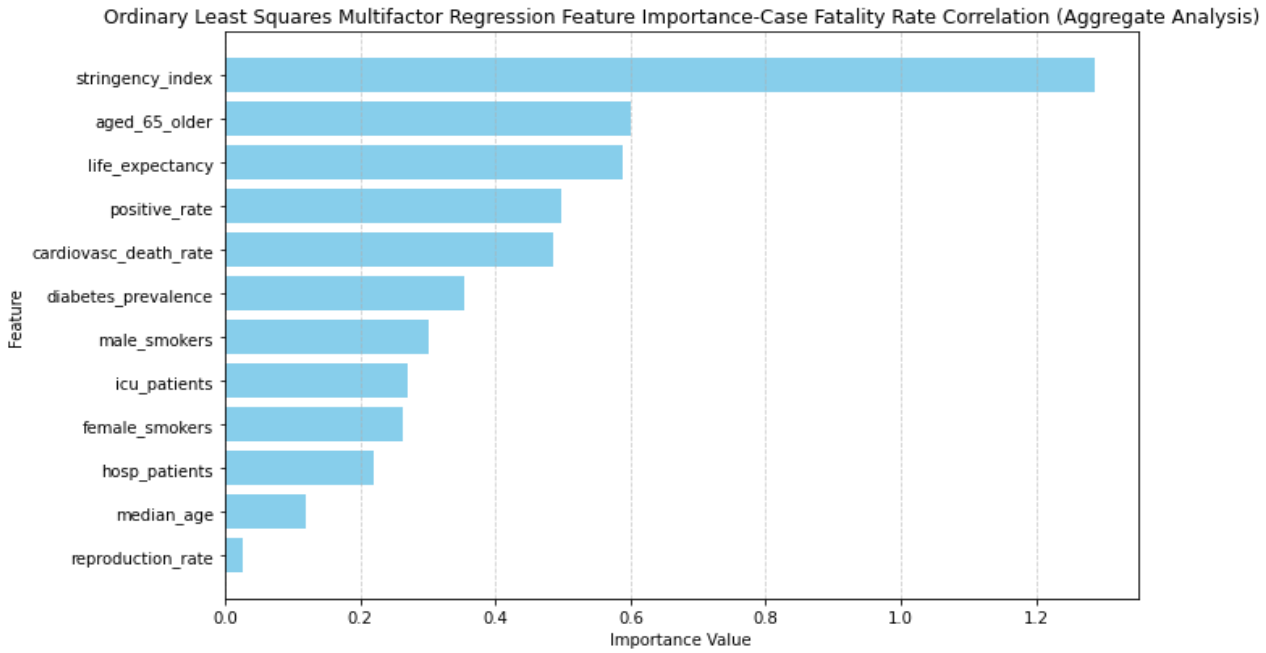

Figure 2: Correlation Analysis for Case Fatality Rate (Aggregate Analysis)

3.2 Forecasting Analysis Results

The summary of the conducted analyses is presented in Table 4, first as an aggregate and then per GDP per capita category (>$50,000, $35,000-$50,000, and <$35,000). Overall, all countries started their vaccination campaigns within the 43 days, starting with Latvia on December 4, 2020, and ending with the UK starting on January 10, 2021. Countries with the higher GDP initiated their vaccination efforts faster than the other countries (15 days vs 26 and 35 days), however, countries with the mid-range GDPs reached the PVIP and SVIP faster than the other two groups, with high and low GDP per capita. PVIP was reached in 37.5 days vs 76 and 131.7 days, and SVIP in 299.2 days vs 336.5 and 380.4 days.

Similar results were observed when median numbers were used, with the mid-range GDP countries again performing better, with the shortest time needed to reach both PVIP (34 days vs 80.5 and 82 days) and SVIP (316 days vs 343.5 and 365 days), and with the highest achieved vaccination rate (74.7% vs 70.6% and 63.3%), for GDP mid-range, high-range, and low-range respectively. Overall, all countries reached an average vaccination rate of 67.8% (mean) and 71.25% (median) at the time they observed the significant CFR drop post-vaccination (SVIP). The highest vaccination rate was achieved in Portugal (89%) and the lowest in Bulgaria (28%).

Analysis of vaccinations by age group in Our World in Data (except for three countries) showed similar distribution by age [20]. The elderly population (60-70, 70-80, and 80+ years of age) achieved the highest vaccination rates in all, but three countries (Latvia, Romania, and Bulgaria), followed by the middle age group (18-24, 25-59). The smallest vaccination rates were observed in the youngest age group (0-17).

The data for the US and UK were not available in the Our World in Data dataset, however, data from official government sites demonstrated the same patterns observed with the rest of the countries [81, 82], supplement Tables S10, S11, and S12. There were no official records available for Serbia at the time of this research. This confirms earlier statements that most countries prioritize elderly and frail populations in their vaccination campaigns. Looking at the countries based on their GDP per capita grouping, the mid-range group on average achieved higher vaccination rates of the elderly population than the countries with higher and lower GDP per capita. These findings support the better performance of the countries in the mid-range

©2024 Great Britain Journals Press

GDP group, demonstrating the importance of prioritizing the needs of the elderly population (age 65 and older and life expectancy) in a pandemic setting. It should be assumed that other factors, such as acceptance and robustness of the vaccination campaign and vaccination mandates imposed by governments played a significant role as well [71].

Table 5 presents the ranking order of the countries based on the time to reach SVIP. The UK observed the SVIP in the shortest amount of time, at 161 days (CFR 3.3%, vaccination rate 63.8%), while Romania reached the same point in 560 days (CFR 2.2%, vaccination rate 41.6%).

Supplemental Tables (Table S1, S2A-B, S3A-B) present all results of all forecasting models, the three foundational (ARIMA, PROPHET, LSTM) and the two hybrid forecasting models (double hybrid: SARIMA-Bidirectional LSTM, and triple hybrid: SARIMA-Prophet-Bidirectional LSTM). The baseline data for each country, as well as the actual historical data from the COVID-19 pandemic are also documented in these supplemental tables.

Table 4: Summary of Results Across 26 Countries

	Aggregate data for 26 countries	Countries with GDP per capita >$50,000	Countries with GDP per capita $35,000-$50,000	Countries with GDP per capita < $35,000
		4 countries (15.4%)	11 countries (42.3%)	11 countries (42.3%)
vaccination start	43 days (Dec 8, 2020 - Jan 10, 2021	15 days (Dec 13 - Dec 28, 2020)	26 days (Dec 8, 2020 - Jan 3, 2021)	35 days (Dec 4, 2020 - Jan 8, 2021)
	mean (range)			
time to reach PVIP*	83.27 days (15-367)	76 days (49-94)	37.5 days (15-75)	131.7 days (16-367)
vaccination rate at PVIP	13.1% (0.1-50)	9.7% (0.9-24.8)	5% (0.4-33.1)	18.6% (1.5-50.1)
time to reach SVIP**	339.31 days (161-560)	336.5 days (296-363)	299.2 days (161-371)	380.4 days (319-560)
vaccination rate at SVIP	67.8% (28-89)	71% (66.4-76.5)	74.2% (63.8-81.8)	60.3% (28-89.1)
	median (range)			
time to reach PVIP	57.5 days (15-367)	80.5 days (49-94)	34 days (15-75)	82 days (16-367)
vaccination rate at PVIP	6.05% (0.1-50)	6.6% (0.9-24.8)	2.4% (0.4-33.1)	9.5% (1.5-50.1)
time to reach SVIP	355.5 days (161-560)	343.5 days (296-363)	316 days (161-371)	365 days (319-560)
vaccination rate at SVIP	71.25% (28-89)	70.6% (66.4-76.5)	74.7% (63.8-81.8)	63.3% (28-89.1)

**PVIP: Primary vaccination inflection point*
***SVIP: Secondary vaccination inflection point*

Table 5: Ranking of the Countries based on the Time to Reach SVIP

Rank	Country	Time (days) to reach SVIP	Vaccination start date	Date SVIP reached	Vaccination rate at SVIP
1	United Kingdom	161 days	Jan 10 2021	Jun 20 2021	63.88%
2	Iceland	201 days	Dec 30 2020	Jul 19 2021	71.64%
3	Denmark	274 days	Dec 8 2020	Sep 8 2021	73.99%
4	Belgium	292 days	Dec 28 2020	Oct 16 2021	74.77%
5	Netherlands	293 days	Jan 8 2021	Oct 28 2021	69.99%
6	Ireland	296 days	Dec 28 2020	Oct 20 2021	76.58%
7	Italy	316 days	Dec 27 2020	Nov 8 2021	79.32%
8	Portugal	319 days	Jan 1 2021	Nov 16 2021	89.10%
9	France	323 days	Dec 27 2020	Nov 15 2021	76.88%
10	Switzerland	329 days	Dec 21 2020	Nov 15 2021	66.42%
11	Finland	333 days	Jan 3 2021	Dec 2 2021	77.16%
12	Spain	337 days	Jan 4 2021	Dec 7 2021	80.84%
13	Cyprus	353 days	Jan 6 2021	Dec 25 2021	71.53%
14	Sweden	358 days	Jan 3 2021	Dec 27 2021	72.39%
15	Luxembourg	358 days	Dec 28 2020	Dec 21 2021	70.99%
16	Serbia	361 days	Jan 8 2021	Jan 4 2022	48.20%
17	Estonia	362 days	Dec 27 2020	Dec 24 2021	63.29%
18	United States	363 days	Dec 13 2020	Dec 11 2021	70.30%

©2024 Great Britain Journals Press

19	Bulgaria	365 days	Dec 29 2020	Dec 29 2021	28.08%
20	Canada	370 days	Dec 14 2020	Dec 19 2021	81.80%
21	Austria	371 days	Dec 27 2020	Jan 2 2022	75.10%
22	Czechia	372 days	Dec 27 2020	Jan 3 2022	65.12%
23	Slovenia	374 days	Dec 27 2020	Jan 5 2022	59.07%
24	Slovakia	386 days	Jan 3 2021	Jan 24 2022	45.73%
25	Latvia	395 days	Dec 4 2020	Jan 3 2022	71.06%
26	Romania	560 days	Dec 27 2020	Jul 10 2022	41.64%

In the dataset used for this research, 65% of countries started their vaccination efforts in December 2020, and 35% started in January 2021. The primary vaccination inflection point representing the first observed reduction in the CFR post vaccination was reached at 83.27 days (mean, range 15-367 days), with 42% of countries seeing the initial impact in less than 50 days, 38.4% in 50-100 days, and 19.2% above 100 days (Figure 3). This reduction was achieved with the initial vaccination rate of 31.1% (mean, range 0.1% to 50%), with 27% of countries reaching the vaccination rate of >25%, 15.3% reaching the rate between 11-25%, and 57.7% reaching the rate of <10% (Figure 4). Finland observed the fastest PVIP in only 15 days (CFR 1.6%, vaccination rate of 1.1%), while Romania had the longest wait to first reduction at 367 days (CFR 3.2%, vaccination rate 27.8%).

The secondary vaccination inflection point (SVIP), representing the most significant reduction in CFR post vaccination, signaling the start of the continuous CFR reduction and turnaround in the pandemic, was reached at 339.31 days (mean, range 161-560 days), with 23.1% of countries observing this impact in less than 300 days, 53.8% from 300-370 days, and 23.1% in more than 370 days (Figure 5). This reduction was achieved with the cumulative vaccination rate of 67.8% (mean, range 8%-89%), with 50% of countries reaching the vaccination rate between 50-75% (Figure 6). Most of the countries reached a significant drop in the CFR in 2021 (73%), out of which 61.5% reached it in the 4th quarter of 2021, 11.5% in the 3rd quarter of 2021, and 27% in early 2022. The highest vaccination rate at this inflection point was achieved in Portugal (89%) on November 16, 2021.

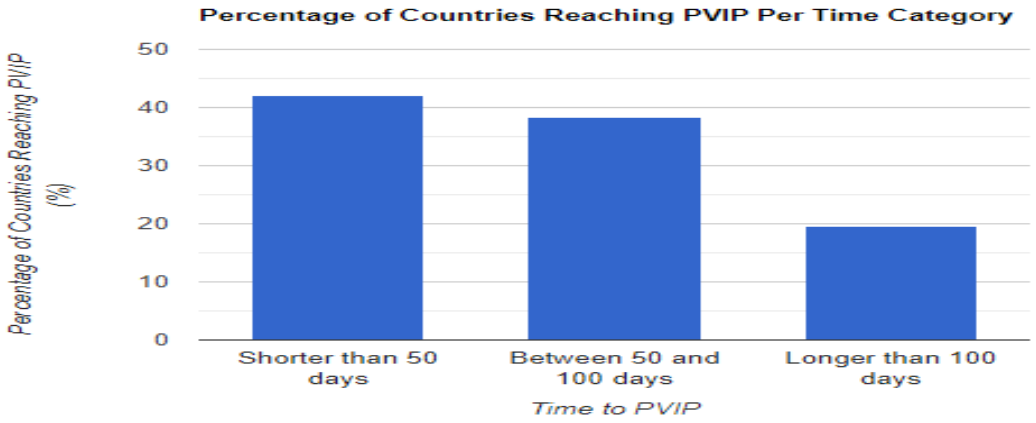

Figure 3: Percentage of Countries Reaching PVIP Per Time Category

©2024 Great Britain Journals Press

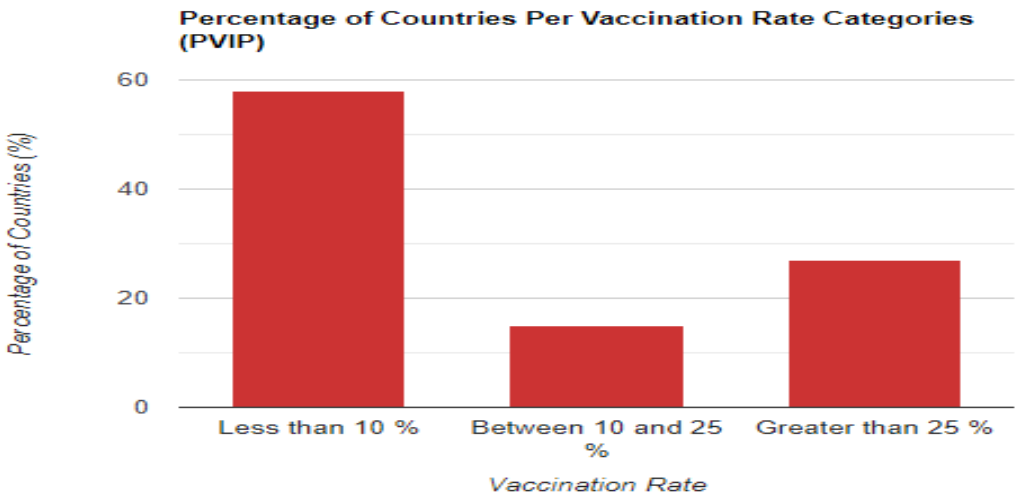

Figure 4: Percentage of Countries Per Vaccination Rate Categories (PVIP)

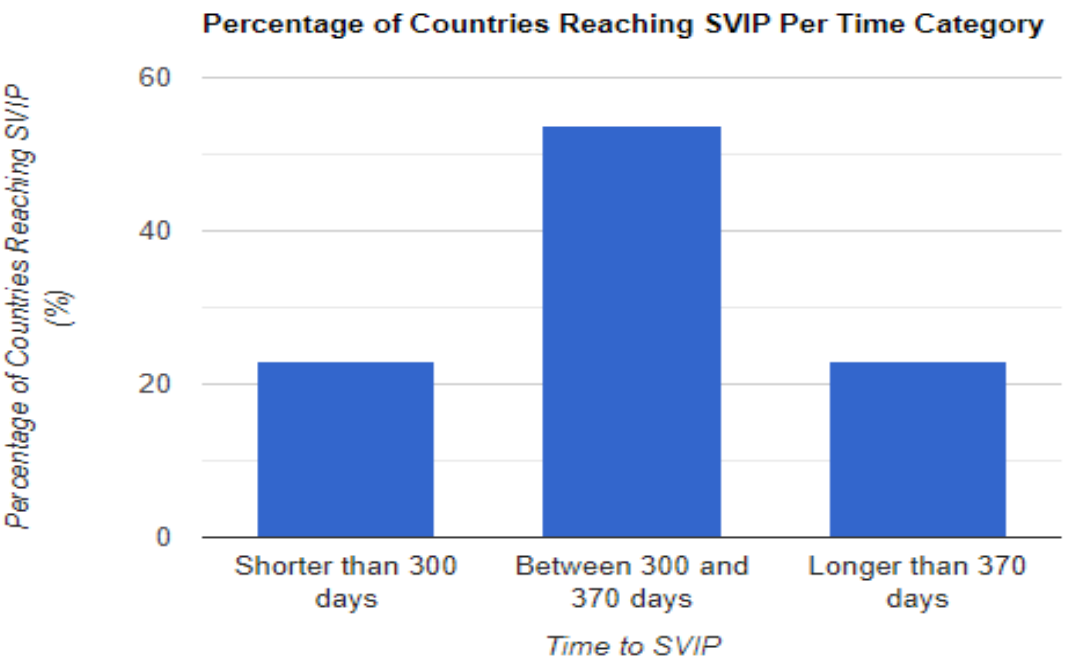

Figure 5: Percentage of Countries Reaching SVIP Per Time Category

©2024 Great Britain Journals Press

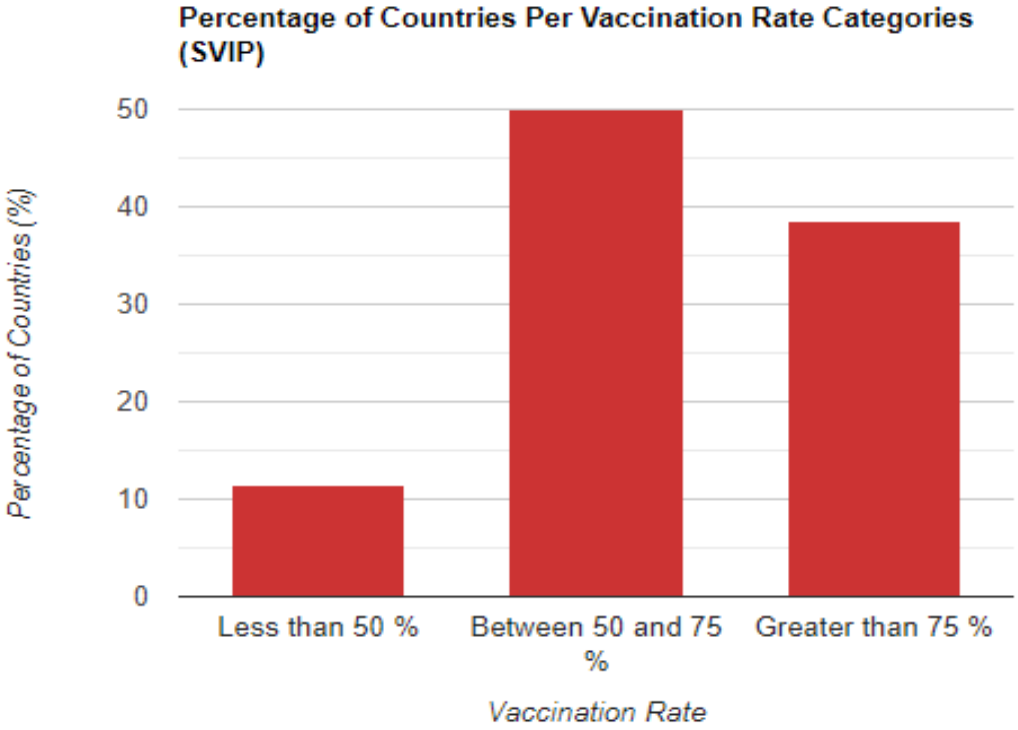

Figure 6: Percentage of Countries Per Vaccination Rate Categories (SVIP)

Overall, at the time of the SVIP, all countries with the exception of three, showed a reduction in the CFRs relative to the CFRs at the beginning of the vaccination. The highest CFR at the time of the SVIP was in Bulgaria (4.1%), followed by the UK (3.32%), and Italy (2.75%). Belgium and Romania had the CFRs that were > 2.0%, and the remaining countries had the CFRs <2.0%. The lowest CFRs were documented in Cyprus (0.42%) and Iceland (0.45%). Bulgaria, Latvia and Slovakia had the CFRs at the SVIP that were higher than the CFR at the vaccination start date, however, all three countries showed a reduction in the CFRs from the PVIP to the SVIP, indicating a positive impact of the vaccination.

3.3 Accuracy and Performance Assessment

Accuracy and performance assessment was conducted across all the models (foundational and hybrid models) evaluating vaccination and case fatality rates: Mean Absolute Error (MAE), Mean Squared Error (MSE), Root Mean Squared Error (RMSE) and Entropy, relative to the actual data. Tables 6-7 showcase the mean and median results for all calculated metrics indicating the superior performance of the triple hybrid model SARIMA-Prophet- Bidirectional LSTM.

3.4 Anomaly and Volatility Analysis Results

Anomaly and Volatility analysis and assessments were conducted across all time-series-analysis and forecasting models utilizing Isolation Forest and Generalized Autoregressive Conditional Heteroskedasticity (GARCH) models. In the Isolation Forest model, precision, recall, and F1-score values above 0.7 indicate good performance. As presented in Tables 8 and 9, both mean and median values were above 0.7, indicating that all forecasting methodologies are performing well and accurately, validating performance of all forecasting models. In the GARCH model, Volatility Performance between 0.7-1, Relative Importance ARCH Term between 0-0.4, and Relative Importance of GARCH Term between 0.3 - 0.9, indicate good performance.

Tables 10 and 11 presented that both mean and median values are within typical and acceptable ranges for all three indicators, suggesting that all forecasting methodologies are performing well

©2024 Great Britain Journals Press

and accurately, validating performance of all forecasting models.

Table 6: Vaccination Rate Forecasting Metrics

Metric	Country	ARIMA	Prophet	LSTM	SARIMA-Bidirectional LSTM Double Hybrid	SARIMA-Prophet-Bidirectional LSTM Triple Hybrid
Mean Absolute Error (MAE)	Mean:	0.273440346	0.269496	0.246185113	0.197624417	0.04688918
	Median:	0.2801870395	0.264832	0.190341017	0.091510384	0.008675794
Mean Squared Error (MSE)	Mean:	0.147081	0.185847	0.184565242	0.12681021	0.022887863
	Median:	0.104444003	0.161433	0.076258508	0.0723305005	0.0000841
Root Mean Squared Error (RMSE)	Mean:	0.333789454	0.321616	0.298212928	0.210208282	0.053976834
	Median:	0.327567389	0.322921	0.31088121	0.187344609	0.009161993
Entropy	Mean:	0.197672158	0.172476	0.093079818	0.111602614	0.10330825
	Median:	0.157320015	0.181081	0.02683001	0.0245333975	0.02033074

Table 7: Case Fatality Rate Forecasting Metrics

Metric	Country	ARIMA	Prophet	LSTM	SARIMA-Bidirectional LSTM Double Hybrid	SARIMA-Prophet-Bidirectional LSTM Triple Hybrid
Mean Absolute Error (MAE)	Mean:	0.423921554	0.240282	0.243192654	0.240685426	0.059632661461538
	Median:	0.271977023	0.211509	0.206126957	0.163648243	0.033323647
Mean Squared Error (MSE)	Mean:	0.430524623	0.225626	0.165527034	0.147206818	0.008526044
	Median:	0.106648124	0.213829	0.0766076	0.062206746	0.001274246
Root Mean Squared Error (RMSE)	Mean:	0.500104124	0.275272	0.271744391	0.303519309	0.063672814
	Median:	0.326569872	0.273384	0.2643577545	0.258133644	0.037807365
Entropy	Mean:	0.199711931	0.19532	0.083534021	0.042455902	0.034290933
	Median:	0.217112239	0.193974	0.0327498355	0.009875701	0.0095256035

Table 8: Isolation Forest: Anomaly Detection for Vaccination Rate

Isolation Forest-Anomaly Detection Results (Vaccination Rate Forecasting)			
Country	Precision	Recall	F1 Score
United States	0.957	0.739	0.8007
Austria	0.9117	0.8159	0.9772
Serbia	0.7469	0.9786	0.8216
Canada	0.9969	0.8121	0.7191
Belgium	0.7331	0.9941	0.8332
Bulgaria	0.7079	0.8811	0.7067
Czechia	0.9397	0.8437	0.7551
Denmark	0.9514	0.8081	0.7378
Estonia	0.7033	0.9454	0.9022
Finland	0.8061	0.8942	0.7076
France	0.7569	0.9209	0.7978
Iceland	0.7113	0.7931	0.7926

©2024 Great Britain Journals Press

Ireland	0.8135	0.8411	0.7034
Italy	0.7614	0.8705	0.8592
Latvia	0.7289	0.8352	0.786
Luxembourg	0.7961	0.7753	0.8538
Netherlands	0.7212	0.7771	0.9907
Portugal	0.8517	0.9156	0.8336
Romania	0.9704	0.7877	0.7137
Slovakia	0.7616	0.904	0.9632
Slovenia	0.8737	0.7902	0.7825
Spain	0.8443	0.868	0.9747
Sweden	0.8305	0.7749	0.973
Switzerland	0.9417	0.7178	0.7002
United Kingdom	0.915	0.8303	0.8497
Cyprus	0.8723	0.9244	0.7774
Mean:	0.8309	0.8476	0.8197
Median:	0.822	0.8382	0.7993

Table 9: Isolation Forest: Anomaly Detection for Case Fatality Rate

Isolation Forest-Anomaly Detection Results (Case Fatality Rate Forecasting)			
Country	Precision	Recall	F1 Score
United States	0.8875	0.7503	0.857
Austria	0.926	0.7301	0.8791
Serbia	0.9929	0.8165	0.8089
Canada	0.797	0.9341	0.7126
Belgium	0.9709	0.7439	0.8172
Bulgaria	0.7817	0.9051	0.9914
Czechia	0.9896	0.9788	0.7884
Denmark	0.8408	0.9157	0.7323
Estonia	0.8036	0.8121	0.8191
Finland	0.9038	0.8677	0.8376
France	0.8538	0.9745	0.7094
Iceland	0.9427	0.9422	0.9627
Ireland	0.8745	0.7822	0.769
Italy	0.9391	0.907	0.9095
Latvia	0.9576	0.9067	0.7518
Luxembourg	0.8179	0.7254	0.996
Netherlands	0.747	0.8287	0.8018
Portugal	0.7876	0.918	0.8372
Romania	0.8899	0.752	0.7196
Slovakia	0.9771	0.9905	0.9455
Slovenia	0.921	0.9264	0.7131
Spain	0.7366	0.9903	0.7089
Sweden	0.7791	0.9988	0.8754
Switzerland	0.8953	0.7339	0.7227
United Kingdom	0.7583	0.7996	0.8798
Cyprus	0.9981	0.7523	0.7227
Mean:	0.8757	0.8609	0.818
Median:	0.8887	0.8864	0.8131

©2024 Great Britain Journals Press

Table 10: GARCH: Volatility Detection for Vaccination Rate

GARCH-Volatility Detection Results (Vaccination Rate Forecasting)			
Country	Volatility Persistence	Relative Importance of ARCH Term	Relative Importance of GARCH Term
United States	0.8282	0.2504	0.852
Austria	0.7063	0.1871	0.6404
Serbia	0.8652	0.3208	0.8104
Canada	0.8244	0.026	0.8845
Belgium	0.714	0.0902	0.4021
Bulgaria	0.7451	0.1982	0.3019
Czechia	0.8241	0.1447	0.5649
Denmark	0.7312	0.0737	0.3504
Estonia	0.8505	0.069	0.6422
Finland	0.7691	0.2895	0.4325
France	0.7524	0.1025	0.4491
Iceland	0.8171	0.063	0.63
Ireland	0.7553	0.0197	0.8928
Italy	0.7087	0.2291	0.3192
Latvia	0.7707	0.1126	0.7709
Luxembourg	0.7432	0.1899	0.4111
Netherlands	0.7774	0.0394	0.5235
Portugal	0.75	0.0377	0.7828
Romania	0.8011	0.0934	0.3291
Slovakia	0.7535	0.0961	0.6822
Slovenia	0.7218	0.2805	0.3256
Spain	0.7524	0.3012	0.4183
Sweden	0.7409	0.1956	0.8429
Switzerland	0.7716	0.1138	0.4444
United Kingdom	0.8017	0.0097	0.7839
Cyprus	0.7527	0.3958	0.6299
Mean:	0.7703	0.1511	0.5814
Median:	0.7544	0.1132	0.5974

Table 11: GARCH: Volatility Detection for Case Fatality Rate

GARCH-Volatility Detection Results (Case Fatality Rate Forecasting)			
Country	Volatility Persistence	Relative Importance of ARCH Term	Relative Importance of GARCH Term
United States	0.7459	0.055	0.5546
Austria	0.7973	0.295	0.6177
Serbia	0.7003	0.1989	0.4148
Canada	0.7955	0.0907	0.5704
Belgium	0.837	0.1485	0.5992
Bulgaria	0.7926	0.1119	0.4248
Czechia	0.8525	0.2854	0.815
Denmark	0.8412	0.0142	0.5472
Estonia	0.7639	0.2216	0.5843
Finland	0.7499	0.1335	0.3002
France	0.8511	0.2473	0.8511

©2024 Great Britain Journals Press

Iceland	0.7068	0.2207	0.3123
Ireland	0.7093	0.3246	0.6198
Italy	0.8087	0.0608	0.8999
Latvia	0.7109	0.0828	0.3823
Luxembourg	0.8555	0.3423	0.6214
Netherlands	0.8424	0.1738	0.3842
Portugal	0.809	0.216	0.7016
Romania	0.7274	0.1294	0.3674
Slovakia	0.8668	0.1789	0.4596
Slovenia	0.846	0.3062	0.7968
Spain	0.8044	0.3552	0.3832
Sweden	0.7273	0.3213	0.602
Switzerland	0.7126	0.3562	0.6668
United Kingdom	0.8057	0.3061	0.5669
Cyprus	0.7119	0.356	0.3568
Mean:	0.7835	0.2128	0.5539
Median:	0.7964	0.2184	0.5687

3.5 Vaccination Inflection Point Score Results

Vaccination Inflection Point score was developed to categorize countries based on their actual time to achieving secondary vaccination inflection point, representing the time of the most significant CFR reduction post vaccination. Countries were categorized into three groups with scores 1, 2, and 3, with a score of 1 indicating the country needing the shortest amount of time to reach their secondary vaccination inflection point.

Table 12 and Figure 7 present the distribution of countries per VIP score. This data indicates that the majority of countries (53.8%) reached the SVIP between 300-370 days (score 2). While there is a broad range in the achieved vaccination rates across different countries, the median values show numerically higher vaccination rates in the countries with the shortest time to SVIP, score 1 (72.75%), over score 2 (71.75%), and score 3 countries (62%).

Table 12: Distribution of Countries per SVIP Score

SVIP Score	Days to SVIP	Distribution of Countries	% of Countries	Vaccination Rate Range
1	< 300	Denmark, Belgium, Iceland, Ireland, Netherlands, UK (6)	23.10%	63.8-76%. median 72.75%
2	300-370	US, Serbia, Canada, Bulgaria, Estonia, Finland, France, Italy, Luxemburg, Portugal, Spain, Sweden, Switzerland, Cyprus (14)	53.80%	28-89%. median 71.75%
3	>370	Austria, Czechia, Latvia, Romania, Slovakia, Slovenia (6)	23.10%	41.6-75.1%. median 62%

©2024 Great Britain Journals Press

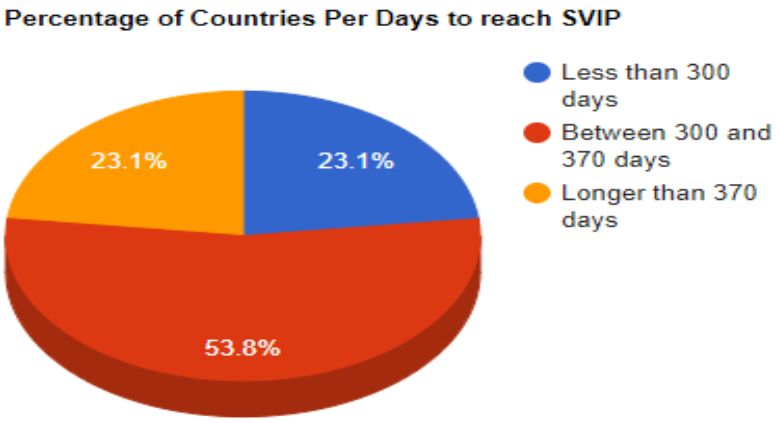

Figure 7: Percentage of Countries per days to reach SVIP

IV. DISCUSSION

The significant negative impact of the COVID-19 pandemic highlighted the need for better preparedness of countries and more sophisticated tools to guide the efforts of public health officials and governments. A wealth of data collected during the COVID-19 pandemic and advanced AI methodologies are allowing researchers to expand our collective knowledge and guide these efforts. This paper builds on the research that highlighted the importance of the non-pandemic predictors in the assessment of pandemic risk [35]. It expands into pandemic predictors and utilizes COVID-19 actual data to refine forecasting tools for future outbreaks. This research was conducted to identify the vaccination inflection points and the time needed to reach the critical cumulative vaccination rate thresholds to observe continuous decrease of the case fatality rates. It was conducted both at the aggregate and country levels, signaling the turnaround point in the pandemic.

The analysis of the actual COVID-19 historical data shows that all of the countries, in aggregate, had the highest fatality rates during the first year of the pandemic. Implementation of the pandemic measures, such as masks, social distancing, school and workplace lockdowns, and testing, had a significant impact on the initial lowering of the case fatality rates. With the introduction of first vaccines in December of 2020, the case fatality rates decreased even further, often reflected as steep downward slopes in graphs. Several types of vaccines were available at the time of the initial vaccination: genetically engineered messenger RNA, viral vector vaccines, and protein subunit vaccine [63]. The initial vaccinations were delivered as single dose or 2-dose vaccines, followed by single dose booster vaccines to improve already established immunity. The first booster dose was approved for use in the third quarter of 2021, followed by two in 2022, and one in 2023, for a total of four booster doses, in developed countries [16]. As of today, there are approximately 40 different vaccines that were approved by regulatory agencies for full emergency use authorization across different countries [36].

In the dataset used for this research, 65% of countries started their vaccination efforts in December 2020, and 35% started in January 2021. On average, looking at the mean values, the time to reach the primary vaccination inflection point, the first reduction in the case fatality rate post vaccination, was on day 83.27 at the vaccination rate of 31%. The secondary vaccination inflection point, representing the most significant and continuous CFR drop post vaccination, was reached at day 339.31 at the average vaccination rate of 67.8%. All four parameters had a very large range, signalizing the presence of outliers. Median values indicate a shorter time to reach the PVIP (57.5 days), lower vaccination rate at PVIP (6.05%), a longer time to reach the SVIP (355.5 days) and a higher overall vaccination rate at SVIP (71.25%). Countries with the mid-level GDP per capita implemented their

©2024 Great Britain Journals Press

vaccination campaigns in the most successful way, securing the shortest times to reach both vaccination inflection points looking at both mean and median values. Regarding the individual countries, Finland was the first country to reach the PVIP in only 15 days with the vaccination rate of 1.1%, while Romania had the longest wait, reaching the PVIP in 367 days with a vaccination rate of 27.8%. The UK observed the most significant CFR reduction (SVIP) in the shortest amount of time in 161 days (vaccination rate 63.8%), while Romania reached the same point in 560 days (vaccination rate 41.6%). The highest vaccination rate at SVIP was achieved in Portugal (89%) on November 16, 2021. The SVIP score was developed to categorize countries based on their actual time to achieving secondary vaccination inflection point. The majority of countries reached the SVIP between 300-370 days, while the countries with the lowest score (shorter time to SVIP) had the highest median vaccination rates. This tool can help with the interpretation of changes in the dynamics of the pandemic.

Looking specifically at the US (Supplement Table S1), PVIP was achieved after 94 days post-vaccination, at a vaccination rate of 24.8% and CFR of 1.8%. The most significant reduction in CFR (SVIP) was achieved at 363 days after the vaccination start date or 269 days after the PVIP date. The vaccination threshold at the SVIP was 70.3% with the CFR of 1.59%. The CFR reduced from 1.82 at the time of start of vaccination to 1.59 at the time when it reached the SVIP. In most countries, including the US, priority for COVID-19 vaccination was given to health care workers, residents and personnel of long-term care facilities, elderly patients, and patients with certain comorbidities. The US was grouped with Switzerland, Luxembourg, and Ireland in the high GDP per capita countries (>$50,000). Within this group, the US was the first country to start the vaccination campaign; however, it needed a longer time than other countries to reach both vaccination inflection points. These results were most likely influenced by the impact of widespread anti-vaccine campaigns, scientific misinformation, and overall lack of readiness of certain parts of the population to support government efforts [21, 22, 23].

It is important to recognize that the impact of vaccination is dependent on many factors, such as speed of implementation of the campaign, availability of vaccines, acceptance of the vaccine by the targeted population, and others. The direct impact of vaccination at the population level will often lag and the data may show some initial misalignment that can be explained. For example, the most significant reduction in CFR in the US was observed in December 2021, signaling the turnaround of the pandemic in the US, with the steady decline of the ratio of total infections and death cases. However, in the next few months in 2022 there was a significant increase in new infections and deaths [20]. While the vaccination rate in the US at that time was reaching 70%, it can be assumed that the increase in new cases was caused by several factors, such as the delay in immunity development post vaccination, breakthrough infections, lack of booster vaccination, higher vulnerability of the unvaccinated population, relaxation of pandemic measures and, most significantly, the emergence of new variants with limited immunity coverage from existing vaccines (e.g., omicron variant BA.2.86 that emerged in Nov of 2021).

To understand the findings and applications of this research, it is important to examine the potential variables that may have influenced the results. This research indicates that there are four most important factors that influence the vaccination, and the case fatality rates in any country. Two are non-pandemic variables (not immediately influenced by the pandemic): percentage of people in the population who are 65 years of age or older, and the life expectancy of the population. An additional two variables are pandemic variables: percentage of people who had a confirmed COVID-19 infection with testing, and the level and scope of the pandemic measures that were implemented. The final ranking order of importance of the four variables was: *stringency_index*, *aged_65_older*, *life_expectancy*, and *positive_rate*. It would be expected that the same factors would be the most important in a potential new pandemic as well,

©2024 Great Britain Journals Press

due to the increased vulnerability of the elderly and sick patient populations to any infectious disease, and the importance of the infection transmission rates and the speed of implementation of response measures. Simply put, if the vaccines were available at the outbreak of COVID-19 and campaigns were implemented fast in targeted populations, the world would not have a pandemic. This is critical learning highlighting the need to take care of the most vulnerable parts of the populations and implementing appropriate procedures for testing, vaccination, and other public health measures.

This research may have been influenced by the inherited challenges of the vaccination process. Published literature highlights the challenges introduced by the disparity in the distribution of COVID-19 vaccines, where the majority of the vaccines were initially delivered to high – and upper middle-income countries vs lower-income countries [64]. This was evident by the differences in times to first vaccination inflection point, demonstrating that lower-income countries had a higher case fatality rate and needed a longer time to observe the CFR reduction as a result of vaccinations, than the higher-income countries. Lack of availability of sufficient doses of vaccines, less organized execution of vaccine campaigns, including the order of vaccination (elderly and immunocompromised population) may have also influenced the results across countries. In addition, factors affecting vaccination acceptance, confidence in safety and efficacy and the risk of side effects, preference for natural immunity, scientifically sounding misinformation, as well as different cultures and political systems, also played a role in the observed vaccination patterns, spread of infection, and mortality of COVID-19 [65, 66, 67, 68, 69, 70].

All foundational forecasting methodologies utilized in this research (ARIMA, Prophet, and LSTM) showed good accuracy and precision, with only small numerical differences in results, relative to the actual values. They performed well and continue to be a true foundational platform for time series forecasting. Utilization of enhancement features to improve limitations of foundational models is already an established approach, and customizing enhancement based on specificities of data allows for more robust analyses. Combining models into hybrids of foundational or foundational with enhancement models is a newer approach requiring validation. The two hybrid forecasting models (double hybrid: SARIMA-Bidirectional LSTM, and triple hybrid: SARIMA-Prophet- Bidirectional LSTM) utilized in this research are both novel models and their validation was conducted by comparing them to foundational models alone, to each other, and to the actual historical data. They both performed well with high accuracy and precision, and better than the foundational models.

However, the performance and accuracy of the triple hybrid SARIMA- Prophet-Bidirectional LSTM model was superior to other models. In addition, the anomaly and volatility detection analyses, conducted using Isolation Forest and GARCH models, validated performance of all forecasting methodologies, reporting all indicators within the typical and acceptable ranges. In summary, all foundational and hybrid models used for forecasting showed comparable results at the primary and secondary vaccination inflection timepoints and performed with high accuracy relative to the actual data. The best performance was observed with the novel triple hybrid SARIMA-Prophet-Bidirectional LSTM, indicating that hybrid models, combining models with enhanced capabilities, can result in higher accuracy and greater sophistication in analysis. Ability to predict the vaccination inflection point and measure its immediate, as well as the most pronounced impacts, allows for a deeper understanding of the dynamics between the vaccination and case fatality rates. In addition, it is important to remember that the data for this research was trained based on the specificities of the COVID-19 pandemic. For the use of these forecasting models for future pandemics, they may need to be re-trained with the data specific to the new pandemic.

The results of this research can guide countries in the assessment of the pandemic risk and inform public health policy makers in creating measures to minimize the impact of any potential infectious

©2024 Great Britain Journals Press

disease pandemic on the people, environment, and socio-economic systems. It is determined that countries can achieve a maximum vaccination rate of 70% with milder measures, and that 90% can be reached only with strict mandates imposed by governments [71]. This highlights the need to plan, organize and execute efficient vaccination campaigns, and improve surveillance and monitoring to substantially reduce morbidity and mortality and avoidance of breakdown of health care systems in countries to control potential new pandemics [72, 73, 74, 75, 76, 77, 78, 79, 80].

V. CONCLUSION AND FUTURE RESEARCH

In conclusion, the research conducted in this paper will add to the knowledge base in the areas of machine and deep learning, and public health. It demonstrates that the novel hybrid time series forecasting models, combining foundational models with enhanced features, provides better performance and higher accuracy over traditional foundational models. The performance and accuracy of the triple hybrid SARIMA-Prophet-Bidirectional LSTM model was superior to other models and was successfully validated with anomaly and volatility detection analyses. In addition, it shows that 42% of countries had seen an immediate effect of vaccination in <50 days, and 23.1% of countries reached the most pronounced impact in <300 days, suggesting the need for improvements. Applying advanced AI methodologies to forecast time to country specific vaccination inflection points, and assessing the vaccination rates relative to the case fatality rates, can provide another useful tool to guide countries in their pandemic risk preparedness.

This paper has several limitations that can be utilized to guide further research, such as: (1) inherited limitations and variabilities of the vaccination campaigns in different countries (supply, distribution, new variants reducing the effectiveness of current vaccines; (2) differences in the health system infrastructures, speed and scope of implementation of other pandemic measures across countries; (3) limitations of the Our Word In Data dataset (e.g., size, completeness, and accuracy, due to the voluntary data reporting and possible underreporting of infection and death cases; and (4) selection of machine and deep learning methodologies and enhancements.

Conflict of Interest

Marco M. Vlajnic and Steven J. Simske declare that there is no conflict of interest.

REFERENCES

1. Muttappallymyalil et al (2022) Vaccination Rate and Incidence of COVID-19 and Case Fatality Rate (CFR): A Correlational Study Using Data From 2019 to 2021. 22 Aug 20. doi: 10.7759/cureus.28210.
2. World Health Organization. (2023). *WHO coronavirus (COVID-19) dashboard*. World Health Organization. Retrieved April 27, 2023, from https://covid19.who.int/.
3. Hospital for Special Surgery. (2021, November 5). *HSS News*. HSS Study Identifies Risk Factor for "Long-Haul" COVID-19 in People with Rheumatic Diseases. Retrieved April 27, 2023, from https://news.hss.edu/hss-study-identifies-risk-factors-for-long-haul-covid-19-in-people-with rheumatic-diseases/.
4. American Hospital Association. (2021). *American Hospital Association homepage: AHA*. American Hospital Association. Retrieved April 27, 2023, from https://www.aha.org/.
5. "Score Data Collection Tool - Who." *World Health Organization*, World Health Organization, from www.who.int/data/data-collection-tools/score# Accessed 8 Oct. 2023.
6. Magazzino C, Mele M and Schneider N (2020) The relationship between air pollution and COVID-19-related deaths: an application to three French cities. Applied Energy 279, 115835.
7. Huang J et al. (2021) The oscillation-outbreaks characteristic of the COVID-19 pandemic. National Science Review 8. https://doi.org/10.1093/nsr/nwa b100.
8. Coccia M. (2021). Effects of the spread of COVID-19 on public health of polluted cities: results of the first wave for explaining the

©2024 Great Britain Journals Press

déjà vu in the second wave of COVID-19 pandemic and epidemics of future vital agents. *Environmental science and pollution research international*, *28*(15), 19147–19154. https://doi.org/10.1007/s11356-020-11662-7.
9. Coccia, M. Pandemic Prevention: Lessons from COVID-19. *Encyclopedia* 2021, *1*, 433-444. https://doi.org/10.3390/encyclopedia1020036.
10. Coccia M. (2021). The impact of first and second wave of the COVID-19 pandemic in society: comparative analysis to support control measures to cope with negative effects of future infectious diseases. *Environmental research*, *197*, 111099. https://doi.org/10.1016/j.envres.2021.111099.
11. Coccia M. (2022). COVID-19 pandemic over 2020 (withlockdowns) and 2021 (with vaccinations): similar effects for seasonality and environmental factors. *Environmental research*, *208*, 112711. https://doi.org/10.1016/j.envres.2022.112711.
12. Coccia M. (2022). Optimal levels of vaccination to reduce COVID-19 infected individuals and deaths: A global analysis. *Environmental research*, *204*(Pt C), 112314. https://doi.org/10.1016/j.envres.2021.112314.
13. Coccia M. (2022). Preparedness of countries to face COVID-19 pandemic crisis: Strategic positioning and factors supporting effective strategies of prevention of pandemic threats. *Environmental research*, *203*, 1116 78. https://doi.org/10.1016/j.envres.2021.111678.
14. Aldila D et al. (2021) Impact of early detection and vaccinat strategy in COVID-19 eradication program in Jakarta, Indonesia. BMC Research Notes 14, 132.
15. Fontanet and Cauchemez (2020) COVID-19 herd immunity: where are we? Nat Rev Immunol 2020 Oct;20(10):583-584.doi: 10.1038/s41577-020-00451-5.
16. Centers for Disease Control and Prevention. (2023, December 7). *Use of updated COVID-19 vaccines 2023–2024 formula for persons aged ≥6 months: Recommendations of the Advisory Committee on Immunization Practices - United States, September 2023*. Centers for Disease Control and Prevention. https://www.cdc.gov/mmwr/volumes/72/wr/mm7242e1.htm.
17. Magazzino, C., Mele, M., & Coccia, M. (2022). A machine learning algorithm to analyse the effects of vaccination on COVID-19 mortality. *Epidemiology and infection*, *150*, e168. https://doi.org/10.1017/S0950268822001418.
18. R. Jeffrey Melton, Robert C. Sinclair (2021) COVID-19 Infection Rates Are Related to Population Rates of Vaccination: A Response to Subramanian and Kumar. https://www.researchgate.net/publication/355929758.
19. Chen Y. T. (2023). Effect of vaccination patterns and vaccination rates on the spread and mortality of the COVID-19 pandemic. *Health policy and technology*, *12*(1), 100699. https://doi.org/10.1016/j.hlpt.2022.100699.
20. E. Mathieu, H. Ritchie, L. Rodés-Guirao, C. Appel, C. Giattino, J. Hasell, B. Macdonald, S. Dattani, D. Beltekian, E. Ortiz-Ospina, and M. Roser. (2020). *Coronavirus Pandemic (COVID-19)*. [Online]. Available: https://ourworldindata.org/coronavirus.
21. Kwok, S. W. H., Vadde, S. K., & Wang, G. (2021). Tweet Topics and Sentiments Relating to COVID-19 Vaccination Among Australian Twitter Users: Machine Learning Analysis. *Journal of medical Internet research*, *23*(5), e26953. https://doi.org/10.2196/26953.
22. Lincoln, T. M., Schlier, B., Strakeljahn, F., Gaudiano, B. A., So, S. H., Kingston, J., Morris, E. M. J., & Ellett, L. (2022). Taking a machine learning approach to optimize prediction of vaccine hesitancy in high income countries. *Scientific reports*, *12*(1), 2055. https://doi.org/10.1038/s41598-022-05915-3.
23. Liew, T. M., & Lee, C. S. (2021). Examining the Utility of Social Media in COVID-19 Vaccination: Unsupervised Learning of 672,133 Twitter Posts. *JMIR public health and surveillance*, *7*(11), e29789. https://doi.org/10.2196/29789.
24. Kir et al (2022) Augmented Artificial Neural Network Model for the COVID-19 Mortality Prediction: Preliminary Analysis of

©2024 Great Britain Journals Press

Vaccination in Turkey. DOI: 10.35377/saucis.05.01.999373.
25. Guha, S., Kodipalli, A. (2023). Deep Learning Sequence Models for Forecasting COVID-19 Spread and Vaccinations. In: Tistarelli, M., Dubey, S.R., Singh, S.K., Jiang, X. (eds) Computer Vision and Machine Intelligence. Lecture Notes in Networks and Systems, vol 586. Springer, Singapore. https://doi.org/10.1007/978-981-19-7867-8_29.
26. Noroozi-Ghaleini, E., & Shaibani, M. J. (2023). Investigating the effect of vaccinated population on the COVID-19 prediction using FA and ABC-based feed-forward neural networks. *Heliyon*, *9*(2), e13672. https://doi.org/10.1016/j.heliyon.2023.e13672.
27. Rashed, E. A., Kodera, S., & Hirata, A. (2022). COVID-19 forecasting using new viral variants and vaccination effectiveness models. *Computers in biology and medicine*, *149*, 105986. https://doi.org/10.1016/j.compbiomed.2022.105986.
28. Xue, J., Chen, J., Hu, R., Chen, C., Zheng, C., Su, Y., & Zhu, T. (2020). Twitter Discussions and Emotions About the COVID-19 Pandemic: Machine Learning Approach. *Journal of medical Internet research*, *22*(11), e20550. https://doi.org/10.2196/20550.
29. Cresswell, K., Tahir, A., Sheikh, Z., Hussain, Z., Domínguez Hernández, A., Harrison, E., Williams, R., Sheikh, A., & Hussain, A. (2021). Understanding Public Perceptions of COVID-19 Contact Tracing Apps: Artificial Intelligence-Enabled Social Media Analysis. *Journal of medical Internet research*, *23*(5), e26618. https://doi.org/ 10.2196/26618.
30. Hussain, A., Tahir, A., Hussain, Z., Sheikh, Z., Gogate, M., Dashtipour, K., Ali, A., & Sheikh, A. (2021). Artificial Intelligence-Enabled Analysis of Public Attitudes on Facebook and Twitter Toward COVID-19 Vaccines in the United Kingdom and the United States: Observational Study. *Journal of medical Internet research*, *23*(4), e26627. https://doi.org/10.2196/26627
31. Cheng, C., Jiang, W. M., Fan, B., Cheng, Y. C., Hsu, Y. T., Wu, H. Y., Chang, H. H., & Tsou, H. H. (2023). Real-time forecasting of COVID-19 spread according to protective behavior and vaccination: autoregressive integrated moving average models. *BMC public health*, *23*(1), 1500. https://doi.org/10.1186/s12889-023-16419-8.
32. Dhamodharavadhani, S., & Rathipriya, R. (2023). Vaccine rate forecast for COVID-19 in Africa using hybrid forecasting models. *African health sciences*, *23*(1), 93–103. https://doi.org/10.4314/ahs.v23i1.11.
33. Kumar, R., Gupta, M., Agarwal, A., Mukherjee, A., & Islam, S. M. N. (2023). Epidemic efficacy of Covid-19 vaccination against Omicron: An innovative approach using enhanced residual recurrent neural network. *PloS one*, *18*(3), e0280026. https://doi.org/10.1371/journal.pone.0280026.
34. Liu, Longjian. (2018). Biostatistical Basis of Inference in Heart Failure Study. 10.1016/B978-0-323-48558-6.00004-9.
35. M. M. Vlajnic and S. J. Simske, "Accuracy and Performance of Machine Learning Methodologies: Novel Assessments of Country Pandemic Vulnerability Based on Non-Pandemic Predictors," in IEEE Access, vol. 11, pp. 90575-90594, 2023, doi: 10.1109/ACCESS.2023.3307495.
36. World Health Organization. (2023, August 8). *Status of covid-19vaccines within who EUL/PQ evaluation process*. Status of COVID-19 Vaccines within WHO EUL/PQ evaluation process. https://extranet.who.int/prequal/sites/default/files/document_files/Status_COVID_VAX_08August2023.
37. Thomas, S. J., Moreira, E. D., Jr, Kitchin, N., Absalon, J., Gurtman, A., Lockhart, S., Perez, J. L., Pérez Marc, G., Polack, F. P., Zerbini, C., Bailey, R., Swanson, K. A., Xu, X., Roychoudhury, S., Koury, K., Bouguermouh, S., Kalina, W. V., Cooper, D., Frenck, R. W., Jr, Hammitt, L. L., ... C4591001 Clinical Trial Group (2021). Safety and Efficacy of the BNT162b2 mRNA Covid-19 Vaccine through 6 Months. *The New England journal of medicine*, *385*(19), 1761–1773. https://doi.org/10.1056/NEJMoa2110345.
38. Katella, K. (2023, October 5). *Comparing the COVID-19 vaccines: How are they different?*. Yale Medicine. https://www.

©2024 Great Britain Journals Press

yalemedicine.org/news/covid-19-vaccine-comparison.
39. F. Pedregosa, G. Varoquaux, A. Gramfort, V. Michel, B. Thirion, O. Grisel, M. Blondel, P. Prettenhofer, R. Weiss, V. Dubourg, J. Vanderplas, A. Passos, D. Cournapeau, M. Brucher, M. Perrot, and E. Duchesnay, "Scikit-learn: Machine Learning in Python," *J. Mach. Learn. Res.*, vol. 12, pp. 2825–2830, Nov. 2011.
40. Nicholson, C., Beattie, L., Beattie, M., Razzaghi, T., & Chen, S. (2022). A machine learning and clustering-based approach for county-level COVID-19 analysis. *PloS one*, *17*(4), e0267558. https://doi.org/10.1371/journal.pone.0267558.
41. Rguibi, M. A., Moussa, N., Madani, A., Aaroud, A., & Zine-Dine, K. (2022). Forecasting Covid-19 Transmission with ARIMA and LSTM Techniques in Morocco. *SN computer science*, *3*(2), 133. https://doi.org/10.1007/s42979-022-01019-x
42. Facebook Open Source. (2023). *Prophet: Forecasting at scale*. Prophet. https://facebook.github.io/prophet/.
43. Pyo, J., Pachepsky, Y., Kim, S., Abbas, A., Kim, M., Kwon, Y. S., Ligaray, M., & Cho, K. H. (2023). Long short-term memory models of water quality in inland water environments. *Water research X*, *21*, 100207. https://doi.org/10.1016/j.wroa.2023.100207.
44. G. Li, N. Yang, A Hybrid SARIMA-LSTM Model for Air Temperature Forecasting. *Adv. Theory Simul.* 2023, 6, 2200502. https://doi.org/10.1002/adts.202200502.
45. Jin, Y.; Wang, R.; Zhuang, X.; Wang, K.; Wang, H.; Wang, C.; Wang, X. Prediction of COVID-19 Data Using an ARIMA-LSTM Hybrid Forecast Model. *Mathematics* 2022, *10*, 4001. https://doi.org/10.3390/math10214001.
46. Y. -C. Jin, Q. Cao, K. -N. Wang, Y. Zhou, Y. -P. Cao and X. -Y. Wang, "Prediction of COVID-19 Data Using Improved ARIMA-LSTM Hybrid Forecast Models," in *IEEE Access*, vol. 11, pp. 67956-67967, 2023, doi: 10.1109/ACCESS.2023.3291999.
47. Hema Priya, N., Adithya Harish, S.M., Ravi Subramanian, N., Surendiran, B. (2022). Covid-19: Comparison of Time Series Forecasting Models and Hybrid ARIMA-ANN. In: Rathore, V.S., Sharma, S.C., Tavares, J.M.R., Moreira, C., Surendiran, B. (eds) Rising Threats in Expert Applications and Solutions. Lecture Notes in Networks and Systems, vol 434. Springer, Singapore. https://doi.org/10.1007/978-981-19-1122-4_59.
48. de Araújo Morais, L. R., & da Silva Gomes, G. S. (2022). Forecasting daily Covid-19 cases in the world with a hybrid ARIMA and neural network model. *Applied soft computing*, *126*, 109315. https://doi.org/10.1016/j.asoc.2022.109315.
49. Wan Mohamad Nawi, W. I. A., K Abdul Hamid, A. A., Lola, M. S., Zakaria, S., Aruchunan, E., Gobithaasan, R. U., Zainuddin, N. H., Mustafa, W. A., Abdullah, M. L., Mokhtar, N. A., & Abdullah, M. T. (2023). Developing forecasting model for future pandemic applications based on COVID-19 data 2020-2022. *PloS one*, *18*(5), e0285407. https://doi.org/10.1371/journal.pone.0285407.
50. Borges, D., & Nascimento, M. C. V. (2022). COVID-19 ICU demand forecasting: A two-stage Prophet-LSTM approach. *Applied soft computing*, *125*, 109181. https://doi.org/10.1016/j.asoc.2022.109181.
51. Long, B.; Tan, F.; Newman, M. Forecasting the Monkeypox Outbreak Using ARIMA, Prophet, NeuralProphet, and LSTM Models in the United States. *Forecasting* 2023, *5*, 127-137. https://doi.org/10.3390/forecast5010005.
52. Shastri, S., Singh, K., Kumar, S., Kour, P., & Mansotra, V. (2020). Time series forecasting of Covid-19 using deep learning models: India-USA comparative case study. *Chaos, solitons, and fractals*, *140*, 110227. https://doi.org/10.1016/j.chaos.2020.110227.
53. Devaraj, J., Madurai Elavarasan, R., Pugazhendhi, R., Shafiullah, G. M., Ganesan, S., Jeysree, A. K., Khan, I. A., & Hossain, E. (2021). Forecasting of COVID-19 cases using deep learning models: Is it reliable and practically significant?. *Results in physics*, *21*, 103817. https://doi.org/10.1016/j.rinp.2021.103817.

©2024 Great Britain Journals Press

54. Z. Li, Y. Wang, Y. Wang, Y. Zheng and H. Su, "Covid-19 Epidemic Trend Prediction Based on CNN-StackBiLSTM," *2022 IEEE 11th Data Driven Control and Learning Systems Conference (DDCLS)*, Chengdu, China, 2022, pp. 970-975, doi: 10.1109/DDCLS55054.2022.9858588.
55. R. R. Maaliw, Z. P. Mabunga and F. T. Villa, "Time-Series Forecasting of COVID-19 Cases Using Stacked Long Short-Term Memory Networks," *2021 International Conference on Innovation and Intelligence for Informatics, Computing, and Technologies (3ICT)*, Zallaq, Bahrain, 2021, pp. 435-441, doi: 10.1109/3ICT53449.2021.9581688.
56. Ali, F., Ullah, F., Khan, J. I., Khan, J., Sardar, A. W., & Lee, S. (2023). COVID-19 spread control policies based early dynamics forecasting using deep learning algorithm. *Chaos, solitons, and fractals*, *167*, 112984. https://doi.org/10.1016/j.chaos.2022.112984.
57. Sah, Sweeti & B, Surendiran & Dhanalakshmi, R. & Mohanty, Sachi & Alenezi, Fayadh & Polat, Kemal. (2022). Forecasting COVID-19 Pandemic Using Prophet, ARIMA, and Hybrid Stacked LSTM-GRU Models in India. Computational and Mathematical Methods in Medicine. 2022. 1-19. 10.1155/2022/1556025.
58. Liu, S., Wan, Y., Yang, W., Tan, A., Jian, J., & Lei, X. (2022). A Hybrid Model for Coronavirus Disease 2019 Forecasting Based on Ensemble Empirical Mode Decomposition and Deep Learning. *International journal of environmental research and public health*, *20*(1), 617. https://doi.org/10.3390/ijerph20010617.
59. Da Silva, T. T., Francisquini, R., & Nascimento, M. C. V. (2021). Meteorological and human mobility data on predicting COVID-19 cases by a novel hybrid decomposition method with anomaly detection analysis: A case study in the capitals of Brazil. *Expert systems with applications*, *182*, 115190. https://doi.org/10.1016/j.eswa.2021.115190.
60. Lesouple, Julien & Baudoin, Cédric & Spigai, M. & Tourneret, Jean-Yves. (2021). Generalized Isolation Forest for Anomaly Detection. Pattern Recognition Letters. 149. 10.1016/j.patrec.2021.05.022.
61. H. Xu, G. Pang, Y. Wang and Y. Wang, "Deep Isolation Forest for Anomaly Detection," in IEEE Transactions on Knowledge and Data Engineering, vol. 35, no. 12, pp. 12591-12604, 1 Dec. 2023, doi: 10.1109/TKDE.2023.3270293.
62. Cai G, Wu Z, Peng L. Forecasting volatility with outliers in Realized GARCH models. *Journal of Forecasting*. 2021; 40: 667– 685. https://doi.org/10.1002/for.2736
63. Assistant Secretary for Public Affairs (ASPA). (2023, December 15). *Covid-19 vaccines*. HHS.gov. https://www.hhs.gov/coronavirus/covid-19-vaccines/index.html.
64. OCHA. (2021, April 20). *Unequal vaccine distribution self-defeating, World Health Organization chief tells Economic and Social Council's Special ministerial meeting - world*. ReliefWeb. https://reliefweb.int/report/world/unequal-vaccine-distribution-self-defeating-world-health-organization-chief-tells.
65. Lane, S., MacDonald, N. E., Marti, M., & Dumolard, L. (2018). Vaccine hesitancy around the globe: Analysis of three years of WHO/UNICEF Joint Reporting Form data-2015-2017. *Vaccine*, *36*(26), 3861–3867. https://doi.org/10.1016/j.vaccine.2018.03.063.
66. Larson H. J. (2018). The state of vaccine confidence. *Lancet (London, England)*, *392* (10161), 2244–2246. https://doi.org/10.1016/S0140- 6736(18)32608-4.
67. Logan, J., Nederhoff, D., Koch, B., Griffith, B., Wolfson, J., Awan, F. A., & Basta, N. E. (2018). 'What have you HEARD about the HERD?' Does education about local influenza vaccination coverage and herd immunity affect willingness to vaccinate?. *Vaccine*, *36*(28), 4118–4125. https://doi.org/10.1016/j.vaccine.2018.05.037.
68. Kim, D., Keskinocak, P., Pekgün, P., & Yildirim, İ. (2022). The balancing role of distribution speed against varying efficacy levels of COVID-19 vaccines under variants. *Scientific reports*, *12*(1), 7493. https://doi.org/10.1038/s41598-022-11060-8.

©2024 Great Britain Journals Press

69. Paul, E., Steptoe, A., & Fancourt, D. (2021). Attitudes towards vaccines and intention to vaccinate against COVID-19: Implications for public health communications. *The Lancet regional health. Europe*, *1*, 100012. https://doi.org/10.1016/j.lanepe.2020.100012.
70. Brumfiel, G. (2021, April 7). *Vaccine refusal may put herd immunity at risk, researchers warn*. NPR. https://www.npr.org/sections/health-shots/2021/04/07/984697573/vaccine-refusal-may-put-herd-immunity-at-risk-researchers-warn.
71. Coccia M. (2022). Improving preparedness for next pandemics: Max level of COVID-19 vaccinations without social impositions to design effective health policy and avoid flawed democracies. *Environmental research*, *213*, 113566. https://doi.org/10.1016/j.envres.2022.113566.
72. Akamatsu, T., Nagae, T., Osawa, M., Satsukawa, K., Sakai, T., & Mizutani, D. (2021). Model-based analysis on social acceptability and feasibility of a focused protection strategy against the COVID-19 pandemic. *Scientific reports*, *11*(1), 2003. https://doi.org/10.1038/s41598-021-81630-9
73. Lalmuanawma, S., Hussain, J., & Chhakchhuak, L. (2020). Applications of machine learning and artificial intelligence for Covid-19 (SARS-CoV-2) pandemic: A review. *Chaos, solitons, and fractals*, *139*, 110059. https://doi.org/10.1016/j.chaos.2020.110059.
74. Peiffer-Smadja, N., Rawson, T. M., Ahmad, R., Buchard, A., Georgiou, P., Lescure, F. X., Birgand, G., & Holmes, A. H. (2020). Machine learning for clinical decision support in infectious diseases: a narrative review of current applications. *Clinical microbiology and infection : the official publication of the European Society of Clinical Microbiology and Infectious Diseases*, *26*(5), 584–595. https://doi.org/10.1016/j.cmi.2019.09.009
75. Putrino, A., Raso, M., Magazzino, C., & Galluccio, G. (2020). Coronavirus (COVID-19) in Italy: knowledge, management of patients and clinical experience of Italian dentists during the spread of contagion. *BMC oral health*, *20*(1), 200. https://doi.org/10.1186/s12903-020-01187-3.
76. Vaishya, R., Javaid, M., Khan, I. H., & Haleem, A. (2020). Artificial Intelligence (AI) applications for COVID-19 pandemic. *Diabetes & metabolic syndrome*, *14*(4), 337–339. https://doi.org/10.1016/j.dsx.2020.04.012.
77. Xylogiannopoulos, K. F., Karampelas, P., & Alhajj, R. (2021). COVID-19 pandemic spread against countries' non-pharmaceutical interventions responses: a data-mining driven comparative study. *BMC public health*, *21*(1), 1607. https://doi.org/10.1186/s12889-021-11251-4.
78. Magazzino, C., Mele, M., & Schneider, N. (2021). Assessing a fossil fuels externality with a new neural networks and image optimization algorithm: the case of atmospheric pollutants as confounders to COVID-19 lethality. *Epidemiology and infection*, *150*, e1. https://doi.org/10.1017/S095026882100248X.
79. Romeo, L., & Frontoni, E. (2022). A Unified Hierarchical XGBoost model for classifying priorities for COVID-19 vaccination campaign. *Pattern recognition*, *121*, 108197. https://doi.org/10.1016/j.patcog.2021.108197.
80. Wu, H., Banerjee, R., Venkatachalam, I., Chougale, P. (2022). Impact of Interventional Policies Including Vaccine on COVID-19 Propagation and Socio-economic Factors: Predictive Model Enabling Simulations Using Machine Learning and Big Data. In: Arai, K. (eds) Intelligent Systems and Applications. IntelliSys 2021. Lecture Notes in Networks and Systems, vol 296. Springer, Cham. https://doi.org/10.1007/978-3-030-82199-9_60.
81. *US coronavirus vaccine tracker*. USAFacts. (2024, January 8). https://usafacts.org/visualizations/covid-vaccine-tracker-states/.
82. Office for National Statistics. (2023, March 26). *Coronavirus (COVID-19) latest insights: Vaccines*. Coronavirus (COVID-19) latest insights- Office for National Statistics. https://www.ons.gov.uk /peoplepopulationandcommunity/healthandsocialcare/condition

©2024 Great Britain Journals Press

sanddiseases/articles/coronaviruscovid19latestinsights/vaccines.
83. Hochreiter, S. & Schmidhuber, J"urgen, 1997. Long short-term memory. Neural computation, 9(8), pp.1735–1780. https://doi.org/10.1162/neco.1997.9.8.1735.

©2024 Great Britain Journals Press

This page is intentionally left blank

©2024 Great Britain Journals Press

Scan to know paper details and
author's profile

Discussion on the Interpretation of the Word "Catalysis, Catalyst"

Jin Jia-Min

ABSTRACT

The main idea of this paper is whether the catalyst participates in the chemical reaction. Chemical Reaction Mode catalysis Mechanism- CRMM considers that catalysts always participate in chemical reactions, and it's a cyclic reaction.

The interpretation on the “Catalysis,catalyst” by.P.Sabatier and M.Boudart principle has encountered serious difficulties, so the CRMM is not reliable. Due to the “catalysis,catalyst” misdirection, As a result, the research and production of catalysts appears in chaos and huge economic losses. The catalytic phenomenon is a physical phenomenon, not a chemical phenomenon, and the catalyst does not participate in chemical reactions. Chinese and foreign scholars should change the interpretation on the “catalysis,catalyst”, or add two new words: “contact and contactor”, it is to give up “catalysis, catalyst “altogether.

Keywords: catalysis catalyst sabatier principle boudart principle.

Classification: LCC Code: QD506

Language: English

Great Britain Journals Press

LJP Copyright ID: 392942
Print ISSN: 2631-8474
Online ISSN: 2631-8482

London Journal of Engineering Research

Volume 24 | Issue 3 | Compilation 1.0

© 2024. Jin Jia-Min. This is a research/review paper, distributed under the terms of the Creative Commons Attribution-Noncom-mercial 4.0 Unported License http://creativecommons.org/licenses/by-nc/4.0/), permitting all noncommercial use, distribution, and reproduction in any medium, provided the original work is properly cited.

Discussion on the Interpretation of the Word "Catalysis, Catalyst"

Jin Jia-Min

ABSTRACT

The main idea of this paper is whether the catalyst participates in the chemical reaction. Chemical Reaction Mode catalysis Mechanism-CRMM considers that catalysts always participate in chemical reactions, and it's a cyclic reaction.

The interpretation on the "Catalysis,catalyst" by.P.Sabatier and M.Boudart principle has encountered serious difficulties, so the CRMM is not reliable. Due to the "catalysis,catalyst" misdirection, As a result, the research and production of catalysts appears in chaos and huge economic losses. The catalytic phenomenon is a physical phenomenon, not a chemical phenomenon, and the catalyst does not participate in chemical reactions. Chinese and foreign scholars should change the interpretation on the "catalysis,catalyst", or add two new words: "contact and contactor", it is to give up "catalysis,catalyst" altogether。

Keywords: catalysis catalyst sabatier principle boudart principle.

Author: Shanghai Research Institute of Materials 200437.

I. INTRODUCTION

Catalysts are widely used in chemical production. However, the catalysis mechanism of the catalyst has always remained in the CRMM. It is more and more Popular for more than 120 years and deep into middle school textbooks, it is deeply rooted in the catalytic academia. But; the author thinks that the CRMM is contrary to the basic principle of thermodynamics。Therefore, the CRMM is error. Who is the cause of this result, whether it is the linguist or the catalysis expert, this paper is to give some explanati.

II. 《CONTACT》AND《CATALYSIS》

In the textbooks of our fathers, You can see the word "contact", but you can't see the word "catalysis". "Catalysis" is a foreign word, it is a translation of <Catalysis, Catalyst >from west.

Different translations can be seen from the【English-Chinese Dictionary】published in different periods:

1. 1963, In the【English-Chinese Dictionary】compiled by Zheng Yili and others published by Beijing Times Press, The translation of these two words is as follows:
   Catalysis: n. Contact reaction,contact action, Catalysis.
   Catalyst: n. Contact agent, Catalyst.
2. In 1974, Shanghai Translation Publishing House, "New English-Chinese Dictionary" compilation group【New English-Chinese Dictionary】about the translation of these two words is:
   Catalysis: n. Catalysis (action).
   Catalyst:.. catalyst Contact agent(Old translation Contact)
3. In 2006, Shanghai Translation Publishing House, Zhou Jilian and other edited the【A NEW ENGLISH -ChINESE ADVANCED LEARNER`S DICTIONARY】about the translation of this word is:
   Catalysis: n. Catalysis.
   Catalyst: n. Catalyst.

©2024 Great Britain Journals Press

It can be seen that the translation of <Catalysis, Catalyst> went from "Catalysis, Contacct" to completely abandoning "Contact' and adopting "Catalysis, Catalyst" for over 40 years.

Taken literally, <Catalysis> has the meaning of a chemical reaction and it belongs to the realm of chemistry. <Contact > on the other hand, is just touch, it belongs to the realm of physics. It is obviously inappropriate to translate one English into two different fields of meaning.

The reason on the change from "Contact" to "Catalysis" came from Western catalytic academics and linguists (dictionaries).

The definition of this《Catalysis, Catalyst》word in Western academia is as follows:

A. Sabatier·s Principle(1902)[1,2]

Sabatier principle proposes the existence of an unstable intermetiate compound formed between the catalyst surface and at least one of the reactants. This intermetiate must be stable enough to be formed in sufficient quantities and labile enough to decompose to yield the final product or products.

B. Boudart Principle(1992年)[1,3]

Ninety years later, an American scholar M. Boudart redefined 《catalysis, catalyst》 like this:

The most fundamental principle in catalysis is that of the catalytic cycle,which maybe based on a redefinition of a catalyst by Boudart: "A catalyst is a substance that transforms reactants into products,through an uninterrupted and repeated cycle of elementary steps in which the catalyst is changed through a sequence of reactive intermediates, until the last step in the cycle regenerates the catalyst in its original form" .

- I call the principles of these two scholars the S-B principles. According to the S-B principle, the linguist (dictionary) was quite right to drop《 Contact》and translate《 Catalysis ,Catalyst》. Unfortunately, it was on the wrong path。Because the interpretation of《catalysis, catalyst》is misleading

In the catalyst handbook [4], CRMM is expressed as follows:

$$R+M=X$$

$$X=P+M$$

Above; R- reactant, M- catalyst, X- intermediate, P- product. The product (P) is not produced directly, but through an intermediate (X).

The catalytic action of biological enzymes is that enzymes participate in the reaction;

$$E+S=ES$$

$$ES=E+P$$

Above; S-reactants (proteins, starches, etc.), E-enzymes, ES-intermediates, P-products. This is the famous Michaelis-Menten mechanism proposed in 1913.[1,5]

For Fe catalysts [3,6], the catalytic process is described asfollows:

$$CO2 +Fe=FeO+CO$$

$$FeO+C=Fe+CO$$

$$CO2 +C=2CO$$

The intermediate of the reaction is the FeO, and The Iron oxide is constantly reduced - oxidized, which is called《Oxygen Transfer Mechanism -OTM》. The OTM here is the author tag.

For alkali metal carbonates [3,7], the catalytic process is described asfollows:

$$M2CO3+2C=2M+3CO$$

$$2M+2H2O=2MOH+H2$$

$$2MOH+CO=M2CO3+H2$$

$$2C+2H2O=3CO+2H2$$

There are two intermediates in the reaction process, namely M and MOH. The catalyst (M2CO3) continuously decomposes and generates a cyclic reaction.

The key points of CRMM are that the catalysts have to participate in the chemical

©2024 Great Britain Journals Press

reaction, and it is a cyclic reaction. There are a intermediate. The catalyst is continuously decomposed and regenerated.

After years of research [8, 9], the author believes that the catalytic phenomenon is a physical phenomenon, not a chemical phenomenon, the catalyst does not participate in chemical reactions, only contact, is the electron donate-accept cycle, is the electron orbital repeated deformation-recovery. Electrocatalysis, photocatalysis, microwave catalysis, laser catalysis are all physical phenomena, but the energy levels are different. The selectivity of the catalyst is also related to the energy level.

Compared with CRMM and Electron Cyclic Donate-Adopt Mechanism-ECDAM or Electron Orbital Deformation-Recovery Mechanism-EODRM, the former is that the catalyst participat in the chemical reaction, and it is a cyclic reaction. The latter is the catalyst does not participate in the chemical reaction, just contact or touch. The former is a chemical phenomenon, the latter is a physical phenomenon.

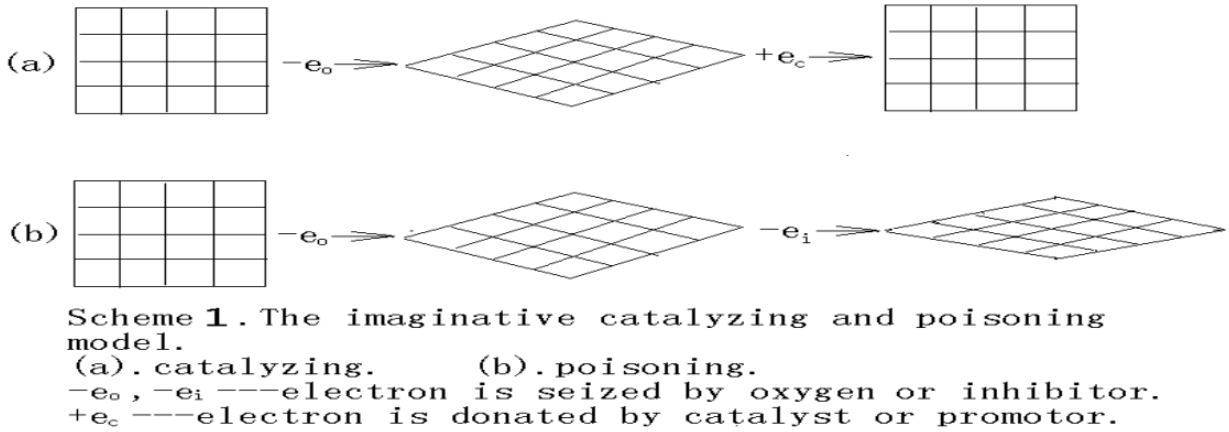

Scheme 1. The imaginative catalyzing and poisoning model.
(a). catalyzing. (b). poisoning.
$-e_o$, $-e_i$ ---electron is seized by oxygen or inhibitor.
$+e_c$ ---electron is donated by catalyst or promotor.

Schememe 1: Is a imagine figure of catalyzing and poisoning

"-e" in schematic diagram 1 indicates that when the suspended electrons on the surface of the carbon particle *(matrix)* or catalyst iron particle *(matrix)* are taken away by oxygen or nitrogen, the carbon or iron matrix tries to regain the take away electrons in order to maintain the original low-energy state electron orbital, and the electron orbital and lattice in matrix must be deformed.

The electrons suspended on the surface of carbon are not free, and their move causes the deformation of the electron orbitals in the carbon or iron matrix, but does not reach the degree of lattice reconstruction. that is no chemical reaction. When this kind of electron pulling occurs, there are two possibilities. One is to donate electrons to the carbon or iron matrix , be "+e", restore the deformed electron orbitals, reduce the fracture energy of the bond, and speed up the reaction, which is the catalyst

1) The other is to further rob the electrons of the carbon or iron matrix, resulting in further deformation of the deformed electron orbitals, resulting in higher bond breaking energy and slower reaction speed, which is the poison agent.
2) Thence; Naturally, two important conclusions are drawn, that is, there is a boundary between catalyst and poison agent, and the activity size of catalyst or *poisonousness* of poison agent is closely related to the electronegativity difference.

II. THE DIFFICULTIES ENCOUNTERED BY CRMM

3, 1 Cyclic Reactions Involving Catalysts are Unlikely to Occur。

- A professor at Shanghai University believes that all catalysts must meet S-B principle, and

©2024 Great Britain Journals Press

London Journal of Engineering Research

those that do not meet this principle are not catalysts. Be visible; The leader of the catalytic academia regards this "principle" as a classic, unimpeachable。 as if this principle provides a theoretical basis for the study of catalysts. The author asserts that if this principle is followed, I am afraid that a catalyst that meets this principle will never be found.

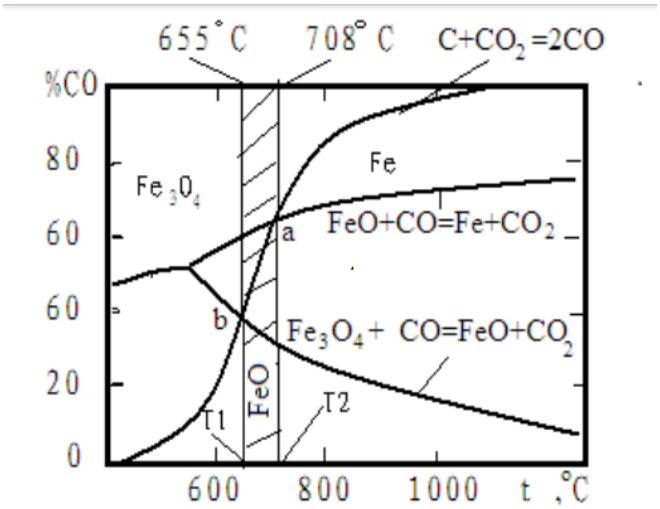

Figure 2: Iron-Carbon-Oxygen Reaction Equilibrium Diagram [10]

For carbon gasification reaction, iron is a catalyst, we have proved this many times by experiments... According to the S-B principle, iron must undergo an oxidation-reduction cycle in order to have catalytic activity. Figure 2 is an iron - carbon - oxygen reaction equilibrium diagram. As can be seen from the figure, the C+CO2=2CO reaction equilibrium curve and FeO+CO=Fe+CO2 reaction equilibrium curve intersect at 708°C. There is only one point in the figure that meets the requirement of the oxidation-reduction cycle reaction, that is, the gas phase composition in the figure is 65%CO, 35%CO2, and the air pressure is 1 atmosphere.

Leave this point, the iron cannot undergo the oxidation-reduction cycle reaction. Above 708°C, the stable phase is iron, the FeO is unstable, and the FeO will be reduced by carbon. Below 708°C, FeO is a stable phase, Fe is unstable, and Fe is oxidized to FeO. Factors affecting the chemical reaction equibrium in addition to temperature, as well as pressure and the form of carbon, if according to the S-B principle, only at 708°C, 1 atmosphere of pressure, carbon in the form of graphite can meet the requirements of the oxidation-reduction cycle reaction, to have catalytic activity, leaving this condition,the cyclic reaction is impossible to occur , iron will lose catalytic activity. In fact, iron has catalytic activity in a wide temperature range (600°-1000°C).

For carbon gasification reaction, alkali metal salt, alkali earth metal salt, transition metals, precious metals, etc., have catalytic activity, but the activity size is different, under the same reaction conditions (such as carburizing box,940°C), so many salts and metals can not be able to decompose-generation, or oxidation-reduction cyclic reaction. The cyclic reaction not only fails to show that many catalysts have catalytic activity under the same reaction condition, but also fails to show that the same catalyst has catalytic activity over a wide temperature range. Therefore, according to the S-B "principle", it can never be found one catalyst.

Besides; The decomposition pressure (equilibrium pressure) of metal oxides has an exponential relationship with temperature, and each metal oxide has a decomposition pressure

©2024 Great Britain Journals Press

curve, which is different. Metal and metal oxide can coexist only on the decomposition pressure curve (2MeO=2Me +O2), and away from this point (temperature, pressure, gas phase composition), Me and MeO cannot coexist. Under certain reaction conditions, it is impossible for many metals or salts with catalytic activity to undergo the cycle reaction of generate and decomposition, and it is impossible to have catalytic activity in a wide temperature range.

According to our determination, in the carburizing box, the catalyst barium carbonate, BaCO3 and BaO can coexist only at 1048°C, leaving this point, the decomposition - formation cyclic reaction is impossible. The actual production temperature is about 940°C, barium carbonate has catalytic activity.

Let me take another popular example. Housewives know that salt has catalytic activity, and a dying coal stove can be saved by sprinkling a handful of salt into it. NaCl is a very stable compound, and it is impossible to undergo decomposition - generation reaction in coal furnaces.

3,2 Intermediate is Impossible to Appear

The most fundamental principle in catalysis is the catalytic cycle, and this cycle is the cycle in which the catalyst participates in. and in order to maintain this cycle, an Intermediate is necessarily needed. The catalyst must form an intermediate with the reactants that is stable, has a certain amount, and is easily decomposed. The catalyst must be continuously decomposed -generated , and from literature can see many, each says his own, completely contrary to the basic principles of thermodynamics.

For example, barium carbonate catalysts can be seen as barium metal (Ba), barium oxide (BaO). Iron catalyst has FeO, carbonate catalyst has Me and MeOH, precious metal catalyst has PtO and so on. The author does not want to make one explanation one by one, only to say that the FeO intermediate,

In the reaction tank of reduction of iron oxide by carbon , tens of kilograms of iron oxide by carbon reduction to sponge iron ingots, the catalyst Iron in the carbon layer cannot undergo an oxidation-reduction cycle。

Moreover, For platinum catalyst, due to the very high decomposition pressure of platinum oxide, it can only exist in the metal state in nature, In a strong reducing atmosphere, it can only appear in the metal state, and it is absolutely impossible to occur oxidation-reduction cycle reaction.

The literature is full of variously discordant intermediates that completely contradict the basic principles of thermodynamics,

3,3. It can be seen from the literature that catalytic experts use the number of "cyclic reactions" per unit time, "TOF", to indicate the activity size of the catalyst, and the total number of cyclic reactions before the catalyst failure to indicate the catalyst life. Since the catalyst participating in the cyclic catalytic reaction does not exist, the intermediate can not appear, the use of “TOF” is obviously out of thin air. It is a pity that the catalytic experts have deceived their readers. As stated above, The definition of ”catalysis, catalyst” by the S-B principle is incorrectthe。Therefore, The interpretation on《catalysis, catalyst》by S-B principle has being mislead。

IV. THE HARM CAUSED BY CATALYSIS'S MISDIRECTION

Due to a misinterpretation of the word "Catalysis", the result was confusion in catalyst research and application. For this reason, the author wrote an article "Some Problems in the research and production of heterogeneous catalysis" [11].

Several examples are given in the article,

- Such as ”The poisoning problem of alumina in the iron base ammonia synthesis catalyst, the poisoning of the Cordierite ceramic Honeycomb support material in the automobile exhaust gas purification catalyst, the poisoning of carbon in the support material of ruthenium ammonia synthesis catalyst, and the CRMM has existence

©2024 Great Britain Journals Press

question. Here are again two examples to illustrate the confusion caused by the misleading S-B principle to the research of catalysts.

1. M.Boudart studied the catalytic effect of Pt on the reactions of C+CO2 = 2CO and C+H2O=CO+H2 [3]. Finally, he used the OTM to explain the catalysis of Pt, that is, the oxidation and reduction reaction of Pt continuously occurs during the catalytic process. The intermediate is the oxide of Pt. On this point, it has been explained before, and will not be repeated here.

   A danger signal can be seen from the literature, some people in the catalytic academia believe that the basic principles of thermodynamics can not guide the research of catalysts, so there are many different intermediate compounds that deviate from the basic principles of thermodynamics. Catalyst research is getting more and more outrageous.

   This is where the misinterpretation of《 Catalysis,catalyst》 word lead us.

2. Mckee. W., who used Controlled Atmosphere Electron Microscopy (CAEM) to study alkali metal oxides and salts, alkaline earth metal oxides and salts, transition metals and oxides, noble metals and other catalysts on the four reactions of C+O2, C+CO2, C+H2O, and C+H2 was studied by referring to 152 literatures and writing 118 pages of articles [10]. In the end, he thought

   "Although it is not yet possible to explain all the observed catalytic effects within one all-encompasing, mechanmistic flamework, on balance specific oxidation-reduction cycles have been conspicuously successful in interpreting the effects of alkli-metal salts,transition metals and oxides ,and the noble metals in the various types of carbon gasification reactions. However, many details of the complex catalytic phenomena still remain obscure and await elucidation by carefully designed experimental and theoretical investigation."

Here he still adopt the OTM. The special oxidation-reduction cycle, but exactly how special it is, it does not say.

Mr. M. Boudart and D.Mckee were both famous American scientists.

From these two examples, it can be seen that scientists have spent a lot of effort trying to solve this mystery, but the result is helpless and end up with nothing definite. The research of catalyst fall into a bottomless pit.

V. CONCLUSION

The author believes that CRMM is deeply rooted in the catalytic academia and popular for more than 120 years. The fundamental reason is that catalytic experts always believe that catalysts participate in chemical reactions.

The inevitable results of participating in the chemical reaction is to appear a series of *trouble*. Such as ; S-B principle, intermediate , catalytic cycle,catalyst repeatedly decomposing- generate or oxidation - reduction and so on.

The author believes that Chinese and foreign s catalytic expert must abandon the inherent idea that catalysts participate in chemical reactions.

The definition of word《catalysis, catalyst》in dictionary should be changed to《contact, contact agent》. Or create a new word to avoid misdirection.

Relevant academic journals and research institutions should remove the word" catalysis" to avoid misleading

The use of CRMM in middle school textbooks to explain the catalytic role of enzymes should be deleted to avoid delaying future generations.
The author's knowledge is shallow, outsider, overreach, inadequacy, please criticize and correct the knowledgeable person.

REFERENCES

1. O. Deutschmann, H. Knozinger, K. Kochloefl, and T. Turex, (2009) 《*Heteroegeneous*

©2024 Great Britain Journals Press

Catalysis and Solid Catalysts》. Wiley-VCH Verlag GmhH & Co. KGaA, Weinheim.
2. P.Sabatier, J. B. J. B. Senderens, *C. R. Acad. Sci.*134 (1902)514.
3. M. Boudart in J. M. Thomas, K. I. Zamaraev (eds): *Perspectives in catalysis,* Blackwell Scientific Publications, London 1992, P.183.
4. 《Catalyst Handbook》, Beijing Chemical Industry Press , *464*(*1982*)
5. L. Michaelis, L. M. Meaten. *Bicchem. Z.*, 49, 333 (1913).
6. P. L. Waker, Jr., M. Shelef, and R. A. Anderson, *Chem. Phys. Carbon* 4, 287, (1968).
7. D. W. Mckee, and D. Chatterji, *Carbon* 16,53 (1978).
8. Jin Jia-min, "*Catalysis of Barium Carbonate in Solid carburizing agent,* "Proceedings of the First Annual Heat Treatment Conference 1963, Beijing Machine Pres,. *389-402*(*1966)*
9. Jin Jia-min, Jiang Guo-yuan, Ren Jia-ying, et al. "Catalysis and poison mechanism of mineral impurities in carbon for carbon reduction of iron oxide". Proceedings of the National Powder Metallurgy Conference (1982).
10. O. A. Esin, P. F. Geld. 《*Phys.-Chem.of Pyrometallurgical processes*》, National Ferrous nonferrous metals Press, 560, (1962).
11. Jin Jia-min, *"Several Problems in the Research and Production of heterogeneous Catalysis*", Guangzhou Chemical Industry, *Vol.43, No.10,47(2015).*

©2024 Great Britain Journals Press

This page is intentionally left blank

©2024 Great Britain Journals Press

Scan to know paper details and
author's profile

Potential Encapsulating Microparticle from Degreased Dry Flour of Guava Seeds

Gustavo Rodrigues de Souza, Armanda Aparecida Júlio, Aldino Neto Venancio, Jaqueline Rodrigues Cindra de Lima Souza, Mario Ferreira Conceição Santos, Renê Chagas da Silva, Fabielle Castelan Marques, Luciano Meniniv & Tércio da Silva de Souza

Universidade Federal

ABSTRACT

Brazil is one of the world's largest producers of guava. The estimated production is approximately 552,393 tons/year. Most guava production is processed to manufacture juices, nectars, pulps, and ice creams. During the processing of guava, about 40% of the waste from the processing of guava consists of seeds, whose disposal causes environmental problems. Within this context, this work aimed to develop encapsulating material from guava seed flour and to study the kinetics, equilibrium, and thermodynamics involved in the microencapsulation process. Initially, the characterization of the guava seeds (carbohydrates, proteins, fibers, and ashes) was carried out, then the seed yield was calculated.

After the characterization, the seed yield was calculated, and these were used to prepare dry and defatted flour. This flour was characterized in terms of solubility, hygroscopicity, bed and compacted density, wettability, morphology, zero load point, and thermal analysis. The experimental parameters of the adsorption process were previously optimized.

Keywords: NA

Classification: LCC Code: TP368

Language: English

Great Britain Journals Press

LJP Copyright ID: 392943
Print ISSN: 2631-8474
Online ISSN: 2631-8482

London Journal of Engineering Research

Volume 24 | Issue 3 | Compilation 1.0

© 2024. Gustavo Rodrigues de Souza, Armanda Aparecida Júlio, Aldino Neto Venancio, Jaqueline Rodrigues Cindra de Lima Souza, Mario Ferreira Conceição Santos, Renê Chagas da Silva, Fabielle Castelan Marques, Luciano Meniniv & Tércio da Silva de Souza. This is a research/review paper, distributed under the terms of the Creative Commons Attribution- Noncom-mercial 4.0 Unported License http://creativecommons.org/licenses/by-nc/4.0/), permitting all noncommercial use, distribution, and reproduction in any medium, provided the original work is properly cited.

Potential Encapsulating Microparticle from Degreased Dry Flour of Guava Seeds

Gustavo Rodrigues de Souza[α], Armanda Aparecida Júlio[σ], Aldino Neto Venancio[ρ], Jaqueline Rodrigues Cindra de Lima Souza[ↀ], Mario Ferreira Conceição Santos[¥], Renê Chagas da Silva[§], Fabielle Castelan Marques[χ], Luciano Menini[ν] & Tércio da Silva de Souza[Θ]

ABSTRACT

Brazil is one of the world's largest producers of guava. The estimated production is approximately 552,393 tons/year. Most guava production is processed to manufacture juices, nectars, pulps, and ice creams. During the processing of guava, about 40% of the waste from the processing of guava consists of seeds, whose disposal causes environmental problems. Within this context, this work aimed to develop encapsulating material from guava seed flour and to study the kinetics, equilibrium, and thermodynamics involved in the microencapsulation process. Initially, the characterization of the guava seeds (carbohydrates, proteins, fibers, and ashes) was carried out, then the seed yield was calculated.

After the characterization, the seed yield was calculated, and these were used to prepare dry and defatted flour. This flour was characterized in terms of solubility, hygroscopicity, bed and compacted density, wettability, morphology, zero load point, and thermal analysis. The experimental parameters of the adsorption process were previously optimized. The adsorption capacity was evaluated in a batch system under a controlled temperature of 25 ± 2°C. From the results obtained, it is possible to infer that the dry and defatted seed flour presented the potential for the proposed purpose, with a high capacity to incorporate the methylene blue dye (~83%). The experimental results showed that the pseudo-second-order model better described the adsorption kinetics.

Finally, thermodynamic results analysis revealed a spontaneous adsorption process (ΔG°= -44.10 kJ mol^{-1}), exothermic (ΔH° = -22.47 kJ mol-1), and with ΔS° = -73 .62 J mol^{-1} K^{-1}, which shows small changes in randomness at the solute-adsorbent interface during adsorption.

Author α ¥: Universidade Federal do Espírito Santo/Departamento de Química e Física, Alto Universitário s/n, Guararema, 29500-000, Alegre-ES, Brasil.

σ ↀ ν Θ: Federal de Educação/ Ciência e Tecnologia do Espírito Santo – Campus de Alegre, BR 482, Rodovia Cachoeiro/Alegre, Km 47, Distrito de Rive - 29520-000 - Alegre-ES, Brasil.

ρ: Universidade Federal Viçosa/Departamento de Química, Avenida P. H. Rolfs,s/n, Campus Universitário, 36570-900 - Viçosa-MG, Brasil.

§: Universidade Federal Viçosa/Departamento de Física, Avenida P. H. Rolfs,s/n, Campus Universitário, 36570-900 - Viçosa-MG, Brasil.

χ: Federal de Educação, Ciências e Tecnologia do Espírito Santo Endereço: Rodovia ES-482, Cachoeiro x Alegre, Morro Grande, Cachoeiro de Itapemirim - ES, CEP: 29311-970, Brasil.

I. INTRODUCTION

The Psidium guajava L. guava is a tropical fruit characterized by a low content of carbohydrates, fats, and proteins and a high content of vitamin C (more than 100 mg/100 g of fruit) and fiber content (2.8-5.5 g/100 g of fruit) [1]. In addition to its nutritional properties, this fruit is very appetizing due to its sensory properties (taste and color) [2-3-4]. Brazil is among the largest guava producers, and guava plantations are concentrated in the Northeast and Southeast regions. Production in the country reached 552, 393 tons in 2021 [5], but the commercialization of the fruit is still national.

©2024 Great Britain Journals Press

Although the fruit is consumed in nature, most guava production is processed to manufacture juices, nectars, pulps, ice creams, jellies and jams, ingredients for preparing yogurts, jellies, and recently, the bittersweet guatchup sauce [6-7].

During the processing stages, there is a large generation of tailings mainly composed of seeds. When improperly disposed of, these tailings can cause environmental damage and consequently become a problem of significant impact on the environment and agro-industries [8].

The waste resulting from the processing of guava is a food with great potential to compose diets for production animals [9] and food for human consumption, as it has already been used in the formulation of guava seed flour for the elaboration of bread [10-11-12]. These seeds are predominantly composed of cellulose, lignin, and lignan, which have favorable characteristics for the development of encapsulating materials, in addition to presenting biodegradability, biocompatibility, and low toxicity [13]. When used as an adsorbent or encapsulating agent, guava seed flour may have promising characteristics. However, using the microencapsulation process can solve many problems, such as increasing the stability, bioavailability, and efficiency of the action of various natural products [14].

Most encapsulating materials are polymers of plant origin due to their biodegradability, biocompatibility, and low toxicity properties [13]. These polymers can be prepared from abundant and cheap agro-industrial waste, such as seeds, peels, and fruit pomace [8]. However, the literature lacks information on this agricultural waste, from the processing of guava to preparing wall material to be used in encapsulating systems, making it possible to carry out studies to identify the potential of dry flour and defatted guava seed.

Thereby the potential of developing an innovative and technological product from low-cost and abundant agricultural waste, the present study aims to prepare to encapsulate material from the dry and defatted flour of guava seeds from agro-industrial waste.

II. EXPERIMENTAL

2.1 Guava Material

The guava waste was acquired at the fruit pulp production unit (PapaFruta®), located in the municipality of Mimoso do Sul, in the southern region of Espírito Santo, and was immediately transported in a thermal box to the Ifes Applied Chemical Laboratory - Campus Alegre. The guava seeds were separated from the residue by mechanical friction via wet and subsequently dehydrated. Their yield and proximate characterization were determined (moisture, mineral content, carbohydrates, proteins, lipids, and fibers). The material was washed with running water and subjected to sun drying for 8 hours; then, they were separated from the rest of the residue and placed in a forced air circulation oven at 55°C for 48 hours.

2.2 Preparation of Dry and Degreased Guava Seed Flour (FSDSG)

The guava seeds were ground in a Willey Marconi® knife mill, MAO 48, with a sieve of 2.0 mm opening and subsequently subjected to granulometric selection in a stainless-steel sieve at 80 Mesh. The flour produced was subjected to lipid extraction in a Soxhlet system (DiogoLab) for 6 hours, using hexane as a solvent. FSDSG was suspended in aqueous HCl solution at a concentration of 0.1 mol L^{-1}, using a 5:1 ratio, and kept under stirring at 1000 Rpm for 3 hours at 25 ± 1°C. Then the material was subjected to quantitative filtration for 24 hours and dried in an oven at 105°C for 1 hour.

2.3 Yield and Properties of FSDSG

FSDSG yield was determined by mass difference, and solubility was calculated according to the method described by Cano-Chauca et al. (2005). Wettability was determined according to the method described by Fuchs et al. (2006). Hygroscopicity was estimated according to the methodology of Cai and Corke (2000). Bed density was conducted following the methods proposed by Jinapong., Suphantharika., Jamnong (2008), and Goula and Adamopoulos (2012) with adaptations. Moisture, ash, protein, lipid, and

©2024 Great Britain Journals Press

fiber contents were determined by standard methodologies proposed by the ASSOCIATION OF OFFICIAL ANALYTICAL CHEMISTS (CUNNIFF-AOAC, 1995). The gravimetric method determined the moisture content by drying in an oven at 105°C (QUIMIS®) until constant weight and mineral matter were obtained by incinerating the material in a muffle furnace at 550°C (QUIMIS®) for five hours. Total nitrogen was determined by the Kjeldahl method and converted into crude protein by the factor 6.25 [15]. Total lipids were determined according to the Soxhlet method using petroleum ether as the solvent and crude fiber according to the Weende method [16]. The carbohydrate content was obtained by the difference [100 – (% moisture - % lipids - % protein - % fiber - % mineral matter)]. The caloric value of the seeds was estimated using the conversion factor of 4 kcal g^{-1} for protein and carbohydrate and 9 kcal g^{-1} for lipids [17]. All assays were performed in triplicate.

2.3.1 Scanning Electron Microscope (SEM)

Morphological analysis of the degreased guava seed was performed on an energy dispersive X-ray spectrometer (EDS) coupled to a scanning electron microscope (SEM) using a JEOL JSM 6010LA SEM. The material had to go through the metallization step, being coated with Au, as it is not a conductor. All images and EDS spectrum were acquired using an acceleration voltage of 20kV and 10 mm working distance. The EDS detector window was beryllium.

2.3.2 InfraRed

The spectra were obtained in the infrared region by Fourier transform coupled with the attenuated total reflectance technique (FTIR-ATR) for products derived from guava seed and were acquired in the spectral range from 400 to 4000 cm^{-1} in the Varian 660-IR equipment.

2.3.3 Structural Property

As isotermas de adsorção/dessorção de nitrogênio foram medidas em um aparelho NOVA 1200 da Quantachrome, usando o degaseificador a vácuo a 80°C por 5h. A área superficial usando o método Brunauer-Emmett-Teller (BET) foi determinada a partir de Multi Point BET. A distribuição do tamanho de poro e do volume de poro foi obtida a partir da Teoria da Densidade Funcional (DFT), que é baseada na modelagem molecular e leva em consideração a interação direta do adsorbato com a superfície adsorvente.

2.3.4 Thermogravimetric Analysis

Nitrogen adsorption/desorption isotherms were measured on a NOVA 1200 instrument from Quantachrome, using a vacuum degasser at 80°C for 5h. The surface area using the Brunauer-Emmett-Teller (BET) method was determined from MultiPoint BET. The pore size and pore volume distribution were obtained from the Density Functional Theory (DFT), which is based on molecular modeling and considers the direct interaction of the adsorbate with the adsorbent surface.

2.3.5 Ponto de Carga Zero

The measurement of pH at zero load point (pHPCZ) was performed based on the method proposed by Mall et al. (2006), which consisted of adding 100 mg of FSDSG in Erlenmeyer containing 50 mL of distilled water with the pH values adjusted between 2.0 and 11.0 through solutions of hydrochloric acid (HCl) and sodium hydroxide (NaOH). The suspensions were kept under constant agitation at 200 rpm for 24 hours at 25°C. The initial and final pH values were measured with a pH meter (MS TECNOPON, Mpa-210). The pHPCZ was measured through the first derivative (ΔpH/initial pH) of the pH behavior curve and assigned to the point where the sums of the charges tend to zero. This procedure was performed in triplicate.

2.4 Adsorption

Methylene blue cationic dye (B. Herzog, Germany) was used as the adsorbate. The previously optimized parameters were used: mass of FSDSG 0.1 g, stirring speed = 200 rpm, and pH = 7.0. Four-milliliter aliquots were taken at predefined time intervals (10, 30, 60, 90, 120, 240, 360, and 480 min) and placed in Falcon tubes, later centrifuged (HERMLE) at 6000 rpm for five minutes. The supernatant was transferred

©2024 Great Britain Journals Press

to a quartz cuvette for reading in a UV-Vis spectrophotometer (Agilent, Cary 60 UV/Vis) at 664 nm, and then the aliquot was returned to the system. All assays were performed in triplicate. The amount of methylene blue (MB) adsorbed on the FSDSG, qe (mg g^{-1}), was calculated by Equation 1 [18-19].

$$q_e = \frac{C_0 - C_e}{w} * V \qquad (Eq.\ 1)$$

Where C_o and Ce (mg L^{-1}) are the initial and equilibrium liquid-phase concentrations of MB, respectively, V (L) is the volume of the solution, and W(g) is the mass of FSDSG used. The same procedure was followed in batch adsorption and kinetic studies, but the aqueous samples were collected at predefined time intervals. MB concentrations were similarly measured. The amount of MB adsorbed at any time, qt (mg g^{-1}), was similarly calculated by Equation 2 (Eq. 2) [18-19].

$$q_t = \frac{C_0 - C_t}{w} * V \qquad (Eq.\ 2)$$

Where C_o and Ce (mg L^{-1}) are the initial and equilibrium liquid-phase concentrations of MB, respectively, V (L) is the volume of the solution, and W (g) is the mass of FSDSG used. The same procedure was followed in batch adsorption and kinetic studies, but the aqueous samples were collected at predefined time intervals. MB concentrations were similarly measured. The amount of MB adsorbed at any time, qt (mg g^{-1}), was similarly calculated by Equation 2 [18-19].

2.5 Adsorption Isotherm and Kinetic Models

The application of adsorption isotherms is very useful in describing the interaction between the adsorbate and the adsorbent of any system. The parameters obtained from the different models provide important information about the sorption mechanisms. For example, there are various equations for analyzing experimental adsorption equilibrium data. The Langmuir and Freundlich models are the most widely used and accepted surface adsorption models for single-solute systems. On the other hand, an interesting trend in isothermal modeling is the derivation in more than one approach, thus leading to the difference in physical interpretation. In this study, the Langmuir and Freundlich isotherms [20] were applied; table 1 shows the equations and parameters of such isotherms. Kinetic models such as pseudo-first-order [21], pseudo-second -order [22], and intraparticle diffusion model [20-21]. were used to understand the adsorption dynamics concerning time for the MB-AC-3 system. The equation and parameters of these models are shown in Table 1.

Table 1: Nonlinear kinetic, isothermal and intraparticle diffusion models

Models	Names	Expression
Isotherms	Langmuir	$Q_e = \frac{q_m b C_e}{1+bC_e}$ $R_L = \frac{1}{1+b\,C_0}$
	Freundlich	$R_l = \frac{1}{1+k_a C_e}$ $q_e = K_f C_e^{\frac{1}{n_F}}$
kinetics	Pseudofirst order	$q_t = q_e[1 - e^{K_1 t}$ $h_0 = K_1 q_e$
	Pseudo Second Order	$q_t = \frac{K_2 q_e^2 t}{1+K_2 q_e t}$ $h_2 = K_2 q_e^2$

©2024 Great Britain Journals Press

intraparticle diffusion	$K_i = \frac{Q_t}{t^{1/2}}$ $q_t = K_{id} t^{0,5} + C$

Source: BEDIN, et al., 2018., CAZETTA et al., 2011

Langmuir's constant Ka; kf = and nF = Freundlich constants; K1 and K2 = Pseudo-first-order and pseudo-second-order constants; h0 = initial adsorption; kid= intraparticle diffusion; C = intercession

Both the adsorption isotherms and the pseudo-first and pseudo-second-order kinetic models were fitted using the nonlinear fitting method, using the Origin 8.5 software. The adequate theoretical models that describe the experimental data of the system were chosen from the correlation coefficient (R^2). In addition, the experimental data were evaluated by the chi-square (χ^2) model (Eq. 3) and by the values of normalized standard deviation (Δqe) (Eq.4) [19-20].

$$X^2 = \sum_{i=1}^{n} \frac{(q_{e\,cal} - q_{e\,exp})^2}{q_{e\,cal}} \qquad (Eq.\ 3)$$

$$\Delta_{q_e}(\%) = 100\sqrt{\frac{\Sigma[(q_{e\,exp} - q_{e\,calc})q_{e\,exp}]^2}{n-1}} \qquad (Eq.\ 4)$$

Where $q_{e\ exp}$ (mg g^{-1}) is the experimental adsorption capacity, calculated q_e (mg g^{-1}) is the adsorption capacity calculated from the kinetic model and n is the number of treatments.

2.5 Thermodynamics

The effect of temperature on the adsorption of MB dye by FSDSG particles was investigated at concentrations of 60; 75, and 90 mg L^{-1} with pH = 7.0, containing 0.1 g of FSDSG, stirring speed = 200 rpm; T = 30, 50, and 70°C kept constant through the use of an incubator bath with magnetic agitation (MARCONI/MA 085/CT). The duration of each trial was eight hours. The thermodynamic parameters of Gibbs free energy change (ΔG °, kJ mol^{-1}), enthalpy change (ΔH °, J mol^{-1}), and entropy change (ΔS°, J mol^{-1} K^{-1}) were calculated from equations 5 and 6 [24-25], Ke is the dimensionless constant obtained from the qe/Ce ratio defined through Equation 5 (Eq. 5), R is the universal gas constant (8.314 J mol^{-1} K^{-1}), and T is the temperature in Kelvin.

$$lnK_e = \frac{\Delta S}{R} - \frac{\Delta H}{RT} \qquad (Eq.\ 5)$$

R is the universal constant of ideal gases, whose value is 8.314 J mol^{-1} K^{-1}, and T is the temperature in Kelvin.

The values of ΔH and ΔS can be determined experimentally. For example, the graph of ln Ke versus 1/T generates a line, and the slope is - ΔH /R, and the linear coefficient corresponds to ΔS/R. With the values of ΔH and ΔS calculated, it is possible to calculate the Gibbs free energy (ΔG) value for a given temperature through Equation 6 (Eq.6).

$$\Delta G = \Delta H - T\Delta S \qquad (Eq.\ 6)$$

III. RESULTS AND DISCUSSION

3.1 General Characteristics and Properties of FSDSG

The encapsulating material developed is of vegetable origin and was obtained from the dried and degreased guava seed. Visually, the product appeared in the form of a fine, loose powder with light cappuccino brown colors. The results regarding the proximate composition, seed yield obtained based on the raw guava waste, properties of the dry and defatted flour of guava seeds, and the yield after standardization of granulometry at 80 mesh are presented Table 2.

©2024 Great Britain Journals Press

Table 2: Centesimal Composition of Guava Seeds and Yield, Characterization of Dry and Defatted Guava Seed Flour and Yield

Centesimal Composition of Guava Seeds and Yield	
seed yield % (m m^{-1})	48.11 ± 0.30
Fiber % (m m^{-1})	58.15 ± 1.32
carbohydrates % (m m^{-1})	18.7 ± 1.0
lipids % (m m^{-1})	10.82 ± 0.20
proteins % (m m^{-1})	8.71 ± 0.30
energy content (kcal $100g^{-1}$)	206.2 ± 5.4
FSDSG Properties and Yield	
FSDSG Yield % (m m^{-1})	34.42 ± 0.14
Solubility % (m m^{-1})	1.95 ± 0.54
Wetability (min)*	10.13 ± 0.02
hygroscopicity (g água $100g^{-1}$)	7.33 ± 1.10
bed density (g cm^{-3})	0.29 ± 0.05
compacted density (g cm^{-3})	0.46 ± 0.04

Buoyancy and submersion time in minutes

3.2 Characterization of the Encapsulating Material

3.2.1 Morphology by Analysis of Energy Dispersive X-ray Spectroscopy Coupled to SEM.

Energy dispersive X-ray spectroscopy provides information on the chemical composition of the elements in the sample. Figure 1 and Table 3 show the relative spectrum and atomic composition of the encapsulating material, respectively, obtained from guava seed, while Figure 2 shows images representing the material's morphology at different scales.

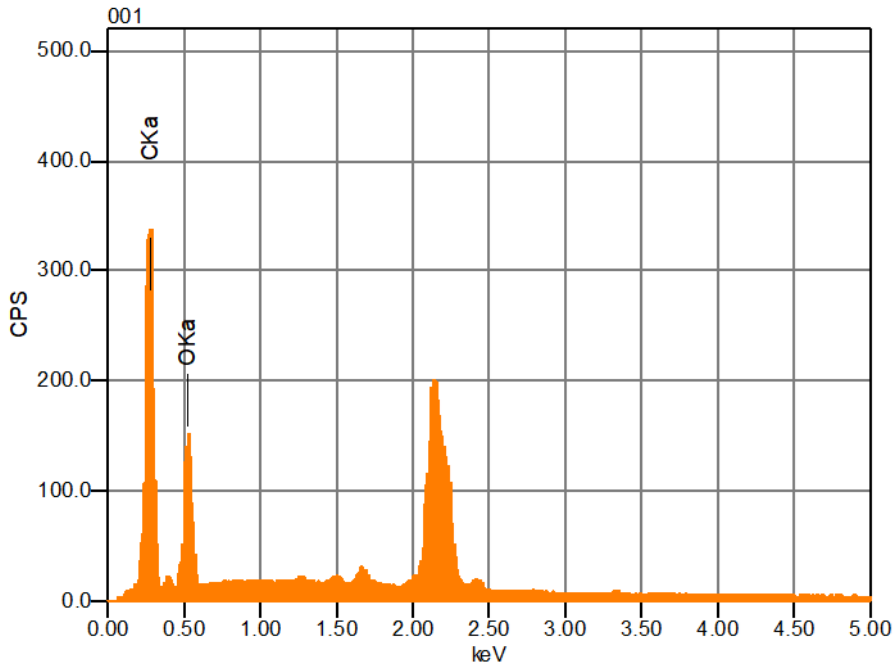

Fig. 1: EDS Spectrum of the Encapsulating Material

©2024 Great Britain Journals Press

Table 3: Elemental Composition of the Encapsulating Material

Elements detected	Mass(%)	atom
C	60,79	67,37
O	39,21	32,63

The EDS analysis indicated that the encapsulating material obtained has only carbon (O) and oxygen (O) in its elemental composition

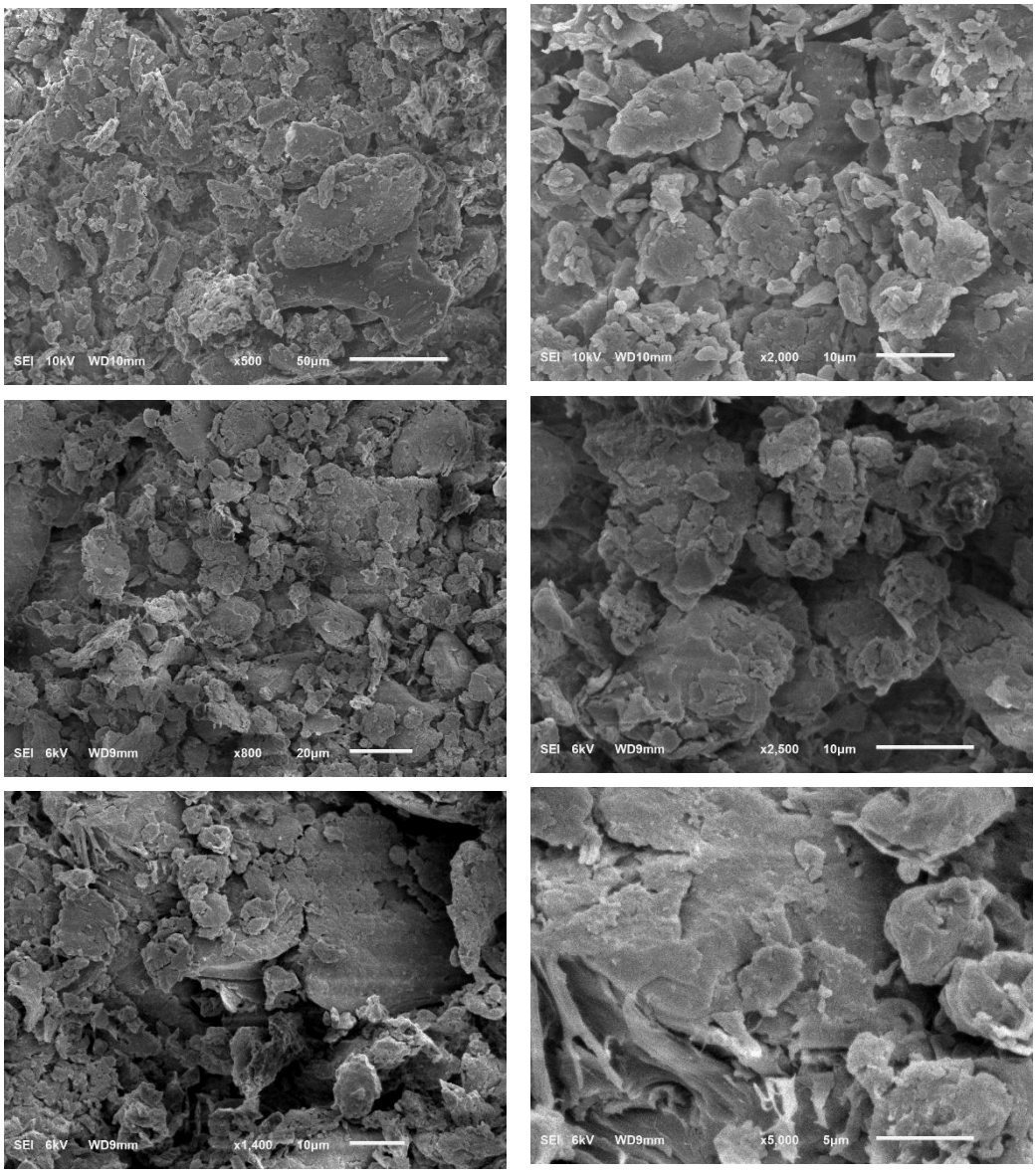

Fig. 2: Micrographs of Encapsulating Material Obtained from Guava Seeds

The SEM images at different scales show that the particles of the encapsulating material developed from degreased guava seeds have geometrically irregular surfaces. This characteristic may favor the process of microencapsulation of other materials in their structure.

3.4 Spectroscopy in the Infrared Region

Analyzing the presence of functional groups in the raw material before and after going through the lipid extraction process indicates whether there was complete removal of the lipid fraction present in the encapsulating material developed (FSDSG),

©2024 Great Britain Journals Press

whose spectra were obtained in the infrared region and are represented in Figure 3.

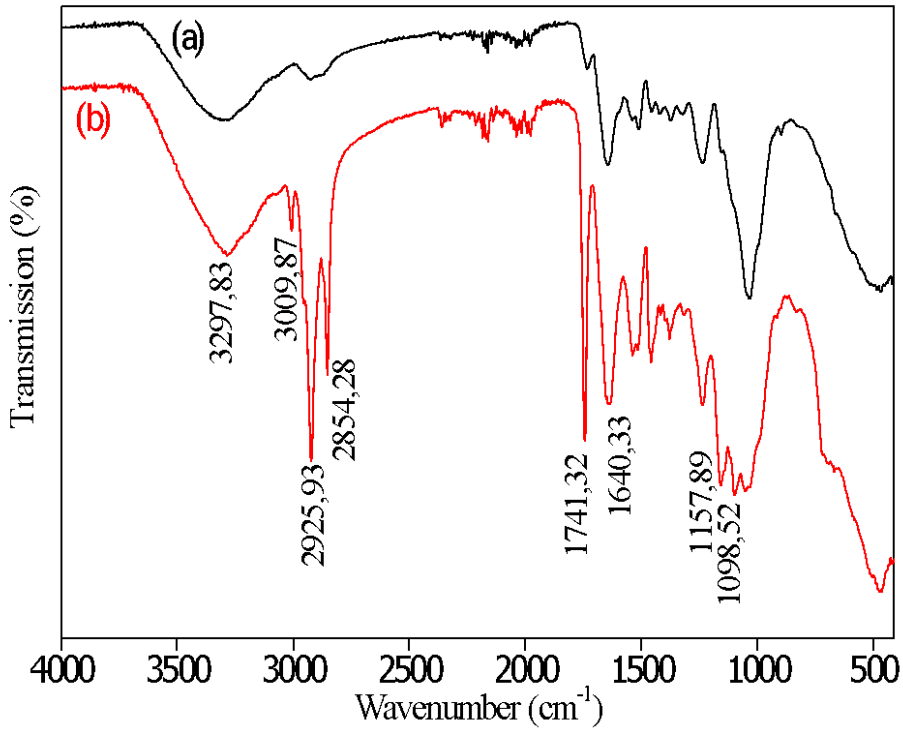

Fig. 3: Spectroscopy in the Infrared Region: (a) Dry and Defatted Guava Seed Flour (encapsulating material), (b) Dry Guava Seed Flour

It is possible to observe in Figure 3(a) that the spectrum of the encapsulating material obtained after the process of removing lipid compounds, has a spectral profile different from that of spectrum 3(b), which represents the guava seed just dry, still with lipid content gift. The spectra have bands in common, highlighting the band present at 3297.83 cm^{-1} due to the stretching of the -OH bond. At 3009.87 cm^{-1}, a band appears that can be attributed to the stretching of the N-H bond associated with amide and is consistent with the band present at 1640.33 cm^{-1}, characteristic of the amide carbonyl group, which is also common in encapsulating material developed, but it is present to a lesser extent. When analyzing spectrum 3(b), there are two bands at 2925.93 and 2854.28 cm^{-1}, which are attributed to stretching of C-H bonds with sp^3 hybridization due to symmetrical and asymmetrical vibrations of the C-H bond. The intense and narrow band present at 1741.32 cm^{-1} is typical of carbonyl stretching (C=O) as described by Pavia et al. (2010), which was consistent with the presence of fatty acid ester present in guava seed, observed in the spectrum (b), thi is the most important in the analysis performed, as it is absent in the encapsulating material, which had the acid content removed, indicating that the material had the lipid fraction successfully removed. The bands in 1157.89 and 1098.52 cm^{-1} can be attributed to the stretching of C-O bonds.

3.5 Propriedade Estrutural

Determining the textural properties of encapsulating material is of great value for the knowledge of its characteristics, as it provides essential information about the material, such as surface area, volume, and pore size, data displayed in Table 4 for the material developed. The N_2 adsorption/desorption isotherms are represented in Figure 4.

©2024 Great Britain Journals Press

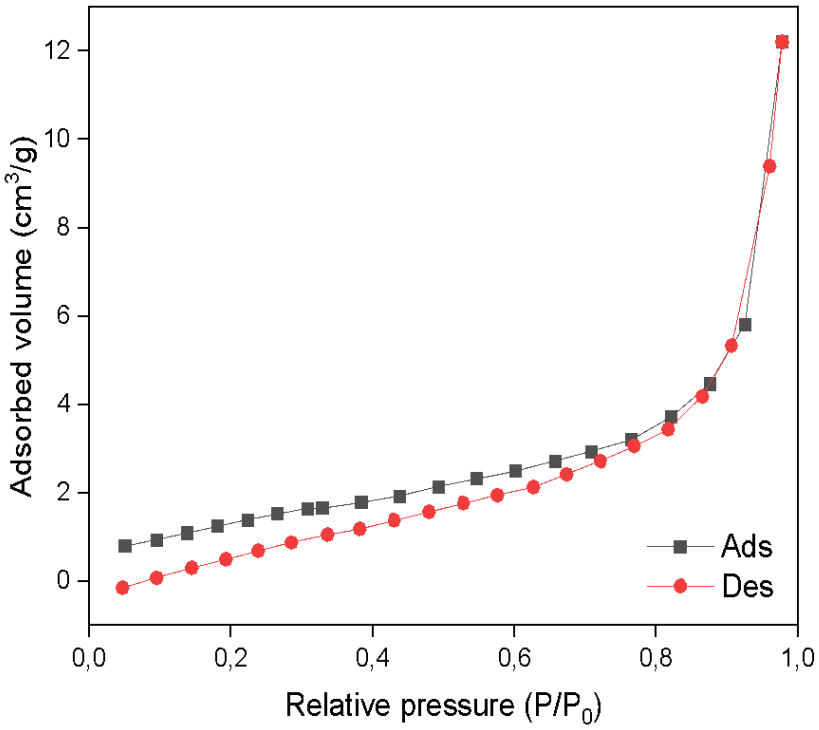

Fig. 4: Isotermas de adsorção/dessorção de N_2 da amostra FSDSG

Table 4: FSDSG sample Texture Properties Obtained from N2 Adsorption/Desorption Analysis

	Surface area (multiPoint S_{BET}) (m^2/g)	pore volume (cm^3/g)*	pore size (nm)*
FSDSG	5.401	$1.342x10^{-2}$	5.438

** DFT method*

Depending on the pore size of a material, it can be classified as macro, meso, or microporous. If the pore diameter exceeds 50 nm, it characterizes a macroporous solid, if the pore size is between 2 and 50 nm, it is characteristic of a mesoporous solid, and if the size is less than 2 nm, it is considered a microporous solid, which subdivided into solid ultra-micropores (pore diameter <0.7 nm), medium-sized micropores (0.7 nm < pore diameter <0.9 nm) and supermicropores (pore diameter >0.9 nm) [25-26]. After analyzing the results obtained in the texture analysis, it was possible to infer that the encapsulating material (FSDSG) is a mesoporous solid due to its pore size of 5.438 nm. The pore size of the material is interesting, as materials with a minimal pore size can make it difficult to encapsulate other materials in their available sites since the material to be encapsulated must be able to access the pore that the encapsulating material does. Following the classification described by the IUPAC, the N_2 adsorption/desorption isotherms have six distinct classifications. Thommes et al. (2015) describe that each isotherm characterizes a solid as a function of the pore size of the adsorption phenomenon. Type I isotherms are typical of microporous solids; types II and IV are characteristics of non-porous solids and macroporous solids, respectively. Types III and V isotherms are typical of systems where the adsorbate molecules interact more with each other than with the solid; finally, type VI

©2024 Great Britain Journals Press

isotherms occur with the adsorption of a gas by a non-porous solid with a uniform surface, which is a rarer phenomenon. The N_2 FSDSG adsorption/desorption isotherms obtained for the material developed here are shown in Figure 4.

Due to the shape of the isotherm obtained for FSDAG, it can be inferred that the isotherm has a type IV isotherm characteristic, as Figure 4 shows a small hysteresis, which characterizes a mesoporous solid, information that corroborates the data obtained in the associated texture analysis and pore size.

3.5 Thermogravimetric Analysis

The thermogravimetric analysis was performed based on pre-defined atmospheric and temperature conditions and allowed the assessment of the material's thermal stability. This technique makes it possible to know the changes that heating can cause in the mass of substances, allowing us to establish the temperature range in which they acquire a fixed, defined, and constant chemical composition, the temperature at which they begin to decompose, and to monitor the progress of dehydration reactions (moisture loss), oxidation, combustion, and decomposition [27]. The result of the thermal analysis of the encapsulating material (FSDSG) obtained from defatted guava seeds is represented in Figure 5, where the mass loss curves (TG) and the mass loss curve derivative (DTG) are exposed.

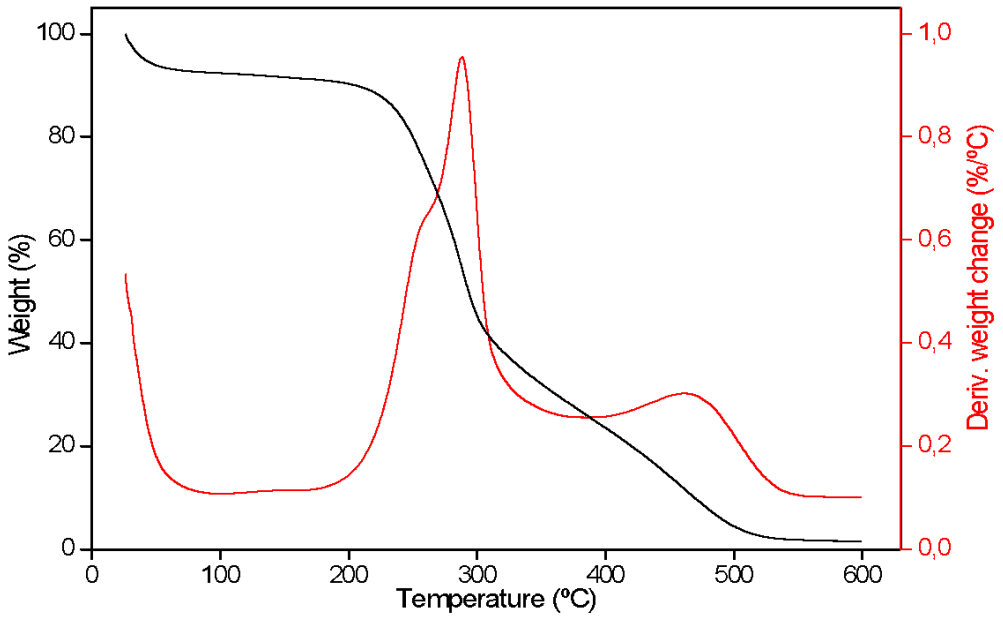

Fig. 5: Mass Loss Curve (TG) and the Derivative of Mass Loss Curve (DTG)

Looking at Figure 5, the mass loss curve of FSDSG showed a mass loss of approximately 8% during the temperature variation from 25°C to 175°C, resulting from the loss of residual water from the sample. However, the significant mass loss occurred between 225°C and 375°C. Through the DTG curve, it was possible to determine the temperature at which the maximum mass change rate (decomposition) is around 288°C, indicating that the material is thermally stable up to a temperature of 225°.

It is essential to know the thermal stability of material under development, as it makes it possible to predict its applications in several areas. For example, when referring to HTST (High-Temperature Short Time), heat treatment processes combine heat, humidity, and mechanical work, profoundly modify the raw materials and provide new formats and structures with different functional and nutritional characteristics [28]. Among these materials

©2024 Great Britain Journals Press

industrialization processes, we can highlight the extrusion process, which has been widely used in the last decades in the food industries due to its numerous advantages such as versatility, continuous production on a large scale, and per unit area low cost. With investment, labor, and energy, the quality of products with better functional, sensory, and nutritional characteristics is a process that does not generate effluents [29].

Aiming at the possible use of FSDSG as an encapsulating material, it is possible to carry out microencapsulation tests up to a temperature close to 225°C, above this value. The material begins the process of degradation of its chemical composition.

3.6 Point of Zero Charge

The point of zero charges (pHpcz) is one of the essential characteristics of the surface of adsorbent material, as it corresponds to the pH value of the liquid surrounding the material when the sum of the positive charges is equivalent to the sum of the negative charges on the surface. The pH_{PCZ} value characterizes the acidity of the material's surface [30-31]. Thus, in an aqueous medium, the particles have a positive surface charge if the pH of the solution is lower than the pH_{PCZ} and a negative surface charge if the pH of the solution is higher than the pH_{PCZ} [32]. The results referring to the determination of the pH_{PCZ} of the FSDSG are shown in Figure 6.

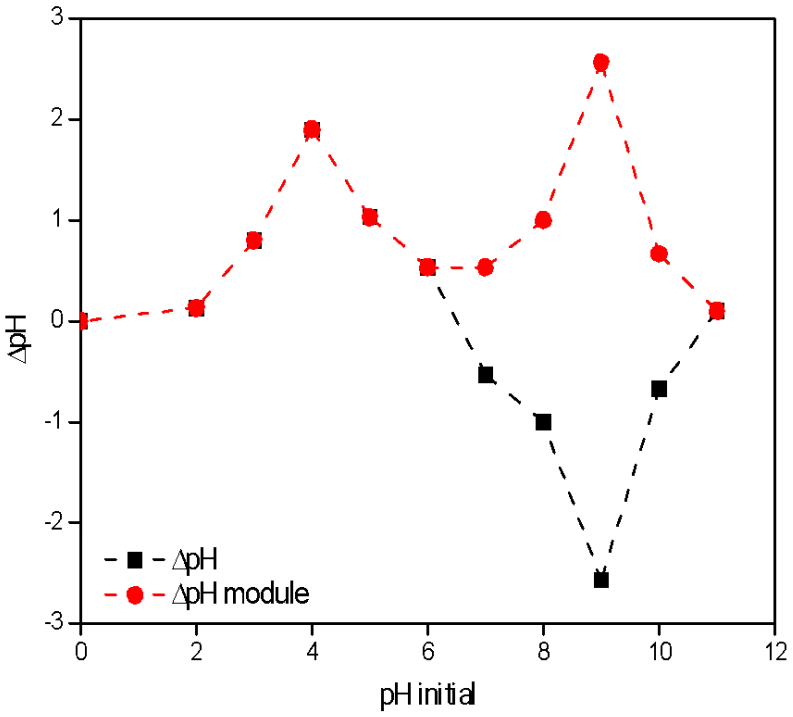

Fig. 6: Determination of pH at Zero Load point of Dry and Defatted Guava Seed Flour at 80 Mesh

To understands the adsorption mechanism, is necessary to determine the pHPCZ. The adsorption of cationic dyes is favored at pH higher than pHPCZ, while the adsorption of anionic dyes is favored at pH lower than pHPCZ [33]. Thus, according to Figure 6, the pHPCZ FSDSG is equivalent to 2.0 and 11.0. In the pH range below 2.0 and above 11.00, the surface charges of the material are predominantly negative. Adsorption, for example, essential (nonpolar) oils, may be preferable at these pH values. Above 2.0 and below 11.00, its surface predominates positive charge, favoring polar molecules' adsorption.

©2024 Great Britain Journals Press

3.7 Adsorption Isotherm

The Langmuir isotherm was obtained through the correlation between Ce/qe as a function of Ce. The values of kL and qm were determined, respectively, from the linear and angular coefficients of the equation obtained by the linear regression of the line, allowed assessing whether the adsorption process is favorable (Table 5).

Table 5: Langmuir Isotherm Parameter Values for MB Adsorption by FSDSG Microparticles

Parameter	Value
Q_{max} (mg g^{-1})	57,95
K_L (L mg^{-1})	8,9645
R_L	0,0037 – 0,0012
R^2 adjusted	0,9613

Analyzing the Langmuir isotherm data, it is evident that the adsorption process fits this model well since the adjusted R^2 value is 0.9613, and the RL values, whose range is between zero and one, indicate that adsorption is favorable [34]. The value of the maximum adsorption capacity, qmax (mg g^{-1}), is essential to identify the adsorbent with the highest adsorption capacity [35]. The value of qmax depends on several factors, such as the adsorbent's characteristics and mass and the adsorbate's volume and concentration. The FSDSG microparticles used in this study showed a promising MB incorporation capacity, showing that they are suitable for incorporating active principles.

The Freundlich isotherm was obtained by correlating ln qe as a function of ln Ce. The kf 1/n values were determined by the linear and angular coefficients of the equation obtained by the linear regression of the line. These parameters and the adjusted R^2 value are represented in Table 6.

Table 6: Values of Freundlich Isotherm Parameters for Adsorption of MB by FSDSG Microparticles

Parameter	Value
K_f (L mg^{-1})	1,0155
1/n	0,5679
n	1,7609
R^2 adjusted	1,0000

Analyzing the data found for this model, it is evident that it has an adjusted R^2 value above 0.9999. Thus, the experimental data fit well to this model, which considers the adsorbent constituted of multiple layers and is applicable for reversible adsorption on heterogeneous surfaces, with available sites with different adsorption energies [36].

The value of 1/n less than 1.0 indicates that the adsorption applies to the range of MB concentrations evaluated in this study [37] and reveals that the adsorption occurs by heterogeneous means, with the high-energy sites being occupied first. Then adsorption occurs at lower-energy sites [38]. The value of n greater than 1.0 shows that the process of adsorption of MB by the FSDSG microparticles was favorable.

3.8 Adsorption Studies

The results for the pseudo-first-order kinetic model were obtained through the linearized Lagergren equation, through the construction of a graph of ln (qe - qt) as a function of time for each value of the initial concentration of MB. The values corresponding to qe for the linearized Lagergren equation were those obtained experimentally (qe exp). The parameters calculated qe (qe calc) and k1 were determined from the linear and angular coefficients of the equations formed by the regression of ln (qe - qt) as a function of time. These parameters and the values of the correlation coefficient (R^2) adjusted normalized standard deviation (Δqe), and the chi-square model (χ^2) are presented in Table 7.

©2024 Great Britain Journals Press

Table 7: Kinetic Parameters for the Pseudo-First-Order model, Chi-square model (χ2), and normalized standard deviation ($\Delta_q e$) of different initial concentrations of MB

	Initial Concentrations (mg L^{-1})				
	30	45	60	75	90
$q_{e\ exp}$ (mg g^{-1})	13.84	19.80	26.02	32.12	37.48
$q_{e\ calc}$ (mg g^{-1})	0.65	16.75	15.7	21.97	32.49
K (min^{-1})	-0.0001	-0.0039	-0.0019	-0.0024	-0.0042
R^2 adjusted	0.0006	0.5006	0.1203	0.2506	0.4590
Δq_e	47.6567	7.6908	20.0860	15.8002	6.6594
X^2	268.1992	0.5536	7.0180	4.6900	0.7670

After analyzing the R^2 values, it is evident that the adsorption process does not present a good fit for the pseudo-first-order kinetic model. Further more, there is a discrepancy between the experimental and calculated qe values. These data suggest that the process of MB adsorption by FSDSG microparticles does not follow this kinetic model.

The k_1 parameter plays a time scaling factor. The higher the value of k_1, the shorter the time taken for the adsorption system to reach equilibrium. Relatively high values of k1 indicate shorter times for the system to reach equilibrium. However, some studies report that the value of k1 may be linked to the dependence or independence of operating conditions [35].

A low correlation coefficient was found with the application of this model. This parameter cannot be used in this work to evaluate the speed with which the system reaches equilibrium. Pseudo-first order kinetics is controlled by diffusion through the boundary layer around the adsorbent solid [35]. Therefore, it is possible to state that diffusion is not the determining step of the process in question since this model did not present a good fit for the experimental data.

In the pseudo-second-order kinetic model for the adsorption of MB by the FSDSG microparticles, the values of q_e exp, q_e calc, and k_2 were obtained using the linearized equation and building a graph t/qt as a function of time for each value of the initial concentration of MB, these parameters and the adjusted R^2 values are shown in Table 8.

Table 8: Kinetic parameters for the pseudo-second order model, chi-square model (χ2) and normalized standard deviation (Δqe) of different initial concentrations of MB

	Initial Concentrations (mg L^{-1})				
	30	45	60	75	90
$q_{e\ exp}$ (mg g^{-1})	13.84	19.80	26.02	32.12	37.48
$q_{e\ calc}$ (mg g^{-1})	14.30	19.72	25.75	31.76	37.21
K_2 (min^{-1})	0.0750	0.0505	0.0382	0.0309	0.0266
R^2 adjusted	0.9982	0.9999	0.9999	0.9999	0.9999
Δq_e	2.3866	0.0606	0.2567	0.2875	0.1807
X^2	0.1080	0.0001	0.0028	0.0043	0.0020

©2024 Great Britain Journals Press

Through Table 8, was possible to observe the data obtained through the adjustment performed by the kinetic model of pseudo-second-order adsorption. This model's correlation coefficient (R^2) was more significant than 0.99 at different concentrations. The applicability of the pseudo-second-order kinetics model was confirmed by the low values of normalized standard deviation (Δqe). Was also possible to observe that the calculated qe values obtained through the adjustment are very close to the experimental q_e.

It is evidenced that K_2 values decrease with increasing concentration. These low values show that the adsorption process is slow, and equilibrium was not reached quickly. The oscillations of these values are linked to the operational conditions and the initial concentration of solute [35].

Kinetic studies are essential tools for understanding the interaction dynamics between the adsorbent and the adsorbate. These provide information that can help model and design adsorption processes. For example, the adsorption kinetics data for MB dye were analyzed using the pseudo-second-order kinetic model shown in Figure 7.

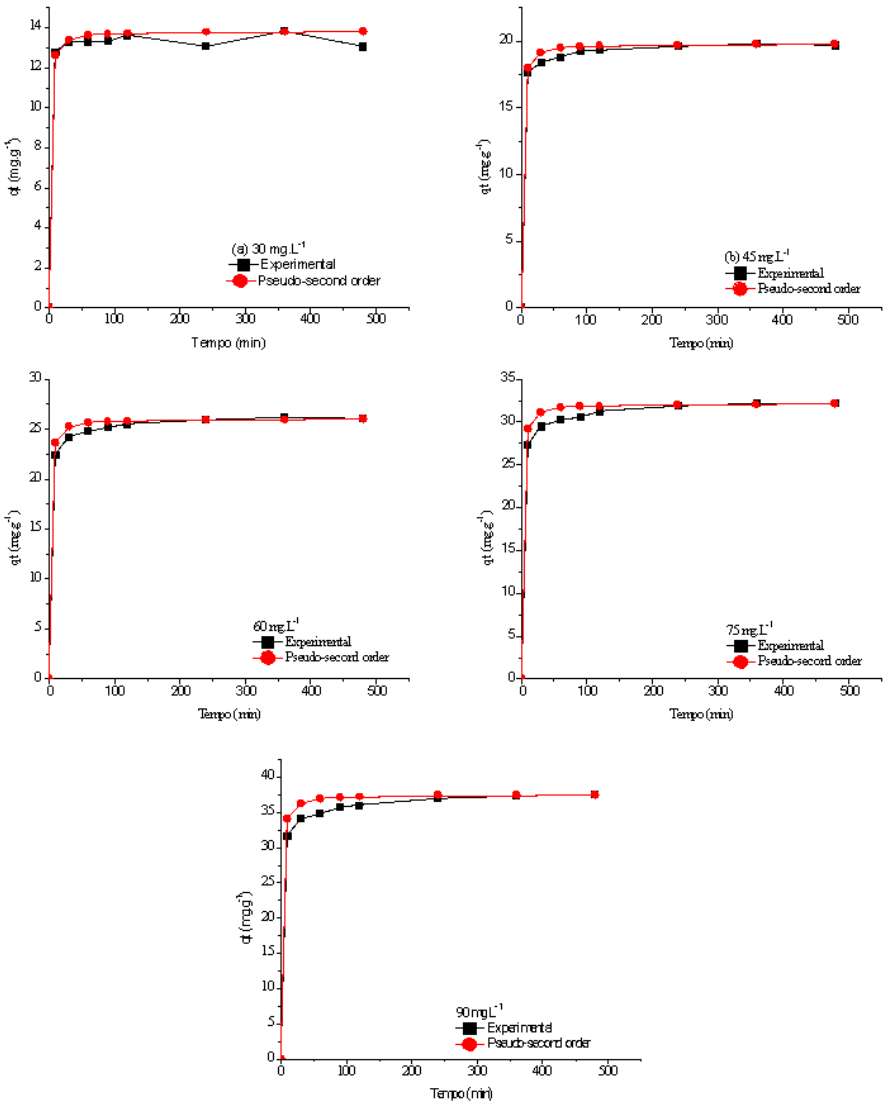

Fig. 7: Non-linear fit of the pseudo-second order kinetic study for different MB concentrations. MB concentrations of 30 (a), 45 (b), 60 (c), 75 (d) and 90 (e) mg L^{-1}

©2024 Great Britain Journals Press

According to Figure 7, the MB dye adsorption system by the FSDSG microparticles reached equilibrium during the first 60 min of the test, demonstrating that the interactions were favorable between the adsorbent and the adsorbate.

The model based on the theory described by Weber and Morris (1963) was applied to the adsorption system to identify the intraparticle diffusion mechanism. The value found through the slope of the line corresponds to the intraparticle diffusion constant (k_{di}). In contrast, the approximate value of the boundary layer thickness (C_i) is obtained at the intercept of the line. The intraparticle diffusion model can generally occur through the following steps: external diffusion, surface diffusion, and pore diffusion [39].

Table 9 shows the values of kdi, C_i, and correlation coefficient (R^2) obtained for the different concentrations. The (R^2) values are smaller than predicted by the pseudo-second-order model, so the experimental q_e value does not agree well with the intraparticle diffusion model.

Table 9: Intraparticle Diffusion Model Constants and Correlation Coefficients for Adsorption

	intraparticle Diffusion		
C_o (mg L^{-1})	K_{di} (mg g^{-1} $min^{-1/2}$)	C_i (mg g^{-1})	R^2
30	0.0404	12.57	0.1191
45	0.0997	17.90	0.7930
60	0.1637	23.10	0.7506
75	0.2167	28.33	0.6929
90	0.2715	32.33	0.8301

The values related to the five different initial concentrations showed two stages of linearity. The first stage was completed in the first 60 min, known as instantaneous adsorption. The second region is the gradual adsorption stage, where intraparticle diffusion is the rate-limiting. The linear behavior did not pass through the origin or close to saturation, which indicates that intraparticle diffusion is not the step that determines the rate of adsorption, so other interaction mechanisms must act simultaneously to control the adsorption process [40-41-42-43].

3.9 Thermodynamic

The thermodynamic study is based on the determination of quantities, enthalpy variation (ΔH°), entropy variation (ΔS°), and variation of Gibbs free energy (ΔG°). By estimating these thermodynamic parameters, it is possible to determine whether the process is spontaneous, exothermic, or endothermic and whether the adsorbent material has an affinity for the adsorbate. In addition, these parameters can provide information regarding the heterogeneity of the adsorbent surface and whether the process involves physical or chemical adsorption [44].

Table 10 shows the values of the Gibbs free energy variation (ΔG°), kc, and adjusted correlation coefficient (R^2), obtained for the adsorption of MB dye by FSDSG microparticles at 60, 75, and 90 mg L^{-1}. From the thermodynamic data, was possible to verify that ΔG° varies from -28.80 to -64.86 kJ mol^{-1}, having significant oscillations during the adsorption process.

Table 10: Values of Gibbs free energy variation (ΔG°), kc and adjusted correlation coefficient (R2) for the adsorption of methylene blue by FSDSG microparticles

Concentration (mg L^{-1})	kc	ΔG° (kJ mol^{-1})	R^2
60	3.52	-44.10	0.9999
75	2.10	-64.86	0.8619
90	1.62	-28.80	0.9295

©2024 Great Britain Journals Press

With the initial concentration of MB of 60 mg L^{-1}, obtaining the highest correlation coefficient (R^2) adjusted for the adsorption was possible. Therefore, this condition was selected to monitor the adsorption process and to determine the values of ΔH, and ΔS. Table 11 shows the values of the Gibbs free energy change ((ΔG° kJ mol^{-1}), kc, enthalpy change (ΔH, kJ mol^{-1}) and entropy change (ΔS, J mol^{-1}) K^{-1}) for the adsorption of MB by the FSDSG microparticles at an initial concentration of 60 mg L^{-1}.

Table 11: Values of (ΔG° kJ mol^{-1}), kc, (ΔH°, kJ mol^{-1}) and (ΔS°, J mol-1 K^{-1}) for the adsorption of AM dye by FSDSG microparticles on initial concentration of 60 mg L-1

T (K)	k_c	ΔG° (KJ mol^{-1})	ΔH° (KJ mol^{-1})	ΔS° (J $mol^{-1}K^{-1}$)
303.15	3.5	-22.34		
323.15	2.4	-46.26	-22.47	-73.62
343.15	1.8	-47.73		

The results concerning the thermodynamics of the adsorption process revealed that it is spontaneous (ΔG° = -46.26 kJ mol^{-1}) and exothermic (ΔH° = -22.47 kJ mol^{-1}). The negative value of ΔS° (-73.62 J mol^{-1} K^{-1}) suggests that the dye molecules are stable on the surface of the adsorbent and that there is a decrease in randomness at the solid-solute interface during adsorption. In addition, the value confirms the affinity of the adsorbent material for the dye.

With increasing temperature, a reduction in adsorption at equilibrium occurs, causing a decrease in kc values and an increase in ΔG°, indicating a reduction in spontaneity. The increase in the value of ΔG° being proportional to the increase in temperature indicates that the lower the temperature, the easier the adsorption [45]. This decrease in adsorption capacity can be explained by the increase in temperature, which possibly causes an increase in MB solubility, which makes its adsorption difficult since the dye will have more affinity with the solvent than with the adsorbent.

Ahmad and Kumar (2010b) reported that the enthalpy change due to chemisorption has values between 84 - 420 KJ mol^{-1}. Thus, enthalpy values below 84 KJ mol^{-1} indicate that the nature of adsorption is physical, involving weak attractive forces [46]. Entropy is entirely linked to disorganization at the adsorbent/adsorbate interface. Positive values of ΔS are interpreted as an increase in disorganization at the adsorbent material interface [40].

IV. CONCLUSION

This work made it possible to prepare good quality encapsulating material with guava seeds, as demonstrated by the characterization tests. In addition, a good yield of flour mass was obtained through cheap and abundant agro-industrial waste. The results showed that the material has promising physical and chemical characteristics as an encapsulating material for the methylene blue dye.

The adsorption of methylene blue by microparticles of dry and defatted guava seed flour is best explained by the pseudo-second-order model, indicating that the adsorption is controlled by sharing or transferring electrons between the adsorbent and adsorbate molecules. Regarding the adsorption equilibrium, the experimental results adjusted all tested isothermal models.

The results referring to the thermodynamics of the adsorption process revealed that it was spontaneous and exothermic. The negative value of ΔS suggests that the dye molecules are stable on the surface of the adsorbent and that there is a decrease in randomness at the solid-solute interface during adsorption. In addition, the value confirms the affinity of the adsorbent material for the dye.

©2024 Great Britain Journals Press

REFERENCE

1. PÉREZ GUTIÉRREZ, R. M., MITCHELL, S., & VARGAS SOLIS, R. Psidium guajava: a review of its traditional uses, phytochemistry and pharmacology. Journal of Ethnopharmacology, 117(1), 1–27, 2008. https://doi.org/10.1016/j.jep.2008.01.025.
2. STEINHAUS, M., SINUCO, D., POLSTER, C., OSORIO, C., & SCHIEBERLE, P. (2008). Characterization of the aroma-active compounds in pink guava (Psidium guajava L.) by application of the aroma extract dilution analysis. Journal of Agricultural and Food Chemistry, 56(11), 4120–4127, 2008. https://doi.org/10.1021/jf8005245.
3. MERCADANTE, A. Z., STECK, A., & PFANDER, H. (1999). Carotenoids from guava (Psidium guajava L.): Isolation and structure elucidation. Journal of Agricultural and Food Chemistry, 47(1), 145–151. https://doi.org/10.1021/jf980405r.
4. GONZÁLEZ, I. A., OSORIO, C., MELÉNDEZ-MARTÍNEZ, A. J., GONZÁLEZ-MIRET, M. L., & HEREDIA, F. J. Application of tristiumuls colorimetry to evaluate color changes during the ripening of Colombian guava (Psidium guajava L.) varieties with different carotenoid pattern. International Journal of Food Sciences and Nutrition, 46(4), 840–848, 2011. https://doi.org/10.1111/j.1365-2621.2011.02569.x.
5. IBGE – Instituto Brasileiro de Geografia e Estatística – SIDRA - Produção Agrícola Municipal 2021 - Tabela 5457 - Área plantada ou destinada à colheita, área colhida, quantidade produzida, rendimento médio e valor da produção das lavouras permanentes (notas). Disponível em https://cidades.ibge.gov.br/brasil/pesquisa/15/0, acesso em 17/out. 2022.
6. EMBRAPA - Coleção Plantar. 66 (2010). A cultura da goiaba [editores técnicos: Flávia Rabelo Barbosa e Mirtes Freitas Lima] – 2ª edição revista e ampliada – Brasília, DF: Embrapa Informação Tecnológica, 2010. 180p. Disponível em: https://ainfo.cnptia.embrapa.r/digital/bitstream/item/128279/1/PLANTAR-Goiaba-ed02-2010.pdf
7. OSORIO, C.; FORERO, D.P.; CARRIAZO, J. G. Characterisation and performance assessment of guava (Psidium guajava L.) microencapsulates obtained by spray-drying. Food Research International, v. 44, n. 5, p. 1174-1181, 2011. https://doi.org/10.1016/j.foodres.2010.09.007.
8. SOUZA, G. R., NASCIMENTO M., E., OLIVEIRA S., P., MERSON, A. A., LIMA S., J. R. C., MARQUES, F. C., SOUZA, T. D. S. Desenvolvimento de material encapsulante a partir da farinha seca e desengordurada de semente de goiaba. Brazilian Journal of Development, v. 6, n. 12, p. 98027-98037, 2020. https://doi.org/10.34117/bjdv6n12-337
   CANO-CHAUCA, M et al. Effect of the carriers on the microstructure of mango powder obtained by spray drying and its functional characterization. Innovative Food Science & Emerging Technologies, v. 6, n. 4, p. 420-428, nov./dez, 2005. https://doi.org/10.1016/j.ifset.2005.05.003
   FUCHS, M. et al. Encapsulation of oil in powder using spray drying and fluidised bed agglomeration. Journal of Food Engineering, v. 75, n. 1, p. 27–35, jun./jul, 2006. doi: https://doi.org/10.1016/j.jfoodeng.2005.03.047
   CAI, Y. Z.; CORKE, H. Production and Properties of Spray-dried Amaranthus Betacyanin Pigments. Journal of food science, Chicago, v. 65, n. 3600, p. 1248–1252, jun./jul. 2006. https://doi.org/10.1111/j.1365-2621.2000.tb10273.x.
   JINAPONG, N.; SUPHANTHARIKA, M.; JAMNONG, P. Production of instant soymilk powders by ultrafiltration, spray drying and fluidized bed agglomeration. Journal of Food Engineering, Essex, v. 84, n. 2, p. 194–205, dez./jan. 2008. https://doi.org/10.1016/j.jfoodeng.2007.04.032.
   GOULA, A. M.; ADAMOPOULOS, K. G. A method for pomegranate seed application in food industries: Seed oil encapsulation. Food and Bioproducts Processing, Rugby, v. 90, n. 4, p. 639-652, set./out, 2012. https://doi.org/10.1016/j.fbp.2012.06.001.
9. SILVA, E. P. D., SILVA, D. A. T. D., RABELLO, C. B. V., LIMA, R. B., LIMA, M. B.,

©2024 Great Britain Journals Press

& LUDKE, J. V. Composição físico-química e valores energéticos dos resíduos de goiaba e tomate para frangos de corte de crescimento lento. Revista Brasileira de Zootecnia, v. 38, n. 6, p. 1051-1058, 2009. Disponível em: https://www.scielo.br/j/rbz/a/vK3tG7XYc9fpHVZc6zd5qNc/?format=pdf&lang=pt.

10. SILVEIRA, MÁRCIA LILIANE RIPPEL et al SILVEIRA, M. L. R., DOS SANTOS, C. O., PENNA, N. G., SAUTTER, C. K., DA ROSA, C. S., & BERTAGNOLLI, S. M. M. Aproveitamento tecnológico das sementes de goiaba (Psidium guajava L.) como farinha na elaboração de biscoitos. Boletim do Centro de Pesquisa de Processamento de Alimentos, v. 34, n. 2, 2017. http://dx.doi.org/10.5380/cep.v34i2.53178.
11. SOARES, D. J., DIOGENES, A., MOURA NETO, L. G., COSTA, Z. R. T., ALVES, V. R., SANTOS, M., & MORAIS, B. Utilização de farinha de resíduos de goiaba na elaboração de pães. Revista CIENTEC, v. 9, n. 1, p. 97-103, 2017. Disponível em: http://revistas.ifpe.edu.br/index.php/cientec/article/view/39/32.
12. THOMAZ, A. U., SOUSA, E. C., LIMA, A., LIMA, R. M. T., FREITAS, P. A. P., SOUZA, M. A. M., & CARIOCA, J. O. B. Elaboração e aceitabilidade de produtos de panificação enriquecidos com semente de goiaba (Psidium guajava L.) em pó. HOLOS, v. 5, p. 199-210, 2014. https://doi.org/10.15628/holos.2014.1895.
13. LUO, Ye WANH, Q. Zein based micro and nano-particles for drug and nutrinet delivery: A review. Journal of Applied Polymer Science. v. 131, n. 16, p. 1-12, 2014. https://doi.org/10.1002/app.40696.
14. SILVA, P. T. D., FRIES, L. L. M., MENEZES, C. R. D., HOLKEM, A. T., SCHWAN, C. L., WIGMANN, É. F., & SILVA, C. D. B. D. Microencapsulation: concepts, mechanisms, methods and some applications in food technology. Ciência Rural, v. 44, p. 1304-1311, 2014. http://dx.doi.org/10.1590/0103-8478cr20130971.
15. GALVANI, F; GAERTNER, E. Adequação da metodologia Kjeldahl para determinação de nitrogênio total e proteína bruta. Embrapa Pantanal-Circular Técnica (INFOTECA-E), 2006. Disponível em: http://www.infoteca.cnptia.embrapa.br/infoteca/handle/doc/812198.
16. WILLIAMS, R. D. e OLMSTED, W. H. A biochemical method for determining indisgetible residue (crude fiber) in feces: lignin, cellulose, and non-water-soluble hemicelluloses. Journal of Biological Chemistry, v. 108, n. 3, p. 653-666, abr/mar, 1935. Disponível em: https://www.cabdirect.org/cabdirect/abstract/19351400053.
17. MERRILL, A. L. e BERNICE, K. W. (1973). Energy Value of Foods: Basis and Derivation. Agriculture Handbook. Washington, DC, ARS United States Departament of Agriculture. Disponível em: https://www.ars.usda.gov/ARSUserFiles/80400525/Data/Classics/ah74.pdf.

    MALL, I.D., SRIVASTAVA, V.C., KUMAR, G.V.A., AND MISHRA, I.M. Characterization and utilization of mesoporous fertilizer plant waste carbon for adsorptive removal of dyes from aqueous solution. Colloids and Surfaces A: Physicochemical and Engineering Aspects, cidade, v. 278, n. 1-3, p. 175-187, 2006. doi: 10.1016/j.colsurfa.2005.12.017. https://doi.org/10.1016/j.colsurfa.2005.12.017.
18. BEDIN, K. C., SOUZA. I. P. A. F., CAZETA, A. L., SPESSATO L. RONIX A. ALMEIDA. V. C.CO2-spherical activated carbon as a new adsorbent for Methylene Blue removal: Kinetic, equilibrium and thermodynamic studies. Journal of Molecular Liquids, v. 269, p. 132-139, 2018. https://doi.org/10.1016/j.molliq.2018.08.020
19. CAZETTA, A. L., VARGAS, A. M., NOGAMI, E. M., KUNITA, M. H., GUILHERME, M. R., MARTINS, A. C., ALMEIDA, V. C. NaOH-activated carbon of high surface area produced from coconut shell: Kinetics and equilibrium studies from the methylene blue adsorption. Chemical Engineering Journal, v. 174, n. 1, p. 117-125, 2011. https://doi.org/10.1016/j.cej.2011.08.058.
20. ROYER, B., CARDOSO, N. F., LIMA, E. C., VAGHETTI, J. C., SIMON, N. M., CALVETE, T., & VESES, R. C. Applications of Brazilian pine-fruit shell in natural and carbonized forms as adsorbents to removal of methylene

©2024 Great Britain Journals Press

blue from aqueous solutions—Kinetic and equilibrium study. Journal of hazardous materials, v. 164, n. 2-3, p. 1213-1222, 2009. https://doi.org/10.1016/j.jhazmat.2008.09.028.

21. MALASH, G. F.; EL-KHAIARY, M. I. Piecewise linear regression: A statistical method for the analysis of experimental adsorption data by the intraparticle-diffusion models. Chemical Engineering Journal, v. 163, n. 3, p. 256-263, 2010. https://doi.org/10.1016/j.cej.2010.07.059.
    MALASH, G.F.; EL-KHAIARY, M. I. Methylene blue adsorption by the waste of Abu-Tartour phosphate rock. Journal of colloid and interface science, v. 348, n. 2, p. 537-545, 2010. https://doi.org/10.1016/j.jcis.2010.05.005.
22. R. HAN, J. ZHANG, P. HAN, Y. WANG, Z. ZHAO, M. TANG. Study of equilibrium, kinetic and thermodynamic parameters about methylene blue adsorption onto natural zeolite. Chemical Engineering Journal, v. 145, n. 3, p. 496-504, 2009. https://doi.org/10.1016/j.cej.2008.05.003.
23. CARDOSO, N.F., PINTO, R.B., LIMA, E.C., CALVETE, T., AMAVISCA, C.V., ROYER, B., CUNHA, M.L., FERNANDES, T.H.M., AND PINTO, I.S., Removal of remazol black B textile dye from aqueous solution by adsorption. Desalination, v. 269, n.1-3, p. 92-103, 2011. Disponível em: https://www.academia.edu/12233601/Removal_of_remazol_black_B_textile_dye_from_aqueous_solution_by_adsorption.
24. GAO, Q., ZHU, H., LUO, W.-J., WANG, S., AND ZHOU, C.-G., Preparation, characterization, and adsorption evaluation of chitosan-functionalized mesoporous composites. Microporous and Mesoporous Materials, v. 193, p. 15-26, jun./jul, 2014. doi: 10.1016/j.micromeso.2014.02.025. https://doi.org/10.1016/j.micromeso.2014.02.025.
    PAVIA et al. Introduction of Spectrocopy. 4ª edição. Cegage Learning, 2010.
25. BARDESTANI, R.; PATIENCE, G. S.; KALIAGUINE, S.. Experimental methods in chemical engineering: specific surface area and pore size distribution measurements - BET, BJH, and DFT. The Canadian Journal of Chemical Engineering, v. 97, n. 11, p. 2781-2791, 2019. https://doi.org/10.1002/cjce.23632.
26. BAE, Y-S.; YAZAYDIN, A. Ö.; SNURR, R. Q. Evaluation of the BET method for determining surface areas of MOFs and zeolites that contain ultra-micropores. Langmuir, v. 26, n. 8, p. 5475-5483, 2010. https://doi.org/10.1021/la100449z.
    THOMMES M.; KANEKO K.; NEIMARK A. V.; OLIVIER J. P.; RODRIGUEZREINOSO F.; ROUQUEROL J.; SING K. S. W. Physisorption of gases, with special reference to the evaluation of surfasse area and pore size distribution (IUPAC Technical Report). Pure and Applied Chemistry. V. 87, p. 1051 - 1070, 2015. https://doi.org/10.1515/pac-2014-1117.
27. CANEVAROLO JR, Sebastião V. et al. Técnicas de caracterização de polímeros. Artliber, São Paulo, v. 430, n. 2004, 2004. Disponível em: https://www.artliber.com.br/amostra/tecnicas_de_caracterizacao_de_polimeros.pdf
28. ZHAO, L. G.; WARRIOR, N. A.; LONG, A. C. A thermo-viscoelastic analysis of process-induced residual stress in fibre-reinforced polymer–matrix composites. Materials Science and Engineering: A, v. 452, p. 483-498, 2007. https://doi.org/10.1016/j.msea.2006.10.060.
29. GUERREIRO, L. Dossiê técnico: produtos extrusados para consumo humano, animal e industrial. Rio de Janeiro: REDETEC, 2007. Disponível em: http://www.respostatecnica.org.br/dossie-tecnico/downloadsDT/MTcy.
30. MAITY, J. AND RAY, S.K. Enhanced adsorption of methyl violet and congo red by using semi and full IPN of polymethacrylic acid and chitosan. Carbohydrate Polymers, v. 104, n. s/n, p. 8-16, mar./abr, 2014. https://doi.org/10.1016/j.carbpol.2013.12.086.
31. GEZICI, O., KÜÇÜKOSMANOĞLU, M., AYAR, A. The adsorption behavior of crystal violet in functionalized sporopollenin-mediated column arrangements. Journal of Colloid and Interface Science, v. 304, n. 2, p. 307-316, 2006. doi: 10.1016/j.jcis.2006.09.0

©2024 Great Britain Journals Press

48. disponível em: https://ur.booksc.eu/book/3654027/7b8f64.
32. KHAN, T.A., CHAUDHRY, S.A., AND ALI, I. Equilibrium uptake, isotherm and kinetic studies of Cd(II) adsorption onto iron oxide activated red mud from aqueous solution. Journal of Molecular Liquids, v. 202, p. 165-175, 2015. https://doi.org/10.1016/j.molliq.2014.12.021.
33. MALL, I.D., SRIVASTAVA, V.C., KUMAR, G.V.A., AND MISHRA, I.M. Characterization and utilization of mesoporous fertilizer plant waste carbon for adsorptive removal of dyes from aqueous solution. Colloids and Surfaces A: Physicochemical and Engineering Aspects, cidade, v. 278, n. 1-3, p. 175-187, 2006. doi: 10.1016/j.colsurfa.2005.12.017. https://doi.org/10.1016/j.colsurfa.2005.12.017.
34. TANHAEI, B., AYATI, A., LAHTINEN, M., AND SILLANPÄÄ, M., Preparation and characterization of a novel chitosan/Al2O3/magnetite nanoparticles composite adsorbent for kinetic, thermodynamic and isotherm studies of Methyl Orange adsorption. Chemical Engineering Journal, v. 259, p. 1-10, 2015. https://doi.org/10.1016/j.cej.2014.07.109.
35. PLAZINSKI, W., RUDZINSKI, W., AND PLAZINSKA, A. Theoretical models of sorption kinetics including a surface reaction mechanism: A review. Advances in Colloid and Interface Science, v. 152, n. 1-2, p. 2-13, nov./dez, 2009. https://doi.org/10.1016/j.cis.2009.07.009.
36. DAHRI, M.K., KOOH, M.R.R., LIM, L.B.L., Water remediation using low cost adsorbent walnut shell for removal of malachite green: Equilibrium, kinetics, thermodynamic and regeneration studies. Journal of Environmental Chemical Engineering, v. 2, n. 3, p. 1434-1444, 2014. https://doi.org/10.1016/j.jece.2014.07.008.
37. MUSYOKA, S.M., MITTAL, H., MISHRA, S.B., NGILA, J.C., Effect of functionalization on the adsorption capacity of cellulose for the removal of methyl violet. International Journal of Biological Macromolecules, v. 65, p. 389-397, jun./jul, 2014. https://doi.org/10.1016/j.ijbiomac.2014.01.051.
38. PERUCHI, L.M., FOSTIER, A.H., RATH, S., Sorption of norfloxacin in soils: Analytical method, kinetics and Freundlich isotherms. Chemosphere, v. 119, p. 310-317, jun./jul, 2015. https://doi.org/10.1016/j.chemosphere.2014.06.008.
WEBER JR, W. J.; MORRIS, J. C. Kinetics of adsorption on carbon from solution. Journal of the sanitary engineering division, v. 89, n. 2, p. 31-59, 1963. https://doi.org/10.1061/JSEDAI.0000430.
39. GUPTA, S. S.; BHATTACHARYYA, K. G. Kinetics of adsorption of metal ions on inorganic materials: a review. Advances in Colloid and Interface Science, Amsterdam, v. 162, n. 1-2, p. 39-58, dez./jan, 2011. https://doi.org/10.1016/j.cis.2010.12.004.
40. AHMAD, R.; KUMAR, R. Adsorptive removal of congo red dye from aqueous solution using bael shell carbon. Applied Surface Science, Amsterdam, v. 257, n. 5, p. 1628-1633, nov./dez, 2010. https://doi.org/10.1016/j.apsusc.2010.08.111.
41. ALZAYDIEN, A. S.; MANASREH, W. Equilibrium, kinetic and thermodynamic studies on the adsorption of phenol onto activated phosphate rock. International Journal of Physical Sciences, Lagos, v. 4, n. 4, p. 172-181, 2009. Disponível em: https://academicjournals.org/journal/IJPS/article-full-text-pdf/B3C1A9F18737.
42. AHMED, M. J.; THEYDAN, S. K. Adsorption of cephalexin onto activated carbons from Albizia lebbeck seed pods by microwave-induced KOH and K2CO3 activations. Chemical Engineering Journal, Amsterdam, v. 211–212, n. 1, p. 200–207, 2012. https://doi.org/10.1016/j.cej.2012.09.089.
43. AHMED, M. J.; THEYDAN, S. K. Fluoroquinolones antibiotics adsorption onto microporous activated carbon from lignocellulosic biomass by microwave pyrolysis. Journal of the Taiwan Institute of Chemical Engineers, Taipei, v. 45, n. 1, p. 219–226, 2014. https://doi.org/10.1016/j.jtice.2013.05.014.
44. ARAUJO, A. L. P., SILVA, M. C. C., GIMENES, M. L., & BARROS, M. A. S. D.

©2024 Great Britain Journals Press

Estudo termodinâmico da adsorção de zinco em argila bentonita bofe calcinada. Scientia plena, v. 5, n. 12, 2009. Disponível em: https://www.scientiaplena.org.br/sp/article/view/680.

45. LI, P., SU, Y.-J., WANG, Y., LIU, B., AND SUN, L.-M., Bioadsorption of methyl violet from aqueous solution onto Pu-erh tea powder. Journal of Hazardous Materials, 2010. 179(1–3): p. 43-48. https://doi.org/10.1016/j.jhazmat.2010.02.054.
AHMAD, R.; KUMAR, R. Adsorptive removal of congo red dye from aqueous solution using bael shell carbon. Applied Surface Science, Amsterdam, v. 257, n. 5, p. 1628-1633, nov./dez, 2010. https://doi.org/10.1016/j.apsusc.2010.08.111.
46. GERÇEL, Ö., ÖZCAN, A., ÖZCAN, A. S., & GERCEL, H. F. Preparation of activated carbon from a renewable bio-plant of Euphorbia rigida by H2SO4 activation and its adsorption behavior in aqueous solutions. Applied surface science, v. 253, n. 11, p. 4843-4852, 2007. https://doi.org/10.1016/j.apsusc.2010.08.111.

Research Highlights

- Encapsulating material from guava seed.
- High capacity to incorporate the methylene blue dye.
- Pseudo-second-order model better described the adsorption kinetics.

©2024 Great Britain Journals Press

This page is intentionally left blank

©2024 Great Britain Journals Press

Scan to know paper details and
author's profile

Study on Pipe Plugging Mechanism based on Polyurethane Magnetic Capsules

Shuai Liu, Bo Peng, Gang Li & Ming Yuan Wang

Jishou University

ABSTRACT

Piping is one of the important causes of accidents in water conservancy facilities such as embankments and dams. Therefore, it is of great practical significance to study the timely plugging after the occurrence of dike piping. Based on the plugging of pipeline magnetic materials, this paper proposes a new method of plugging piping holes with PMC. Combined with the experimental method, the effects of different ratios of oily and waterborne polyurethane and the amount of magnetic powder on the plugging effect of PMC were investigated. The main results are as follow:(1) Under the same ratio of oily polyurethane and waterborne polyurethane, the more the magnetic content in the mixture, the easier the PMC is adsorbed by the strong magnetic field at the water inflow, and the more the magnetic material and polyurethane capsule are gathered in the water inflow.

Keywords: magnetic materials; piping; oily polyurethane; waterborne polyurethane; magnetic capsules.

Classification: UDC Code: 628.2

Language: English

Great Britain Journals Press

LJP Copyright ID: 392944
Print ISSN: 2631-8474
Online ISSN: 2631-8482

London Journal of Engineering Research

Volume 24 | Issue 3 | Compilation 1.0

© 2024. Shuai Liu, Bo Peng, Gang Li & Ming Yuan Wang. This is a research/review paper, distributed under the terms of the Creative Commons Attribution-Noncom-mercial 4.0 Unported License http://creativecommons.org/licenses/by-nc/4.0/), permitting all noncommercial use, distribution, and reproduction in any medium, provided the original work is properly cited.

Study on Pipe Plugging Mechanism based on Polyurethane Magnetic Capsules

Shuai Liu[α], Bo Peng[σ], Gang Li[ρ] & Ming Yuan Wang[ω]

ABSTRACT

Piping is one of the important causes of accidents in water conservancy facilities such as embankments and dams. Therefore, it is of great practical significance to study the timely plugging after the occurrence of dike piping. Based on the plugging of pipeline magnetic materials, this paper proposes a new method of plugging piping holes with PMC. Combined with the experimental method, the effects of different ratios of oily and waterborne polyurethane and the amount of magnetic powder on the plugging effect of PMC were investigated. The main results are as follow:(1) Under the same ratio of oily polyurethane and waterborne polyurethane, the more the magnetic content in the mixture, the easier the PMC is adsorbed by the strong magnetic field at the water inflow, and the more the magnetic material and polyurethane capsule are gathered in the water inflow. The comprehensive analysis shows that the magnetic capsule has the best plugging effect on piping when the content of magnetic material is 45g and 60g.(2) In the case of the same amount of magnetic materials, the ratio of oil polyurethane and waterborne polyurethane used in the test is 1:1,1:2,1:3,2:3, respectively. The water inflow curve is basically the same, and the more the proportion of oil polyurethane in the mixed polyurethane grouting fluid, the faster the PMC reacts with water, the less the final water inflow, and the four mixed polyurethane slurry ratios selected in the test can achieve better plugging effect. The research in this paper provides a good theoretical and experimental basis for piping rescue technology and magnetic material plugging in the future.

Keyword: magnetic materials; piping; oily polyurethane; waterborne polyurethane; magnetic capsules.

Author α σ ρ ω: School of Civil Engineering and Architecture, Three Gorges University, Yichang 443002 China.
ρ: School of Civil Engineering and Architecture, Jishou University, Zhangjiajie 427000,China.

I. INTRODUCTION

With the rapid development of the national economy, flood control and disaster reduction have become the top priority. As of 2019, the number of reservoirs in China has reached nearly 100,000, becoming the country with the largest number of reservoirs in the world [1-5]. Various types of reservoir dams are accompanied by a long history, and often do not have good maintenance, and various problems have emerged one after another [2]. Among them, the piping damage caused by leakage accounts for 51.2% of the total number of accidents. It can be seen that the research on piping plugging has become very important [6-12].

Grouting and water plugging technology is one of the most common methods to control water inrush disasters [13-16]. Although polyurethane in traditional grouting materials has a good effect on plugging piping, polyurethane slurry has the characteristics of rapid dispersion, emulsification and expansion when encountering water, which will cause some problems on how polyurethane slurry enters the piping channel [17]. The most commonly used grouting method in the process of engineering piping plugging is the high-pressure grouting method. This method is used to inject polyurethane slurry into the piping channel, and the piping outlet has compressive resistance, which

©2024 Great Britain Journals Press

may cause secondary damage to the already sealed hole. Therefore, based on the research of magnetic material plugging, this paper proposes a new type of polyurethane magnetic capsule to plug the piping method, and through the self-designed piping simulation test device, to carry out in-depth research on the plugging mechanism of magnetic capsules.

At present, magnetic materials are not widely used in engineering applications, mainly for structural safety research under magnetic induction. TaeseoKu [18] studied the influence of nanoparticles on grouting performance under water-rich conditions. The results show that the application of nanoparticles can effectively improve the grouting reinforcement performance. Mu et al [19-20] used the piezomagnetic effect to study the force-magnetic relationship model of the interface between steel and reinforced concrete. Zhao et al [21-22] plunged magnetized water into concrete and found that the performance was greatly improved. Some scholars have mixed magnetized steel fibers into concrete for magnetic induction orientation, which greatly enhances the shear strength and flexural stiffness of weak areas of buildings. Liu et al[23] used the attractiveness of ring magnets to magnetic materials and combined with high-strength adhesives to solve the leakage problem of diameter pipelines. Hu et al [24] added the magnetic material to water, and then added the amount of polyvinylpyrrolidone and suspension aid A to make the magnetic material suspend in water. The plugging performance and plugging mechanism of the magnetic material were studied by a self-made plugging simulation device. The results show that the greater the magnetic force of the electromagnet, the better the plugging effect of the magnetic material. The closer the electromagnet is to the outlet of the hole, the more the magnetic material is accumulated, and the better the plugging effect is. It can be seen that the application of magnetic materials in the field of grouting reinforcement and fracture anti-seepage plugging engineering has great development space and research value.

Based on the previous research on magnetic material plugging, this paper proposes to add magnetic materials to polyurethane capsules, and then use the adsorption force of magnets on magnetic materials to achieve the purpose of plugging piping. In order to better study the plugging mechanism of magnetic capsules, a single-tube piping simulation test device was independently designed to explore the effects of different ratios of oily and waterborne polyurethane, and the amount of magnetic powder added on the plugging effect of PMC.

II. MATERIALS AND METHODS

2.1 Experimental material

The polyurethane grouting fluid used in the experiment is mainly hydrophilic (water-soluble) polyurethane and hydrophobic (oil-soluble) polyurethane. The appearance of hydrophilic polyurethane is light yellow transparent liquid, and the appearance of hydrophobic polyurethane is dark brown liquid. The magnetic material is micron spherical Fe_3O_4 magnetic powder with a content of 99% Fe_3O_4, which has a good magnetization effect and lower cost than nano-Fe_3O_4 magnetic powder. In addition, the test also requires additives, buckets, magnetic rings, transparent acrylic tubes and other reagents and materials, as shown in table 1 below.

©2024 Great Britain Journals Press

Table 1: Experimental drugs and materials used in plugging experents

Name	Model
Polyurethane slurry	Hydrophilic(water-soluble)、Hydrophoblc（oil soluble）polyurethane
Magnetic materials	Grain diameter 5-10μm ferriferrous oxide（Fe_3O_4）magnetic powder
Suspending agent	Sodium silicate
Floatation agent	RON's reagent
Empty capsule	00 glutinous rice hollow capsule
Clear acrylic tube	Outside diameter 25mm、Inner diameter 21mm
Plastic bucket	10L
Tank connector 6-point set	External 25 PVC pipe
Nanda 703 silicone rubber	Net weight 45g
Ru iron boron magnetic ring	Outside diameter 36mm*thickness2.5mm/internal diameter 25.5mm

2.2 Test instrument

The instruments used in this experiment mainly include: a number of disposable rubber head droppers, a number of 2000ml measuring cylinders, a number of disposable plastic bowls, electronic scales, glass rods, timers, electric agitators, and self-made piping plugging simulation devices.

2.3 Self-made piping plugging simulation devices.

The simulation test device is mainly composed of a bucket, a water tank joint 6-pack (with a PVC ball valve), a transparent acrylic tube, and a Ru Tie B magnetic splicing, as shown in Figure 1. A 35mm round hole is opened on the side wall of the plastic bucket near the bottom of the bucket, and the inner and outer wires in the water-based joint set are connected to the bucket at the opening. Then the outlet of the water tank joint is connected to the transparent acrylic tube, and each interface is sealed with silicone rubber to prevent water leakage. A simple single-tube piping simulation test device is completed by putting 20 Ru Tiepeng strong magnetic rings on the outer wall of the transparent acrylic pipe outlet.

Figure 1: Physical diagram of self-contained pipe plug simulation device

©2024 Great Britain Journals Press

2.4 Self-made polyurethane magnetic capsules

Waterborne polyurethane and oily polyurethane were mixed in a certain proportion, and then a certain amount of magnetic material was added, and then stirred evenly with a glass rod, and then injected into the hollow capsule using a disposable rubber dropper. PMC as shown in Figure 2 were fabricated.

Figure 2: Polyurethane magnetic capule physical picture

2.5 Test scheme

The amount of magnetic material added in the (PMC) will affect the adsorption effect of the magnetic ring at the outlet of the pipe, and the ratio of the oil in the capsule and the waterborne polyurethane will also directly affect the plugging performance of the pipe. In this paper, the orthogonal experimental design method is used to prepare the oil-based polyurethane and waterborne polyurethane in the ratio of 1:1,1:2,1:3,2:3 of the 500g mixture, respectively, adding 15g, 30g, 45g, 60g of magnetic powder.PMC with different ratios of oil-based polyurethane and waterborne polyurethane and different amounts of magnetic powder were prepared to explore the different ratios of oil-based polyurethane and waterborne polyurethane, and the effect of the amount of magnetic powder on the plugging and piping effect of PMC . The specific parameters are shown in Table 2. Table 2 lists the orthogonal array of 4 factors of 16 experiments in this study, and each factor changes at 4 levels (the name of the experiment is represented by numbers 1~4).

Table 2: Magnetic capsule material ratio

Trial number	Oil-based polyurethane(g)	Waterborne polyurethane (g)	O/W	Magnetic Material content
1	250	250	1:1	15
2				30
3				45
4				60
5	175	325	1:2	15
6				30
7				45
8				60
9	125	375	1:3	15
10				30
11				45
12				60
13	200	300	2:3	15
14				30
15				45
16				60

©2024 Great Britain Journals Press

In this magnetic capsule plugging test, if the amount of magnetic material added in the water is too much, it will also affect the circulation of the PMC in the pipeline, so only 180g of magnetic material is added to 10L of water. The particle size of the magnetic material particles is small and the density is large, and the water solubility is poor. Therefore, the magnetic material is added to the water, and it is easy to accumulate in the water and cannot be stably suspended in the water. In order to make the magnetic powder have good dispersion in water, it is necessary to add 2% concentration of polyvinylpyrrolidone (PVP) and 0.1g suspension aid A [24].

During the test, an electric stirrer was used to stir the PMC in the bucket at a uniform speed, so that it could smoothly enter the water gushing pipeline, and a 2L measuring cylinder was placed at the water gushing port to record the water inflow. By observing the water inflow at the water inlet at different times, the effect of different proportions of PAM on plugging piping was evaluated. A timer is used to record the amount of water gushing every 10 seconds in the first minute, and then every 1 minute until there is no water flowing out of the outlet. In order to ensure the accuracy of the test values, each group of tests was repeated three times, and the average value was taken as the final test result.

III. EXPERIMENTAL RESULTS AND ANALYSES

3.1 Study on the effect of the amount of magnetic material on the PMC plugging piping

When the ratio of oil-based polyurethane grouting material and water-based polyurethane grouting material in 500g mixed polyurethane grouting liquid is 1:1,1:2,1:3 and 2:3 respectively, the PMC prepared when the magnetic material content is 15g, 30g, 45g and 60g respectively are compared and analyzed. The curve of the change of the water inflow at the outlet of the pipe during the test is shown in figure 3.

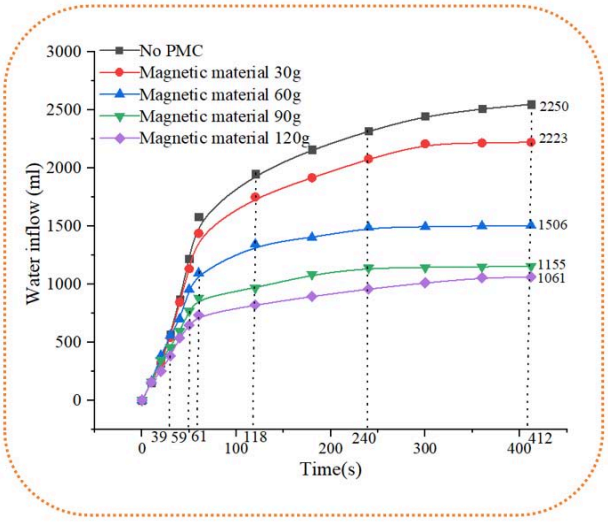

(a)Oilypolyurethane:waterbore polyurethane=1:1

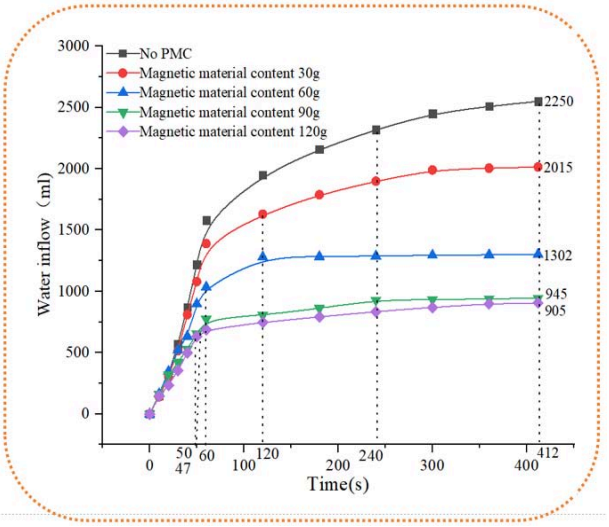

(b) Oily polyurethane:waterbore polyurethane=1:2

©2024 Great Britain Journals Press

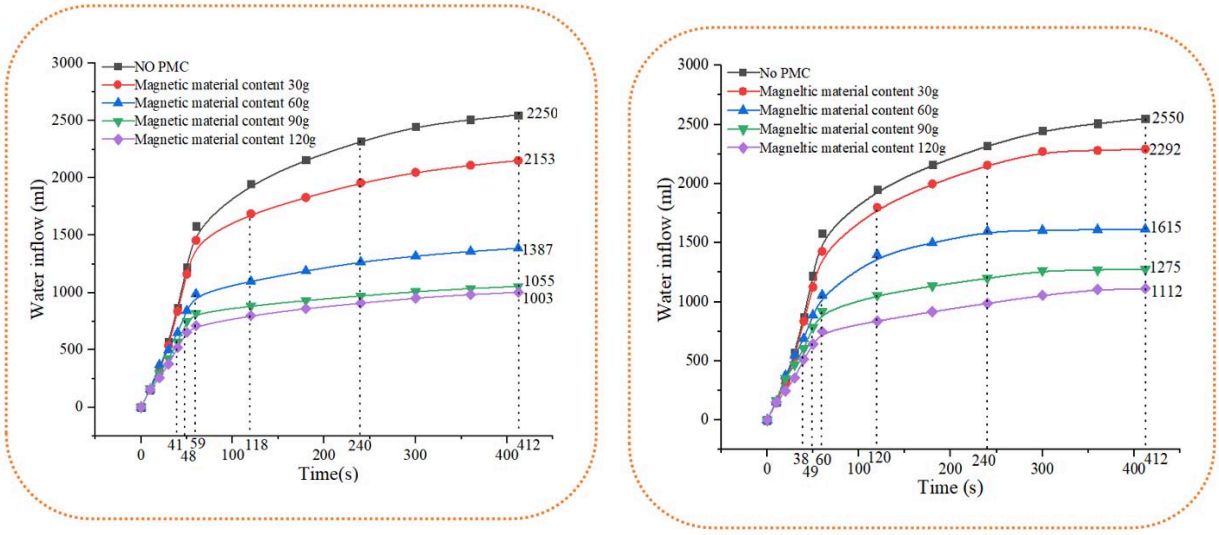

(c)Oilypolyurethane:waterbore polyurethane=1:3 (d)Oily polyurethane:waterbore polyurethane=2:3

Figure 3: Variation curve of water inflow at pipe outlet at the ratio of oily polyurethane and waterborne polyurethane

It can be seen from Fig.3 that in the case of only using magnetic materials to block the piping, the water inflow at the piping outlet is as high as 2250ml, and after using the PMC, the water inflow decreases significantly. In the test process of using magnetic materials to block the piping, the magnetic materials enter the piping channel under the action of water flow. Due to the strong magnetic magnetization at the piping outlet, the magnetic materials are gradually adsorbed and accumulated in the pipeline, reaching the effect of plugging the piping. After the magnetic materials are completely blocked, there are still a small amount of water droplets seeping out, and the strong magnetism at the piping outlet is taken away after a certain period of time. At this time, the water leakage is serious, and some magnetic materials in the channel will be lost with the water flow. The channel blocked by PMC has no water seepage after taking away the strong magnetism at the piping outlet, and the plugging effect is good. This is because the magnetic capsule is adsorbed by the strong magnetism at the piping outlet and gathers at the piping outlet, so that the water flow velocity decreases instantaneously. With the erosion of the water flow, the shell of the magnetic capsule melts after a period of time, and the internal mixed polyurethane grouting fluid reacts with water and expands rapidly, enriching the interior of the pipeline and making it reach a better plugging effect. This shows that when plugging the piping, the method of using PMC and magnetic material to block the piping can have better results.

By observing Fig.3 (a), it can be seen that when the amount of magnetic materials is 15g, 30g, 45g, and 60g, the final water inflow at the piping mouth is 2015ml, 1302ml, 945ml, and 905ml, respectively. The addition amount of magnetic material in the mixture of PMC with the ratio of oily polyurethane to waterborne polyurethane of 1:1 also has a certain effect on plugging piping. The water inflow at the piping outlet gradually decreases with the increase of the amount of magnetic material. When the amount of magnetic material is 60g, the water inflow is the least. And the growth rate of water inflow decreases with the increase of the amount of magnetic material added. Observing the curve of water inflow change when the amount of magnetic powder material is 15g, 30g, 45g and 60g respectively, it is found that the growth rate of water inflow has a significant downward trend after 38s, 49s, 60s and 120s respectively, and the time inflection point of the growth rate decreases with the increase of the amount of magnetic material. The increase of the amount of magnetic material is advanced, indicating that the closer the occurrence point is, the faster the water flow rate in the pipeline decreases. This is because when the PVC ball valve is opened, the magnetic material and magnetic capsule suspended in the water enter the piping channel with the water flow, and are strongly magnetically adsorbed at the

©2024 Great Britain Journals Press

piping mouth. The more magnetic materials added to the PMC, the easier the strong magnetic adsorption, so that the magnetic material and polyurethane magnetic capsule PMC gather at the piping mouth, the water flow rate decreases rapidly, and the longer the time, the more magnetic materials accumulated in the piping channel, and at the same time, the number of magnetic capsules entering the pipeline will decrease. When the content of magnetic material is 15g, the time inflection point of the growth rate of water inflow is greatly different from that of the other three different contents. Therefore, the number of PMC in the channel with 60g magnetic powder content is less, while the number of PMC with 45g and 60g content is not much different. From the figure, the amount of magnetic materials is 30g, 45g, 60g.

By observing Figure 3 (b), it can be seen that when the ratio of oily polyurethane and waterborne polyurethane is 1:2, the amount of magnetic material is 15g, 30g, 45g and 60g respectively, the PMC plugging test is configured, and the final water inflow at the outlet of the pipe is 2223ml, 1506ml, 1155ml and 1061ml respectively. Compared with the experiment using only magnetic material to block the piping, it can be concluded that the addition of PMC has a better effect on blocking the piping, and the more the amount of magnetic material added, the less the water inflow at the final piping outlet. Comparing and analyzing Fig.3(a) and Fig.3(b), it can be found that in the case of the same amount of magnetic materials, the time inflection point of the decrease in the growth rate of water inflow basically does not change much, and the change law of water inflow is the same. With the increase of the amount of magnetic materials, the growth rate of water inflow at the piping port is lower, which indicates that the ratio of oily polyurethane and waterborne polyurethane has no effect on the number of magnetic capsules entering the piping channel. It also shows that the ratio of mixed polyurethane has no effect on the effect of PMC plugging piping. It can also be seen from Fig.3(b) that when the content of magnetic materials is 45g and 60g, the growth rate of water inflow is relatively slow after the time inflection point, and the water inflow is also less. Compared with Fig.3(a), it can be seen that the ratio of oil-soluble polyurethane to water-soluble polyurethane has a certain influence on the reaction time of polyurethane magnetic materials. Based on the above analysis, it can be seen that when the ratio of oil polyurethane and waterborne polyurethane is 1:2, the PMC prepared with 45g and 60g of magnetic material content has the best rush protection piping effect.

It can be seen from Fig.3(c) that when PMC is used, the water inflow at the final piping outlet is 2292ml, 1615ml, 1275ml and 1112ml respectively when the dosage of magnetic material is 15g, 30g, 45g and 60g respectively, and when the dosage is 60g, the water inflow is the least, indicating that the addition of magnetic material in polyurethane capsule has a certain effect on plugging piping loopholes, and the more the amount of magnetic material added, the less the water inflow at the final piping outlet. By comparing and analyzing Figure 3(a), Figure 3(b) and Figure 3(c), it can be found that in the same magnetic material content and different mixed polyurethane ratio, the final water inflow of the piping mouth is different, which shows that the mixed polyurethane ratio has a certain influence on the final water inflow. Under the condition of the same amount of magnetic material blending, the position of the inflection point at each time does not change much, and the change law of the water inflow growth rate is the same. The growth rate becomes smaller with the increase of time after the time inflection point, and the more the amount of magnetic material is, the less the water inflow is. These indicate that the ratio of the mixed polyurethane has little effect on the strong magnetic adsorption magnetic capsule at the nozzle, and has a small effect on the number of magnetic capsules accumulated in the pipeline. By observing Fig.3(c), after comprehensive analysis, when the ratio of oily polyurethane to waterborne polyurethane is 1:3, it is found that when the amount of magnetic material is 45g and 60g, the plugging time is shorter and the total water inflow is less.

From Figure 3(d), it can be seen that when the magnetic material content is 15g, 30g, 45g and 60g, the time inflection points of the water inflow growth rate are 118s, 59s, 48s and 41s, respectively. The

©2024 Great Britain Journals Press

water inflow of the final piping outlet is 2153ml, 1387ml, 1055ml and 1003ml, respectively.When the content is 45g and 60g, the difference of the final water inflow is small, which indicates that when the magnetic material content is greater than 45g, the increase of the magnetic material has little effect on the final water inflow. By comparing and analyzing Figure 3(a)~Figure3 (d), it can be seen that in the four water inflow curve changes, the position of the time inflection point where the water inflow growth rate decreases has little change, and the curve change rule is basically the same. This shows that the mixed polyurethane ratio has a certain influence on the final water inflow, but it has little effect on the effect of the strong magnetic adsorption PMC at the outlet of the pipe. By analyzing the final water inflow of each diagram, it can be concluded that the ratio of oily polyurethane and waterborne polyurethane has a certain influence on the reaction time of polyurethane magnetic materials. Therefore, if the index of water reaction time of PMC is selected, when the ratio of oily polyurethane to waterborne polyurethane is 2:3, and the dosage of magnetic material is 45g and 60g, the magnetic capsule has the best plugging effect on piping.

In summary, the above analysis of the water inflow curve of the four mixed polyurethane ratios shows that the amount of magnetic material in the PMC determines the number of PMC staying in the piping channel when plugging the piping. With the increase of magnetic material admixture, the effect of plugging piping is also gradually enhanced. When the content of magnetic material is 45g and 60g, the magnetic capsule has the best plugging effect on piping. When the amount of magnetic material is more than 45g, it has little effect on the final water inflow of the piping port. This is because the magnetic material will reduce the speed of the PMC to react with water, so the water plugging effect will be weakened.

3.2 Study on the ratio of mixed polyurethane to the plugging piping performance of magnetic capsules

The same content of magnetic materials was added to the mixed polyurethane slurry with the ratio of oily polyurethane to waterborne polyurethane of 1:1,1:2,1:3 and 2:3, respectively. The effects of capsules prepared by mixed polyurethane slurry with different ratios on the plugging of piping were compared and analyzed. The test conditions are the same as those in Section 3.1, and the content of magnetic materials is selected as 15g, 30g, 45g and 60g respectively. The change curve of water inflow at the piping outlet during the test is shown in Fig.4.

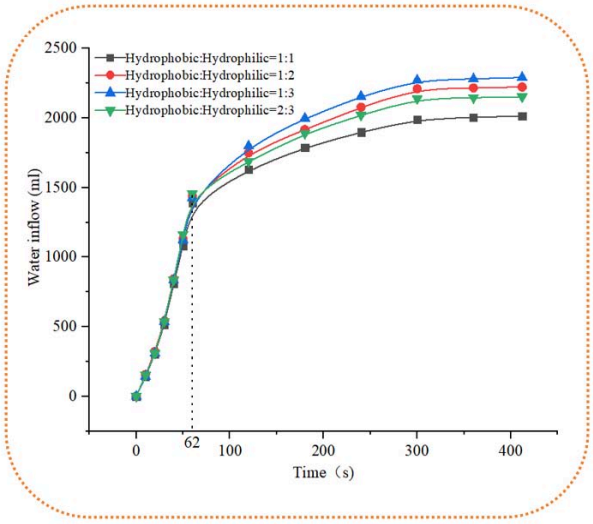

(a)Magnetic material content 15g

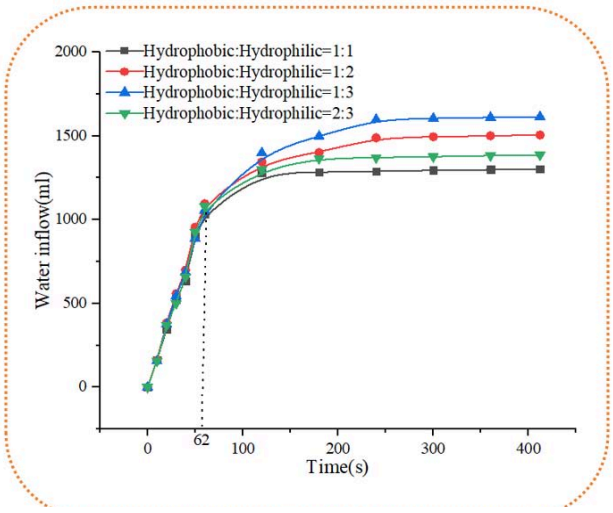

(b)Magnetic material content 30g

©2024 Great Britain Journals Press

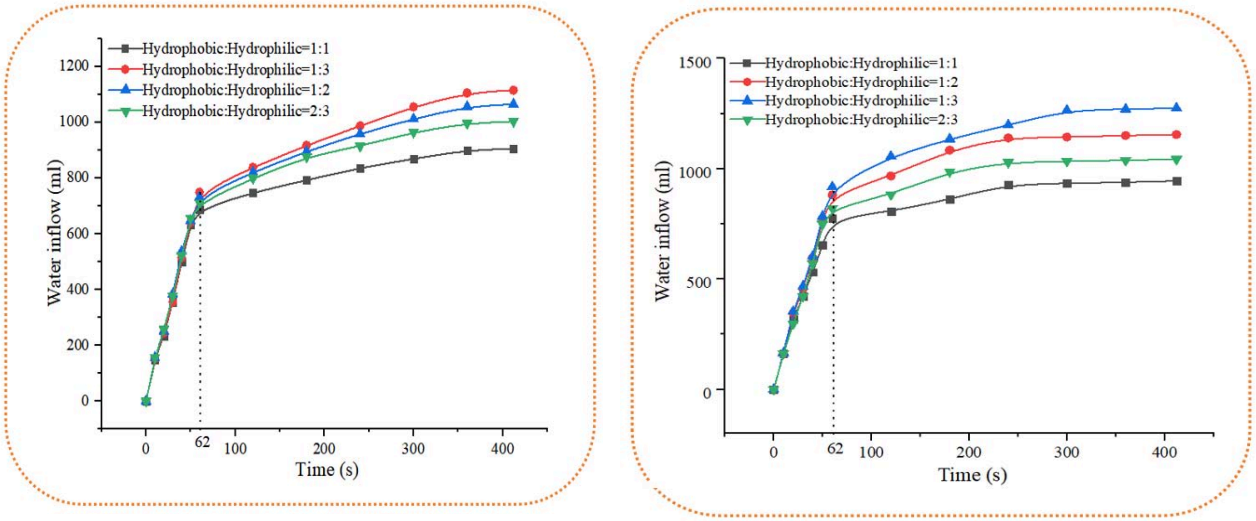

(c) Magnetic material content 45g (d)Magnetic material content 60g

Fingure 4: Variation curve of water inflow at pipe outlet with different magnetic material content

It can be seen from Fig.4 (a) that when the content of magnetic material is15g, the change trend of the four curves is basically the same. The water inflow of the pipe gushing port increases rapidly before 62s, and the water inflow increases slowly after 62s. The main reason is that before 62s, the PMC and the magnetic material entered the piping channel, the capsule shell did not begin to melt, and the polyurethane did not contact with water to react. After 62s, the capsule shell completely melted, and the mixed polyurethane slurry inside the capsule gradually reacted with water until the reaction was complete. The reaction rate of oil-soluble polyurethane:waterborne polyurethane=1:1>oil-soluble polyurethane: waterborne polyurethane =2:3 > oil-soluble polyurethane waterborne polyurethane = 1:2 > oil-soluble polyurethane: waterborne polyurethane=1:3, the more the proportion of oil-soluble polyurethane, the faster the reaction rate, the less the final water inflow. It can be seen that the four water inflow change curves basically coincide before 62s. This is because after the PVC ball valve is just opened, the water flow is large, and the strong magnetism at the piping mouth is difficult to adsorb the PMC when the magnetic material content is 15g. The magnetic material suspended in the water flow is easily magnetized, gradually accumulated at the channel mouth, and the water flow decreases randomly. At this time, the PMC will stagnate in the channel with the water flow into the channel, and the number is small. After 62 s, the four change curves have little change in water inflow. This is due to the reaction of polyurethane magnetic capsule PMC with water, which has the effect of blocking the channel. Although the PMC with a magnetic material content of 15g has a certain effect on piping plugging loopholes, it takes a long time.

By observing figure 4(b), it can be seen that when the magnetic material content is 30g, the PMC begins to react in the channel. From the change of the rate of the four water inflow curves, the speed of the reaction of the PMC with water is reflected. The earliest water inflow of the curve changes the least, and the reaction speed is the fastest. The speed of the reaction rate is oily polyurethane: waterborne polyurethane =1:1 > oily polyurethane: waterborne polyurethane = 2:3 > oily polyurethane: waterborne polyurethane = 1:2 > oily polyurethane: waterborne polyurethane =1:3. It is concluded that the content of oily polyurethane is proportional to the reaction rate. Comparing Fig.4(a) and Fig.4(b), it can be seen that the effect of PMC plugging piping vulnerability when the magnetic material content is 30g is better than that when the content is 15g.Since the magnetic material content is 30g, the reaction speed is faster, and the number of PMC retained in the channel is also more.

It can be seen from Fig.4(c) that the more the content of oily polyurethane in the PMC, the faster the reaction rate. The reaction rate of these four curves is as follows: polyurethane: waterborne polyurethane = 2:3 > oily polyurethane: waterborne polyurethane = 1:3 > oily polyurethane:

©2024 Great Britain Journals Press

waterborne polyurethane = 1:2 > oily polyurethane : waterborne polyurethane = 1:1. By comparing and analyzing Figure 4(a) ~ Figure 4(c), it can be seen that the reaction speed is the fastest when the magnetic material content is 30g, while the reaction speed slows down when the magnetic material content is 45g. The main reason is that the number of polyurethane magnetic capsule PMC in the channel is very small, which has little effect on the reaction speed. Inside the PMC, the more the mixed polyurethane content, the faster the reaction speed will be.

By observing figure 4(d), it can be seen that the four curves in the figure have the same change trend and the same reaction speed. Therefore, when the content of magnetic material reaches 60g, the ratio of mixed polyurethane in polyurethane magnetic capsule PMC has no effect on the reaction speed of the capsule in water. This is mainly because when the amount of magnetic material is 60g, the content of mixed polyurethane in polyurethane magnetic capsule PMC is relatively small, so the ratio of mixed polyurethane has little effect on its reaction. By comparing and analyzing figure 4(a)~(d), it can be seen that the influence of magnetic material content on the plugging of piping holes by is 30g > 45g > 15g > 60g. In the four pictures, after 62s, the PMC began to react with water. The more the content of magnetic materials in the capsule, the less the water inflow in 62s. This shows that the glutinous rice hollow capsule has the effect of delaying the reaction of mixed polyurethane with water, and the more the content of magnetic materials, the easier it is to be adsorbed by the strong magnetic at the water inlet, and the less time it takes to accumulate the magnetic materials in the channel, and the water inflow decreases rapidly.

In summary, the ratio of mixed polyurethane grouting fluid will affect the reaction rate of PMC in water. In the case of the same amount of magnetic material, the more oil polyurethane content, the faster the reaction rate. According to the size of the reaction speed, it can adapt to the plugging of different water potential of piping holes. If the piping mouth is large and the water potential is large, the PMC with the ratio of oil polyurethane to waterborne polyurethane of 2:3 is selected. If the water potential of the piping port is small and the water flow is slow, the polyurethane magnetic capsule PMC with a ratio of 1:2 of oily polyurethane and waterborne polyurethane with slower reaction speed is selected. Under the action of strong magnetism at the piping port, the magnetic material and PMC are accumulated in the piping channel, so that it can achieve the effect of quickly plugging the piping vulnerability. The PMC with a ratio of 1:1 and 1:3 of oil polyurethane and waterborne polyurethane has a moderate reaction speed, which is suitable for most emergency piping projects.

IV. SUMMARY

Aiming at the problem of piping leakage, based on the plugging of magnetic materials, combined with the use of polyurethane grouting fluid, this paper prepares PMC, and explores the performance of polyurethane magnetic capsule PMC in rushing and protecting piping. The main conclusions are as follows :

In this paper, polyurethane grouting fluid, magnetic material and hollow capsule were selected for the preparation of PMC. The mixed polyurethane grouting fluid and Fe_3O_4 magnetic powder were uniformly mixed, and then the rubber dropper was injected into the meltable starch hollow capsule.

The water inflow of the PMC is less than the water inflow of the magnetic material, which shows that the PMC has a good effect in the process of plugging the piping hole, which can make up for the fact that the magnetic material can not completely block the channel, and there are still water seepage defects in the channel.

In the PMC, different amounts of magnetic materials were added to study the effect of magnetic material content PMC on the plugging effect of piping holes. The test results show that the amount of

©2024 Great Britain Journals Press

magnetic material not only affects the effect of strong magnetic adsorption at the piping mouth, but also affects the effect of polyurethane magnetic capsule PMC plugging piping. The more the amount of magnetic material, the better the effect of strong magnetic adsorption, but the less the content of polyurethane in the capsule, the slower the reaction rate with water, and the worse the piping plugging effect. When the content of magnetic material is 45g, the plugging effect is the best, and when the content of magnetic material is greater than or less than 45g, the plugging effect is poor.

In the study of mixed polyurethane grouting liquid ratio of polyurethane magnetic capsule PMC plugging piping performance of the test process, under different magnetic material content, PMC and water reaction time after 62s, indicating that the starch capsule has a certain delay effect on the reaction of polyurethane and water. The higher the content of oily polyurethane in the mixed polyurethane grouting fluid, the faster the reaction rate of the polyurethane magnetic capsule PMC, and the faster the final water inflow. In the case of the same amount of magnetic material, the change trend of the water inflow curve of the PMC prepared by different ratios of mixed polyurethane slurry is basically the same, indicating that the four ratios of oil polyurethane and waterborne polyurethane are selected : 1:1,1:2,1:3,2:3, which has little effect on the effect of plugging piping holes.

Author Contributions: Conceptualization, G.L. and S.L.; Methodology, G.L. and S.L.; Investigation,B.P. and M.W; formal analysis, S.L.; Writing—original draft, S.L. and B.P. All authors have read and agreed to the published version of the manuscript.

Informed Consent Statement: Not applicable.

Data Availability Statement: The research data are included within the article, and further data are available from the corresponding author upon request.

Conflicts of Interest: The authors declare no conflict of interest.

REFERENCE

1. Study on plugging model of piping magnetic material in dike foundation [D]. China University of Mining and Technology.
2. Zhao Yu.Research on control theory and application of anti-seepage reinforcement of dams [D]. Tianjin University, 2009.
3. Wang Fuming, Li Jia, Shi Mingsheng, et al. Research and application of new technology for anti-seepage reinforcement of dams [J]. Acta Hydroelectrica Sinica, 2016.35 (12): 1-11.
4. Qu Wei. Discussion on anti-seepage reinforcement technology of dam in water conservancy project [J]. Engineering construction and design, 2016 (18): 163-164.
5. Turkmen S. Treatment of the seepage problems at the Kalecik Dam (Turkey)[J]. Engineering Geology, 2003, 68: 159-169.
6. Dai Q, Lin F, Wang X, et al. Detection of concrete darn leakage using an integrated geophysical technique based on flow-field fitting method[J]. Journal of Applied Geophysics, 2017, 140:168-176.
7. Dong H, Chen J, Li X. Delineation of leakage pathways in an earth and rockfill dam using multi-tracer tests[J]. Engineering Geology, 2016, 212: 136-145.
8. XU Qiang. Research on dam risk analysis method [D]. Dalian: Dalian University of Technology, 2008.
9. Ding Liuqian, Zhang Qiyi, Yao Qiuling. Analysis of the characteristics of piping hazards in the Yangtze River Basin in 1998 [J]. Water Conservancy and Hydropower Technology, 2007 (02): 44-45 + 69.
10. Zhou Yinghu. Study on the seepage failure mechanism and control measures of river levees [D].Anhui : Hefei University of Technology, 2006.

©2024 Great Britain Journals Press

11. Zhao Erfeng.Monitoring data analysis theory and evaluation method of dam safety [M]. Nanjing: Hohai University Press, 2018: 21-25.
12. Zhao Xinzhong, Yang Jian, Ma Jinchao, et al. [J]. Henan Water Conservancy, 2002 (04):40.
13. Huang Kun. Experimental study on water plugging mechanism of organic grouting materials under engineering water inrush conditions [D]. Wuhan University of Light Industry, 2018. DOI: 10.27776 /d.cnki.gwhgy.2018.000244.
14. Lian Youwu. Discussing the dangerous situation and emergency protection of dike loopholes [J]. Henan Water Conservancy, 2006 (08):8.
15. Jiao 's income increase. [J]. Science and technology information, 2010 (33): 370.
16. LIU Zirui, JIANG Kezheng. Study on piping in levees and dams [J]. China Water Transportation (2nd half month), 2017, 17 (05): 197-199.
17. Li Wanrong. Experimental study on piping plugging by new polyurethane magnetic capsule [D]. China University of Mining and Technology, 2020. DOI: 10.27623 / d.cnki.gzkyu.2020.000146.
18. Taeseo Ku, Subramaniam Palanidoss, Yunhuo Zhang, Practical configured microtremor array measurements (MAMs) for the geological investigation of underground space[J], Underground Space,2020(04).
19. Mu Ru, Zhao Quanming, Tian Wenling. Preparation and properties of unidirectional steel fiber reinforced cement slurry [J]. Journal of Hebei University of Technology, 2012,41 (2): 101-104.
20. Song Heyue, Ding Yining. Review on the research methods of spatial distribution of steel fibers in concrete matrix [J]. Journal of Materials Science and Engineering, 2015,33 (05): 768-775.
21. Li Yueguang, Yi Shuguo, Zhang Linbo, Xu Ronghua. Research status and development prospect of magnetized water cement concrete [J]. Journal of Materials Science and Engineering, 2019,37 (02): 331-338.
22. Zhao Huawei, Dai Xueling, Zeng Xiantao, Liu Yanbin. Experimental Study on Reducing Dust Content of Shotcrete by Magnetized Water [J]. Journal of Mining and Safety Engineering, 2008 (03): 371-374.
23. Liu Fangli, Cai Xiaojun. Study on the sealing scheme of annular magnet pressure bonding for large diameter pipeline [J].New technology and new process, 2012 (08): 39-41.
24. Hu Shanshan. Research on suspension process and plugging performance of magnetic materials [D]. China University of Mining and Technology, 2019.

©2024 Great Britain Journals Press

Scan to know paper details and
author's profile

Innovative Approaches to CO2 Emission Reduction and Application

Jin Jia Min

ABSTRACT

This article discribes how limestone and iron ore can become raw materials for energy production by relying on carbon gasification reaction (C+CO2=2CO). Converting a lime calcining kiln into an electric gas producer is the most economical-effective emission reduction, achieving "0" capture cost.

The total CO2 discharged from the two industries of cement and steel is 3.664 billion tons, which can produce 3729.952 billion m3CO, equivalent to 1,376.4 billion m3 of natural gas, equivalent to the energy transported by 25 Nord Stream 2 lines annually. Unfortunately, it is currently wasted。

The water-gas instead of the direct combustion of coal should be a feasible technical route. A profitable water-gas technology route should be more welcome. The technical route of Emission Reduction-ER is much better than the CCS technical route.

Keywords: ER CO2 lime carbon gasification emission reduction sponge iron electric heating water-gas CCS CO gas steelmaking.

Classification: DDC Code: TD885.5.C3

Language: English

Great Britain Journals Press

LJP Copyright ID: 392945
Print ISSN: 2631-8474
Online ISSN: 2631-8482

London Journal of Engineering Research

Volume 24 | Issue 3 | Compilation 1.0

© 2024. Jin Jia Min. This is a research/review paper, distributed under the terms of the Creative Commons Attribution-Noncom-mercial 4.0 Unported License http://creativecommons.org/licenses/by-nc/4.0/), permitting all noncommercial use, distribution, and reproduction in any medium, provided the original work is properly cited.

Innovative Approaches to CO_2 Emission Reduction and Application

Jin Jia Min

ABSTRACT

This article discribes how limestone and iron ore can become raw materials for energy production by relying on carbon gasification reaction ($C+CO_2=2CO$). Converting a lime calcining kiln into an electric gas producer is the most economical-effective emission reduction, achieving "0" capture cost.

The total CO_2 discharged from the two industries of cement and steel is 3.664 billion tons, which can produce 3729.952 billion m^3CO, equivalent to 1,376.4 billion m^3 of natural gas, equivalent to the energy transported by 25 Nord Stream 2 lines annually. Unfortunately, it is currently wasted。

The water-gas instead of the direct combustion of coal should be a feasible technical route. A profitable water-gas technology route should be more welcome. The technical route of Emission Reduction-ER is much better than the CCS technical route.

Keywords: ER CO_2 lime carbon gasification emission reduction sponge iron electric heating water-gas CCS CO gas steelmaking.

Author: Bao Weifang Shanghai Research Institute of Materials (200437).

I. INTRODUCTION

Climate warming and frequent extreme climate events pose a serious threat to human life and survival. Scientists primaly attribute this to the greenhouse gas- CO_2; So many methods of capturing CO_2 have emerged.

According to a report in the People's Daily CHina on October 10, 2021, the 26 CCS units have been put into operation worldwide in 2020, capturing a total of 40 million tons of CO_2. The CCS technology is difficult to promote, because of the expensive of capture and storage.

This paper proposes that using coal directly to capture the CO_2 eleased in the production of lime and iron should be an economical and feasible method, which can fully utilize the natural resources and open up a new way of energy production. The use of water-gas as power plant fuel has remarkable emission reduction effect and reduced coal consumption.

The author has written an article, 《The Technology of Producing Sponge Iron, Lime, and Nitrogen-Free Type Gas Simultaneous with Encloseed Heating Furnace.》[1], The paper is complementary and expanded.

©2024 Great Britain Journals Press

II. THE COAL IS USED TO DIRECTLY CAPTURE CO_2 RELEASED DURING CALCINATION OF LIMESTONE.

2.1 An Argument Question

The author once wrote an article titled《A chemical reaction can save mankind》[2,3]. Discribing the carbon gasification reaction ($C+CO_2=2CO$). but didn't receive the attention it deserved. Some scholars argue that neither Emission Reduction-ER nor energy enhancement occurs before and after the carbon gasification reaction. Furthermore; they assert that heat lose may result in more to lose than gain. For the carbon-water reaction ($C+H_2O=CO+H_2$), the same problem exists.

But the author believes that the source of question is that some scholars do not take into account the results of "after used" of CO gas. The Consequence on relying on the carbon gasification reaction is described later in this paper, limestone becomes raw material for producing energy. opening up a new way of energy production. So this result seems like a strong proof that the statement of《carbon gasification reaction can save the earth and mankind》is not wrong.

2,2 The lime calciner should be transformed into an electric heat gas generator

Achieving 'o' capture costs。

The chemical equation associated with calcination of limestone is as follows:

$$CaCO_3=CaO+CO_2 \qquad \Delta H^{o}_{298k}=177.4kj/mol\ [4] \tag{1}$$

$$C+CO_2=2CO \qquad \Delta H^{o}_{298k}=162.297kj/mol\ \ ZN=3.48^{***} \tag{2}$$

$$CaCO_3+C=CaO+2CO \qquad \Delta H^{o}_{298k}=339.697kj/mol\ \ ZN=1.67 \tag{3}$$

$$2CO+O_2=2CO_2 \qquad \Delta H^{o}_{298k}=-566kj/mol \tag{4}$$

$$C_{(graphite)}+CO_{2\,(g)}=2CO_{(g)} \quad \Delta H^{o}_{298k}=172.53kj/mol \tag{5}$$

Stored energy index ZN= stored energy/consumed energy. The stored energy is the energy released after the gas is completely burned. The energy consumed includes the energy absorbed by the reaction, heat loss (including furnace gas, furnace wall, slag, product).

Equation (1), (2) is a well-known old equation that has been used in industrial production for a long time. The Lime produce depends on the equation (1).

The blast furnace ironmaking, sponge iron production, producing gas in generator ,surface carburizing of steel parts, sintered steel production, cemented carbide production, vacuum deoxidation of alloy powder etc. These are totally dependent on this reactions (2). To metallurgists, they are very familiar with this reaction. Therefore, I do not want to say more here.

Reaction (3) is endothermic reaction, or energy storage reaction. It is the result of adding the two equations (1)+(2)=(3).

The theoretical storage energy index ZN=566/339.69=1.67, including 10% heat loss, storage energy index ZN*==566/339. 697X1.1=1.51. The energy storage index is greater than 1, which means that the energy consumption of production process is zero for producing lime and CO gas at same time.

According to the calculation of equation (1), we can get:

A. To produce 1 ton of lime, the limestone decomposes and releases $400M^3CO_2$ or 785.7 kg CO_2.
B. To Produce 1 ton of lime, 3167857kj of heat was absorbed. Equivalent to 880 kwh of electricity.

©2024 Great Britain Journals Press

According to the calculation of equation (3), it can be obtained that:

To produce 1 ton of lime, while 800M³ of CO gas (without nitrogen) can be produced. The Nitrogen free type CO gas comes from a closed furnace body or hearth.

C. To produce 1 ton of lime, absorbed 6066018kj heat. Converted into electrical power is1572kwh. Thereinto; 880kwh is heat absobed by limestone decomposition, account for 55.97%。692kwh is heat absobed by carbon gasification, account for 44%.
D. The production of 1M³ nitrogen-free type CO gas requires 2.1 KWh of electricity, factor in 20% heat loss, it is 2.5 kwh of electricity.

Due to the slow burning rate of limestone, large heat loss is caused by calcination,

According to the calculation of the reaction formula(2), the production of 1m³ gas requires 1.08 kwh of electricity and 0.27 kg of carbon. The calorific value of 1m³ CO gas is 3045kcal, the caloricity of 1kwh is 860 kcal, the selling price about is 3 yuan, the use of valley power production, the cost is 0.3 yuan。 After the comparison in regard to the economy and energy consumption,it can be found that there is a large profit space. There is no "more harm than good".

The (0) capture cost is achieved because the production of lime also produces gas at same time, and the price of gas is much greater than the price of lime, and lime becomes a by-product.

The rough calculation shows that unprofitable situations seem unlikely.

Fortunately, the making temperature required for limestone calcination and producing gas is the consistent of 1050°C.. In addition; The carbon gasification reaction rate is much greater than the calcinate rate of limestone, the former is measured in seconds, but the calcination of limestone is measured in hours, the heat transfer of the porous lime layer is slow, The burn-through rate of limestone at 1100°C, is 1.6cm/h, and the burn-through rate becomes the control step or slowest step of the lime produce process. The rate of carbon gasification reaction does not affect the lime produce。

It is worth mentioning that the use of carbon capture CO_2 has the potential to increase lime productivity and reduce production costs. Because the condition of limestone decomposition is that the decomposition pressure (P_{CO_2}) of calcium carbonate must be greater than the partial pressure of CO_2(p^*_{co2}) in the furnace gas. At 1050°C, when the carbon gasification reaction reaches equilibrium, the CO_2 content in the gas phase is almost zero, $P_{CO_2}>>>P^*_{CO_2}$. The $P^*_{CO_2}$ in the furnace gas is almost zero, so it is conducive to the decomposition of calcium carbonate and improve the decomposition rate of limestone。 So increasing productivity.

At present; The steel heat treatment furnaces and powder metallurgy sintering furnaces were used extensively in industrial production, these furnace bodies are closed all and can be used to produce gas and lime, Only the stock box is filled with limestone and carbon powder.

Of course, if a supplementary gasification chamber with a cross-sectional area 5-10 times larger than that of the furnace hearth and about 1 m long is added at the tail of the furnace, the CO_2 in the gas is reduced to less than 1%, which may be a complete gas producer. As for the combined furnace type, it remains to be practiced.

In addition, it is necessary to increase the gas washing device and gas storage tank.

According to the Internet, the production of 1 ton of lime in the calcination furnace requires 600-900 kg of coal***, the equivalent carbon content is 516-774 kg, take the middle value of 645 kg, 645 kg of carbon after burning to produce 2365 kg (645x3.67=2365)of CO_2. adding 785.7 kg of CO_2 released by limestone decomposition. that is to say to produce 1 ton of lime, the total CO_2 emission is 3150 kg(2365+786=3151).

©2024 Great Britain Journals Press

The production of 1 ton of lime, the release of 3.151 tons of CO2, of which 2.365 tons of CO2 from coal combustion, accounting for75% of emissions.

With electric heating instead of carbon heat has a significant emission reduction effect, especially the use of valley electricity, it is more economical. Therefore, it is the most effective and economical technical route to transform lime kiln into electric gas producer. The CCS route simply doesn't compare.

In 2016, the consumption of lime is 3.248 billion tons, and the amount of CO_2 emitted should be 10.2 billion tons, accounting for 31% of the global total emissions of 33 billion tons, which is a large emitter. The authors argue that capturing CO_2 focus should be the lime kiln.

To sum up, the transformation of lime calciner into gas producer and the

production of lime and gas at the same time is an economical and effective emission reduction technical route, and there is no difficult technical problem.

***:The data quoted on the Internet differs greatly from the theoretical data of 122.3 kg/ton lime.required for carbon, which is estimated to be the data of calcination in round kilns。

2.3 CO gas is produced to use limestone, Open up new ways of producing energy

According to online data, in 2016, the global production of cement is 5 billion tons, with China accounting for 2.5 billion tons. It is calculated that the consumption of limestone used to produce cement should be 5.8 billion tons.Based on the CaO content of cement being approximately 65%, this equats to a limestone consumption of 5.8 billion. The amount of CO_2 released from the calcination of this limestone is 2.552 billion tons, Thereinto; the content of carbon is 696 million tons, and the content of oxygen is 1.856 billion tons. The 2,552 billion tons is 7.73% of the total global CO_2 emissions of 33 billion tons。

If carbon gasification reaction $C+CO_2=2CO$ is used, the CO_2 is converted into CO gas. According to the equation(2); One ton of carbon can converts 3.67 tons of CO_2 into CO. 2.552 billion tons of CO_2 would require 696 million tons of carbon or 770 million tons of standard coal. Of the 2.552 billion tons of CO_2, the carbon content is 696 million tons, which is 809 million tons of standard coal, which is larger than the annual extraction of the United States or India.

According to equation (3), 1 ton of CO_2 can produce 1018 M^3 of CO, 2.552 billion tons of CO_2 can produce 2,600 billion M^3 of CO,

The calorific value of natural gas is 8000-8500kcal/m^3, and the median value is 8250kcal/m^3. The calorific value of CO is 3045kcal/m^3, and the calorific value of natural gas is 2.71 times that of CO gas. 2,600 billion cubic meters of CO gas is equivalent to 959.4 billion cubic meters of natural gas. It is equivalent to the annual transport capacity of 17.4 pipelines of the Nord Stream 2 line. (The design transport capacity of Nord Stream Line 2 is 55 billion m^3 per year). Europe needs 570 billion m^3 of gas per year, and 959.4 billion cubic meters of gas is almost enough to meet the annual gas demand of two European countries.

People celebrate the discovery of 100 billion cubic meters of natural gas fields, while every year 10 PCs 100 billion gas fields are wasted and ignored. They are to go to war for one natunal gas pipeline, killing each other, giving the lives of many, young men, war is the most stupid act of mankind. If the expense of the war is used for technological transformation and the lime kiln is transformed into an electric gas producer, mankind can enjoy a peaceful and happy life forever.

©2024 Great Britain Journals Press

Three-quarters of carbon and oxygen element in gas come from limestone, which has become a raw material for energy production, opening up a new way of energy production.

If limestone can be recycled to use, there is no need to worry about energy depletion. When the coal runs out, the wood carbon can be used in gasification reaction instead of coal.

III. THE USE OF COAL TO DIRECTLY CAPTURE THE CO_2 RELEASED DURING THE PRODUCTION OF SPONGE IRON

The formula for carbon reduction of iron oxide is:

$$Fe_2O_3+3C=2Fe+3CO \quad \Delta H^{o}_{298k}=447.4kj/mol \tag{6}$$

The actual carbon reduction of iron oxide is carried out in steps, that is:

$Fe_2O_3 \rightarrow Fe_3O_4 \rightarrow FeO \rightarrow Fe$. The longest reduction process is FeO reduction.

The reaction is endothermic, and the theoretical storage energy index ZN=844/447.4=1.89. After accounting for 10% heat loss, the storage energy index ZN*= 1.70. The ZN is greater than 1, which means that the energy consumption of the production process is zero.

According to the calculation of the reaction formula, the production of one ton of sponge iron while producing 600 M^3 of nitrogen-free type CO gas requires 0.321 tons of reducing agent carbon or standard coal 357 kg. From the results of our repeated determination of the reduction gas phase composition, in the reduction stage of FeO, For thermodynamic and kinetic reasons, the reduction gas phase always contains about 25% CO_2, which must be converted to carbon monoxide with carbon outside the reduction reaction zone.That is just to put some carbon powder at the top of the reaction tank.

From the formula of Fe_2O_3, the content of iron is 70% and the content of oxygen is 30%. According to the network, in 2023, the global crude steel production is 1,888.2 million tons, (China's crude steel production is 1,019 million tons, accounting for 53.97% of the world).

According to the crude steel production, the application amount of refined iron ore should be 2.697 billion tons, of which the oxygen content should be 809 million tons, and these Oxygen with carbon combine to produce CO_2,. Its weight is 1.112 billion tons.

When we add the CO_2 released by the decomposition of limestone and the CO_2 released by the production of ironmaking, and we get 3.664 billion tons of CO_2 (25.52+11.12= 3.664 billion tons), if it is converted into CO rely on carbon gasification reaction, it is 3,729.95 billion m^3 CO gas, this value equivalent to 1,376.36 billion $m^3$of natural gas, and that`s equivalent of 25 Nord Stream 2 lines energy delivered in a year。

At present; So much energy is thrown away。

We used a sealed small iron box (120x60mm)[6], which was filled with iron ore powder and carbon. The carbon powder was added with Fe, Co, Ni, Cu Ag, S etc. catalysts or poisons to study their catalytic and poison effects on carbon reduction of iron oxide. The catalytic activity was determined according to the flow rate of the reduction gas release, the composition and the carbon content in the sponge iron. The CO content in the released reducing gas fluctuates at 75%, and there is about 25% CO2, which is the CO2 we need to add carbon to converte to CO.

©2024 Great Britain Journals Press

IV. USING WATER TO REDUCE CO_2 EMISSIONS

Using water to reduce CO_2 emissions is based on the reaction equation:

$$H_2O+C=H_2+CO \quad \Delta H^{\circ}_{298k}=39488 \text{ kcal/kgmol.(liquid)} \quad (6)$$

$$28380 \text{ kcal/kgmol.(vapour)}$$

This is an old reaction that everyone knows. The equation clearly tells you that gas contains 50% hydrogen. Using this water-gas gas as a power plant fuel, the CO_2 content of the flue gas can be reduced remarkable.

The carbon in the equation can be any kind of carbon, such as; plastic, rubber, paper, cloth, bituminous coal, peat, firewood, wood chips, feces, animal carcasses, and so on. Different raw materials have different hydrogen content in the gas.

4.1 Carbon

Carbon reacts with water:

$$C_{(graphite)}+H_2O_{(g)}=H_{2(g)}+CO_{(g)} \quad \Delta H^{\circ}_{298k}=+131.382kj/mol[6], \quad ZN=4.35 \quad (7)$$

This reaction is endothermic reaction, or energy storage reaction, the theoretical energy storage index of the reaction ZN=4.35, if the 20% heat loss is included, ZN*= 3.62, the energy storage index is greater than 1, This means that the production process uses zero energy.The gains and losses feared by some scholars are unlikely to materialize.

According to the reaction calculation, 1 ton of carbon requires 1.5 tons of water to produce 3733 m^3 of nitrogen-free type water-gas, and the calorific value of water-gas is 3048 kcal/m^3.

4.2 Plastic

$$\text{PE type plastic; } C_2H_4+2H_2O=4H_2+2CO \quad (8)$$

$$\text{PP type plastic; } C_3H_6+3H_2O=6H_2+3CO \quad (9)$$

According to equation (8), (9), a ton of PE or PP type plastic and 1.3 tons of water can produce 4800 m^3 of nitrogen-free type gas, the content of hydrogen in the gas is 67%. Once this water-gas is used as fuel for power plants, CO_2 emissions can be reduced by 67%

People are very worried about white pollution. Her Majesty the Queen has called on scientists to save the planet .Because the sea is also seriously pollute The author believes that the white pollution can be eliminated by using water and electricity, and the plastic islands floating in the Pacific Ocean can be a good raw material for the production of gas. The energy storage index of these two reactions is estimated to be higher than 4.35, so it is unlikely that the gains will outweigh the losses. In a strongly reducing atmosphere, toxic dioxin gases are unlikely to occur.

Thankfully; In the lab we have done experiments and got beautiful blue flames.

4.3, Rubber

$$C_5H_8+5H_2O=9H_2+5CO \quad (10)$$

According to equation (10), a ton of waste rubber and 1.32 tons of water can produce 4600 m^3 of nitrogen-free type gas, and the content of hydrogen in the gas is 64%.

©2024 Great Britain Journals Press

4.4. Starch (C_6H_{1005})

$$2C_6H_{1005}+12H_2O=1017H_2+12CO \quad (11)$$

According to equation (11), a ton of starch plus 0.1 tons of water can produce 10700 M^3 of nitrogen-free type gas, and the hydrogen content in the gas is 98.83%, almost all hydrogen.

4.5 Starch

$$2C_6H_{1005}+12H_2O=1017H_2+12CO \quad (12)$$

According to equation (12), a ton of starch plus 0.1 tons of water can produce 10700 m^3 of nitrogen-free type gas, and the hydrogen content in the gas is 98.83&, almost all hydrogen.

4.6. fat ($C_{57}H_{11006}$)

$$C_{57}H_{11006}+57H_2O=5560H_2+57CO \quad (13)$$

According to equation (13), a ton of fat plus 0.087 tons of water can produce 10760 M^3 of nitrogen-free type gas, and the hydrogen content in the gas is 98.98%, almost all hydrogen.

As can be seen from the above, using water to produce water-gas, the minimum hydrogen content of gas is 50%. If animal carcasses are used as raw materials, the hydrogen content is almost 100%. The emission reduction effect is even more significant.

According to online data, power plants account for about 70 percent of global CO_2 emissions of 33 billion tons per year. That is, 330x0.7= 23.1 billion tons, if all the world's thermal power plants are converted to water-gas as fuel, 50% emissions reduction is 11.55 billion tons, an astonishing figure. Therefore, using water to reduce CO_2 emissions is also the very effective and economical way.

Using water to reduce CO_2 emissions has many advantages;

One of the biggest advantages is that resources are abundant, the price is cheap, and the production cost of gas is low.

Another advantage is that an infinite number of Bioenergy is utilized and It is easy to realize coal gasification in rural areas, while protecting the environment. Once the global rural coal gasification, energy depletion, environmental pollution, climate warming three problems troubling mankind should be solved.

Fortunately, the laboratory research on the production of water-gas using plastic, waste paper, wood chips, pig skin and pig manure as raw materials has been basically completed. There's video to prove it.

The author holds that the use of water and biological energy to produce water-gas is the only way for human beings, because the resources are rich and continuous, both to provide energy, but also to protect the environment, protect the climate, conducive to human survival.

V. CONCLUSION

The three technical schemes share several commonalities; Firstly, a closed furnace body or hearth; Secondly, a consistent operating temperature of 1050°C; Thirdly, the complete utilizztion of natural resources. Fourth, the direction of the flow of gas and furnace charge must be the same, from low to high temperature.

©2024 Great Britain Journals Press

Fiveth, the emissions reduction, reducing emissions at the source. It is more cost-effective than capture.

The author believes that the most economical and effective emission reduction is the replacement of carbon heat by electric heating, The limestone calcining kiln must be transformed into electric gas generator. the simultaneous production of lime and gas, and the realization of '0' capture cost.

The author holds that; Using carbon gasification reaction, limestone becomes raw material of energy production, opening up a new way of energy production, which is of great significance. The author considers that "A chemical reaction can save mankind" is not wrong。

Using coal to capture the carbon dioxide released by the production of sponge iron, the production cost of iron is reduced, and the oxygen in the iron oxide is fully utilized. Once sponge iron becomes raw material of steelmaking; blast furnaces, sintering furnaces, coke ovens, converter will be eliminated, there will be a technological revolution in the metallurgical industry.

Using water and bioenergy to produce water gas, it should be a feasible technical route to change direct combustion to indirect combustion. It is the technological route that human beings must take. It is also the technical route to realize coal gasification in rural areas. In particular, the use of valley power to produce gas, there is a large profit space.

Any of the above three technologies are more economical - efficient - than the CCS technology route。

Finally; The authors argue that the $C+CO_2=2CO$ and $C+H_2O=H_2+CO$ reactions could save the earth and humanity. One is the use of limestone, the other is the use of bioenergy, both resources are rich, the source of constant.

Electricity, cement, steel are the three pillars of the national economy, both energy consumption, but also large carbon dioxide emissions, relying on electricity, water, coal; Relying on carbon gasification reaction and carbon water gas reaction, the author believes that it can economically and effectively solve the three major problems of energy exhaustion, environmental pollution and climate warming. Let mankind live in peaceful and happy life forever.

Finally；To compare the two technical routes of ER and CCS, it is obvious; The ER technological route has great advantages.

The author is shallow knowledge, not self-evident, talking on paper, a brick to attract jade, expectations of insightful criticism and correction.

REFERENCES

1. J. M. Jin, The Technology of Producing Sponge Iron, Lime, and Nitrogen-Free Type Gas Simultaneous with Encloseed Heating Furnace. *Metallurgical Engineering*, 2021,8(2),47-55. https://doi.org/10.12677/meng.2021.82007.
2. J. M. Jin, Making Use of CO_2 Capture for Saving Earth and Human-A Comparison of "Carbon Capture and Storage-CCS" and "Carbon Capture and Storage Energy-CCSE", *Global Journal of Human Social Sciences: H*. 2020,20(2) 17-20. DOI:10.17406/GJHSS.
3. J. M. Jin, Water can Protect Earth and People-A Comparison of Two Energy Storage Reactions. *International Journal of chemistry, 2023,15(1),26-30*.
4. M. A. Glinkof. metallurgical furnace (Chinese). commercial press。p308.
5. JANAF Termochemical Tables, 2d. ed., NSRDS-NBS 37 (1971).

©2024 Great Britain Journals Press

6. J. M. Jin, W .F. Bao, Study on the Mechanism of Heterogeneous Catalysis (2). The Relative Catalytic Activities of Fe,Co,Ni,Cu,Ag and SiO_2 in the carbon Catalyzed Gasification Reaction. *Journal of Meterials Sceince and Chemical Engeneering* 6,191–20 (2018. https//doi.org/10.4236/msce.201864018.

©2024 Great Britain Journals Press

Great Britain Journal Press Membership

For Authors, subscribers, Boards and organizations

Great Britain Journals Press membership is an elite community of scholars, researchers, scientists, professsionals and institutions associated with all the major disciplines. Great Britain memberships are for indivi - duals, research institutions, and universities. Authors, subscribers, Editorial Board members, Advisory Board members, and organizations are all part of member network.

Read more and apply for membership here:
https://journalspress.com/journals/membership

For Authors

Author Membership provide access to scientific innovation, next generation tools, access to conferences/seminars/ symposiums/webinars, networking opportunities, and privileged benefits. Authors may submit research manuscript or paper without being an existing member of GBJP. Once a non-member author submits a research paper he/she becomes a part of "Provisional Author Membership".

For Institutions

Society flourish when two institutions Come together." Organizations, research institutes, and universities can join GBJP Subscription membership or privileged "Fellow Membership" membership facilitating researchers to publish their work with us, become peer reviewers and join us on Advisory Board.

For Subscribers

Subscribe to distinguished STM (scientific, technical, and medical) publisher. Subscription membership is available for individuals universities and institutions (print & online). Subscribers can access journals from our libraries, published in different formats like Printed Hardcopy, Interactive PDFs, EPUBs, eBooks, indexable documents and the author managed dynamic live web page articles, LaTeX, PDFs etc.

GO GREEN AND HELP
SAVE THE ENVIRONMENT

JOURNAL AVAILABLE IN

PRINTED VERSION, INTERACTIVE PDFS, EPUBS, EBOOKS, INDEXABLE DOCUMENTS AND THE AUTHOR MANAGED DYNAMIC LIVE WEB PAGE ARTICLES, LATEX, PDFS, RESTRUCTURED TEXT, TEXTILE, HTML, DOCBOOK, MEDIAWIKI MARKUP, TWIKI MARKUP, OPML, EMACS ORG-MODE & OTHER

support@journalspress.com
www.journalspress.com

*THIS JOURNAL SUPPORT AUGMENTED REALITY APPS AND SOFTWARES

© COPYRIGHT 2024 GREAT BRITAIN JOURNALS PRESS